# Expansion of Cancer Cells in Self-Sorting Microwells

F. Abali

UNIVERSITEIT TWENTE.


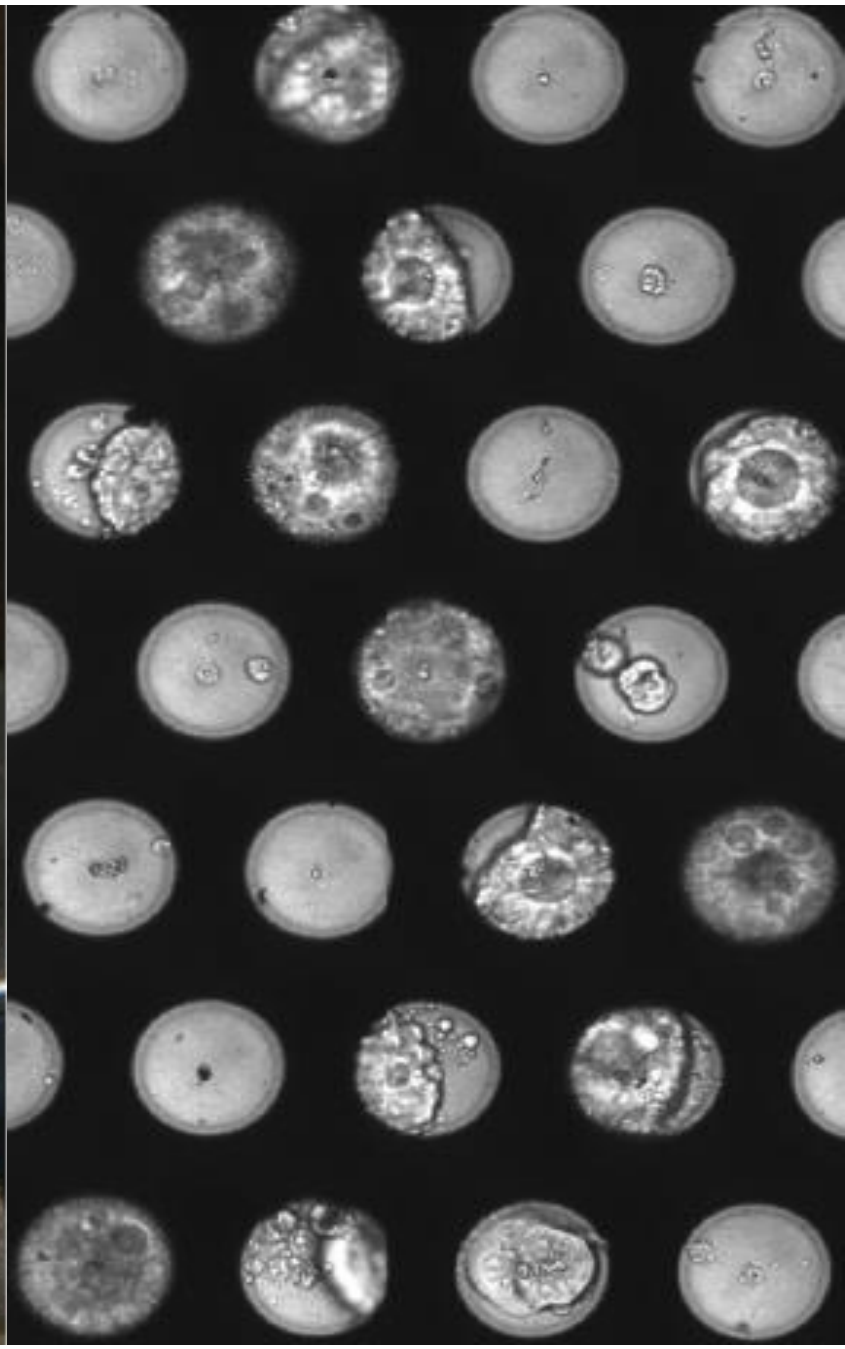

**Title**

# Expansion of Cancer Cells in Self-Sorting Microwells

**Author**
Fikri Abali

**Date**
6 juli 2016

**Department**
Medical Cell Biophysics Group (MCBP)
University of Twente

Carré, room C4439
Dienstweg 1
7522ND Enschede
The Netherlands

**Supervisors**

Prof. Dr. L.W.M.M. Terstappen
MCBP, University of Twente

Dr. M. Katika
MCBP, University of Twente

MSc J. Swennenhuis
MCBP, University of Twente

MSc K. Andree
MCBP, University of Twente

**External evaluator**

Prof. Dr. M. Karperien
Developmental Bioengineering, University of Twente

# Preface

This thesis represents the results of my master assignment performed as a student in the group Medical Cell BioPhysics (MCBP) at the University of Twente. During this period I had a great time and have been introduced to interesting research topics performed by this group and enthusiasm shown by the members of the MCBP group. The success of any project depends largely on the encouragement and guidelines of many others, and this was very true also for my master assignment. Due to the help and supervision of many at the group, I was enabled to finish my thesis.

First, I would like to thank Prof. Leon Terstappen for giving me the opportunity to perform my thesis in his department and work in a great laboratory. I would also like to express my gratitude to Madhu whose supervision and experience were fundamental for my project. Thank you for all the guidance, enthusiasm and advice on the practical part of my study.

Thank you also to the guys of VyCAP, Michiel for the preparation of many microwells, Joska for the help during some of the experiments and Arjan for his support and feedback. Also thanks to Christian for his help with the FACS machine. I would also like to thank Hugo and Koen for kindly providing primary CRC cells. Furthermore, I would like to thank Joost, who knows so much and is always ready to provide new insights and constructing feedback. Finally, big thanks to all my fellow students for their assistance during all the moments I needed a hand.

# Abstract

Metastasis is the major cause of death in patients diagnosed with invasive cancer. Blood contains two types of cancer-derived materials that are susceptible to detailed molecular analysis: intact circulating tumor cells (CTC) and (ctDNA). CTCs from peripheral blood hold important information that may represent a "liquid biopsy" and may be used for personalized treatment and real-time monitoring of cancer patients. However, the isolation and characterization of these CTCs is extremely difficult because of their rarity and heterogeneity. Although technically challenging, the growth of CTCs from patients could overcome these difficulties. In order to better understand cellular processes in metastasis and CTC heterogeneity, a controlled way for the isolation and sorting of single CTCs and their clone formation is greatly needed.

This report is composed of two parts: part 1 of this thesis describes a self sorting microfluidic chip with 6400 microwells in an array format, applied for cell culture. Obtained results showed that cells can be seeded into each microwell of the chip automatically by filtration using a small pressure, followed by week-long culture and detection of cell growth. Growth of LNCaP cell was shown to be low when compared to MCF-7 cells. In addition the growth of 3D tumor organoids in the microwells was shown to be feasible. Organoids derived from primary cells were established in microfluidic wells and maintained in culture for weeks.

Cell growth efficiency in microwells was shown to be dependent on cell-type. Primary CRC cells displayed the highest growth efficiencies. The addition of BME showed to induce cell growth in microwells. However, the growth from single cells was still very low. In contrast increasing the cell number per microwell resulted in an increase in growth efficiency for MCF-7 cells and primary CRC cells.

Subsequently, we showed that microfluidic chip enables the retrieval of cells for continued culture or analysis. Single cells or cell grown in the microwells from a single clone could be recovered from the microwells by punching. Recovered cells proliferated after punching and gave rise to larger cell colonies.

In part 2 the methylation status of GSTP1 gene was determined. MSPCR analysis was exploited to determine the presence of GSTP1 methylation in plasma derived from prostate cancer patient. Methylation of the GSTP1 gene was detected in plasma samples from all patients but not in healthy individuals. The detection of methylation in cell-free ctDNA can allow highly specific diagnosis of prostate cancer. Therefore ctDNA could be used a diagnostic marker for cancer.

# Table of Contents

# 1 Introduction

## 1.1 Cancer

Cancer is a leading cause of death with approximately 14 million new cases worldwide and accounted for 8.2 million deaths in 2012 [36]. This number is expected to rise by about 70% over the next 2 decades [36]. Cancer is a generic term for a large group of diseases that can affect any part of the body. One defining feature of cancer is characterized by the rapid development of abnormal cells that grow uncontrollably beyond their usual boundaries, and which have the ability to infiltrate and destroy normal body tissue and organs [37]. Normally, the body forms new cells when they are needed and old cells will be replaced by new ones. However, genetic changes can result in abnormal proliferation of cells and a mass can be formed called a tumor. Although the precise mechanisms for cells to adapt a tumorigenic/malignant phenotype are still unknown, the majority of the cancer types arises from 6 hallmarks and include; sustaining proliferative signaling, evading growth suppressor, activate invasion/metastasis, enable replicative mortality, induce angiogenesis and resist cell death [37]. During cancer development cells acquire one or more of these hallmarks which can result in a malignant phenotype.

Approximately 90% of the cancers found in human are malignancies of epithelial origin [41]. Although there are many kinds of cancer, only a few occur frequently. The four most common cancers, found in human and accounting for more than half of all cancer cases, are those of the breast, prostate, lung, and colon/rectum. Lung cancer, by far the most lethal, is responsible for nearly 30% of all cancer deaths [41].

## 1.2 Liquid Biopsy

The development of personalized medicine for patients with cancer depends on the identification of the molecular targets reflecting their disease. Currently, the genetic make-up of solid tumors is obtained through invasive surgical procedures [1-3]. This procedure cannot be performed on regular basis and only provides limited information about tumor heterogeneity. Tumors cells continuously change at the molecular level [4]. Therefore we need to consider whether biopsies fully reflect patient's disease. In addition, while therapies matched to the molecular fingerprint of individual patient's tumor biopsies has shown to be promising at first. Overtime drug resistance and relapse is common [5]. In order to identify new drugs, there is a need to monitor tumor evolution and determine mechanism which gives rise to tumor resistance. The development of non-invasive methods for the detection and monitoring of cancer is still a challenge. The presence of tumor cells and tumor DNA in blood of cancer patients has been considered for non-invasive detection and monitoring of patient tumors as a liquid biopsy. This non-invasive method can yield information about the genetic profile of cancers (primary and metastasis) as well as offering the opportunity to track genomic transformation. These minimally invasive liquid biopsies can be performed at multiple intervals to monitor disease and tailor cancer therapy [1,3,6].

## 1.2.1 Circulating Tumor Cells

About 90% of deaths from cancer are due to metastasis [7]. The formation of metastasis at distant places is a complex process that includes several biological phenomena [7]. Tumor cells originating from the primary tumor travel through the circulatory system and initiate tumor growth at distant sites (Fig. 1.1). It is believed that CTCs undergo phenotypic changes providing them with the ability to penetrate in to the blood stream [7, 8]. These changes are accompanied by a process known as epithelial to mesenchymal transition (EMT). EMT results in an enhanced invasive potential by the loss epithelial characteristics and the adaptation of a mesenchymal phenotype [7, 10-11]. Once transformed cells detach from the primary tumor, migrate and invade into the blood or lymphatic circulation system. CTCs travel throughout the body and infiltrate in various organs and tissues [11]. Next, CTCs adapt to environment, undergo mesenchymal to epithelial transition (MET) and finally colonize. An important factor to metastasis and tumor growth is the ability to stimulate angiogenesis leading to the formation of new blood vessels, hereby providing tumor cells nutrients [11]. CTCs show to be very heterogeneous populations of cells, some cells that have metastasized beyond their organ of origin remain dormant and resistant to therapies. CTCs which do grow and start new tumors may not respond to cytotoxic drugs or targeted therapies [11].

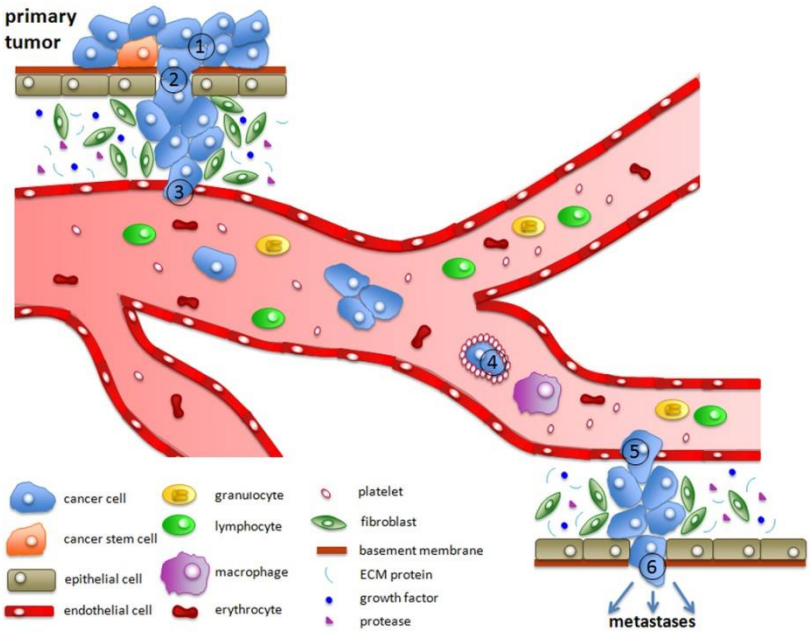


**Figure 1.1:** The process of metastasis is depicted. Cancer cells acquire an invasive phenotype and intravasite in the circulatory. CTCs survive in the circulation and arrest at distant organ sites followed by extravasations. Finally, cells adapt and initiate micrometastasis, colonization and formation of macroscopic metastasis sites. Image adapted from [11].

## 1.2.2 Circulating Tumor DNA

Circulating tumor DNA (ctDNA) is the portion of circulating DNA specifically derived from cancer cells and is present both bound and unbound to leukocytes and erythrocytes[9,12-13].The presence of ctDNA in blood is thought to arise from apoptotic or necrotic tumor cells or by active secretion from immune cells [9]. Although most ctDNA is bound, some portion can be identified in body fluids. Elevated concentrations of cell-free ctDNA fragments have

been found in blood plasma and serum of cancer patients with various types of cancer. Moreover, bodily fluids from several types of cancer have been successfully used for the molecular detection of neoplasia, including stool in colon and pancreatic cancer, urine in bladder and prostate cancer, sputum and bronchial lavage fluid in lung cancer and recently it was found that urine also contains ctDNA fom tumors originating from different organs [9].

# 1.3 Characterization of CTCs and ctDNA

## 1.3.1 DNA methylation

DNA methylation is an epigenetic process that affects cell function by change in gene expression and involves the covalent addition of a methyl group to the 5-carbon of cytosine [14-16]. DNA methylation play important role in human development through the regulation of cell differentiation that influence cell fate [42].

The DNA methyltransferase (DNMT) famillie of enzymes catalyze the transfer of methyl groups to cytosine in a CpG dinucleotide. In humans, approximately 70-80% of all DNA is methylated when located at CpG dinucleotides in non-transcribed DNA regions [14]. DNA methylation is largely found in cytosines within 5-CpG dinucleotides. This covalent modification of DNA functions as an important regulator of gene expression [14]. However, CpG dinucleotides are also found in transcribed parts of the genome. Here, CpG dinucleotides are clustered in regions known as CpG islands. The length of a CpG island is typically between 0.5-2 kb and located near promoter regions in highly expressed genes (50% of all human genes) [14]. For non-cancerous (normal) cells, CpG islands are unmethylated and associated with active genes and able to participate in active transcription. In cancer cells, many CpG islands exhibit abnormal hypermethylation, resulting in gene silencing. Many of these inactivated genes code for proteins that act as tumor suppressor or play roles in important processes including DNA repair, hormonal responses, tumor-cell invasion/metastasis and cell cycle control [14]. It is therefore commonly accepted that inactivation of certain tumor-suppressor genes occurs as a consequence of hypermethylation within the promoter regions [14]. Several studies have indicated a broad range of genes silenced by DNA methylation in different cancer types. However, the target genes that are inactivated by CpG hypermethylation differ between cancer types [17].

For example in prostate cancer, hypermethylation of the Glutathione S transferase P1 (GSTP1) gene is found in the majority (>90%) of primary prostate carcinomas but not in normal prostatic tissue [14]. The GSTP1 protein is involved in the metabolism, detoxification and elimination of potentially toxic foreign compounds, protecting cells from DNA damage. The deactivation of GSTP1 gene can result in an increased sensitivity to DNA damage and an increase in cancer initiation. GSTP1 methylation is the most common genetic alteration thus far described in prostate cancer [14]. The exact mechanisms resulting in the subsequent GSTP1 methylation and gene silencing is still unknown. However, it is likely that accumulation of genetic mutations resulting from inactivated GSTP1can give rise to growth advantage to cells.

Currently, for the early detection of prostate cancer, the prostate-specific antigen (PSA) test is used. The test detects a change in PSA concentration. Although, the PSA test is extremely sensitive it has drawbacks, including false positive results. Further tests, primarily prostate biopsy, are required to obtain a positive prostate cancer diagnosis. These invasive procedures are expensive and uncomfortable for the patient [14]. New biomarker for the detection of prostate cancer and others types of cancers need to be identified and characterized. Biomarkers based on the detection of changes in the DNA methylation status of genes could be ideal candidates. Therefore the detection of methylation status in body fluids (e.g. urine or serum) containing CTCs or ctDNA might be a valuable screening tool.

## 1.3.2 Detecting DNA methylation

Bisulfite treatment of DNA is the foremost method used to discriminate between methylated and unmethylated DNA. This method, first described by Frommer and colleagues was recognized as a revolution in DNA methylation [18]. Today, bisulfite conversion is regarded the gold-standard for detection of DNA methylation and is an efficient approach to identify 5-methyl-cytosine (5mC) at single base-pair resolution [18-19]. In this reaction (Fig. 1.2), all cytosines are converted to uracil, but those that are methylated are resistant to this modification and remain as cytosine. Following, DNA amplification, uracil will be recognized as thymine while 5mC will remain cytosines. This method enables 5mCs to be distinguished from unmethylated cytosines. A subsequent PCR or sequencing process is necessary to determine the methylation status in the gene of interest by using specific methylation primers after the bisulfite treatment.

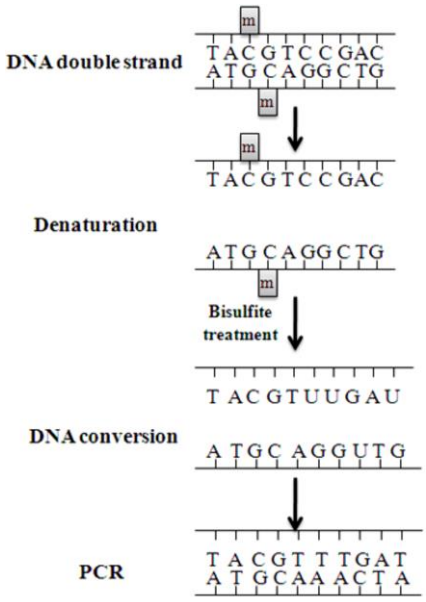


**Figure 1.2**: Principle of DNA methylation analysis using bisulfite conversion. Exposure of DNA to bisulfite converts unmethylated cytocines to uracil whereas 5mC remains unaffected. After PCR amplification of converted DNA, uracils are converted to thymines. DNA methylation can be determined with sequencing methods or PCR. Image adapted from [19].

However, the process of DNA conversion using bisulfite has an important limitation. Due to the prolonged exposure to the aggressive chemical conditions (low pH and high temperature),

required to deaminate the unmethylated cytosines, there is a great extend of DNA degradation which can reach the level of 90% [20]. On the other hand, less aggressive treatments carry the risk of not converting efficiently all unmethylated cytosines, which results in an overestimation of methylation levels.

Apart from the use of bisulfite to determine the DNA methylation status of DNA, methyl binding domain 2 protein (MBD2) has been used to specifically separate methylated CpG islands from unmethylated DNA. *In vivo*, MBD2 binds specifically to methylated CpGs via its MBD resulting in gene silencing. For the enrichment of methylated DNA MBD2 protein is coupled to magnetic beads which enable the separation of methylated and unmethylated DNA. Enriched DNA can be sequenced or subjected to bisulfite for PCR applications.

# 1.4 In vitro culture of CTCs

CTCs are promising new biomarkers which could be useful for prognostic prediction and monitoring of therapies in patients with solid tumors. Moreover, CTC research opens new opportunities for understanding the biology of CTC and the process of metastasis in patients with cancer. However, isolation of CTCs from a background of millions ($10^6$–$10^7$) of peripheral mononuclear blood cells remains challenging [38, 39]. The identification and characterization of CTCs requires extremely sensitive and specific analytical methods, which are usually a combination of complex enrichment and detection methods. Thorough investigation of CTCs is limited by the very low number present in the peripheral blood of cancer patients, ranging from 1-10 cells per 10 mL blood [35]. Most of these cells, which are thought to be involved in metastasis, die in the circulation, presumably due to the loss of matrix-derived survival signals or circulatory shear stress. Nonetheless, the establishments of functional CTC cell line models from cancer patients have the potential to identify treatments that most effectively target the changing mutational profile of the primary tumor. These models might be useful for the testing of new drugs specifically targeting CTCs.

Several group aimed to generate CTC lines isolated from a spectrum of cancers types. First, Skolorova's group used a size based separation method to isolate urothelial CTCs. The enriched CTCs fraction was cultured directly on the separation membrane, or transferred from the membrane and cultured on a plastic surface. However, the generated cultures could not be kept in culture for a prolonged period (only 2 weeks) [21]. Second, Cayrefourcq *et al*. focused on establishing a colon CTC line. In this research study, blood samples from 71 patients with metastatic colon cancer was negatively enriched and the CD45(-) cells were cultivated in non-adherent culture conditions. The authors have provided the experimental proof that CTCs isolated from the blood of a colon cancer patient are able to give rise to a permanent cell line. The established cell line could be maintained in culture for more than 2 years, showed epithelial properties with stem-cell like characteristics, epithelial/mesenchymal phenotype and tumorigenic properties when transplanted into immunodeficient mice [22]. In prostate cancer Gao *et al*. succeeded in establishing a 3D organoid system for the long-term culture of CTCs derived from peripheral blood of castration resistant metastatic patients [23]. The group of Zhang *et al*. focused on lung cancer and developed a novel in situ capture and

culture methodology for ex vivo expansion of CTCs using a 3D co-culture model. Tumors from CTCs were cultivated from 14 of 19 early stage lung cancer patients, using a three dimensional co-culture model (fibroblasts and CTCs), to support tumor development [24].
In a proof-of-concept study, Yu *et al*. aimed to cultures CTCs from six patients with estrogen receptor–positive breast cancer. After testing a range of culture conditions, they found that CTCs proliferated best as tumor spheres when cultured in serum-free media supplemented with epidermal growth factor (EGF) and basic fibroblast growth factor (FGF) under hypoxic conditions. Non-adherent culture conditions were critical, because CTCs senesced after a few cell divisions in adherent monolayer culture [34]. Three of five CTC lines tested were tumorigenic in mice. Genome sequencing of the CTC lines revealed preexisting mutations in a few genes and newly acquired mutations in the estrogen receptor gene (ESR1), PIK3CA gene, and fibroblast growth factor receptor gene (FGFR2). Drug sensitivity testing of CTC lines with multiple mutations revealed potential new therapeutic targets [34].
Finally, scientist from the Clevers lab reported the *in vitro* culture of CTC from prostate cancer. The culture system described was developed by adapting and optimizing the culture conditions that were previously used to establish mouse and human small intestine and colon organoids [25].
These discussed examples indicate that the establishment of functional CTC cell line models is feasible. The isolation and *in vitro* culture of CTCs may provide an opportunity to noninvasively monitor the changing patterns of drug resistance and study CTC heterogeneity in individual patients. To achieve this goal, the development and optimization of efficient culture strategies combined with efficient and gentle cell isolation methods is of great importance.

### 1.4.1 Organoid model

Traditionally, *in vitro* 2D cell culture models were used for the investigation of tumor behavior and for the determination of effective anti-tumor therapies. Although, monolayer cultures provided interesting and promising activities, 2D cultures could not always be confirmed in clinical settings or in animal studies [26]. This is due to the inability to mimic the extracellular microenvironment where cells reside in tumor tissue. When cells are removed from a tumor and grown in a monolayer on tissue culture plastic, the loss of these cell-substrate changes their behavior and results in an inadequate model for understanding biology or establishing appropriate therapies.
In native tissues, cells are embedded in extracellular matrix (ECM) that provides not only architectural support, but also chemical and mechanical stimuli to cells [26-27]. *In vitro* and *in vivo* studies have demonstrated the importance of cell-ECM interactions in the tumor microenvironment. For instance stiffness of the matrix was shown to induce tumor cell growth, modulate cell signaling and enhance cell invasion [27]. When cells are removed from a tumor and grown in a monolayer on tissue culture plastic, the loss of these interactions changes their behavior and results in an inadequate model for understanding biology or establishing appropriate therapies. Therefore, 2D cultures on tissue culture plastic affect tumor

cell behavior in terms of growth, adhesion, morphology and migration and do not reflect true properties of tumors *in vivo*.

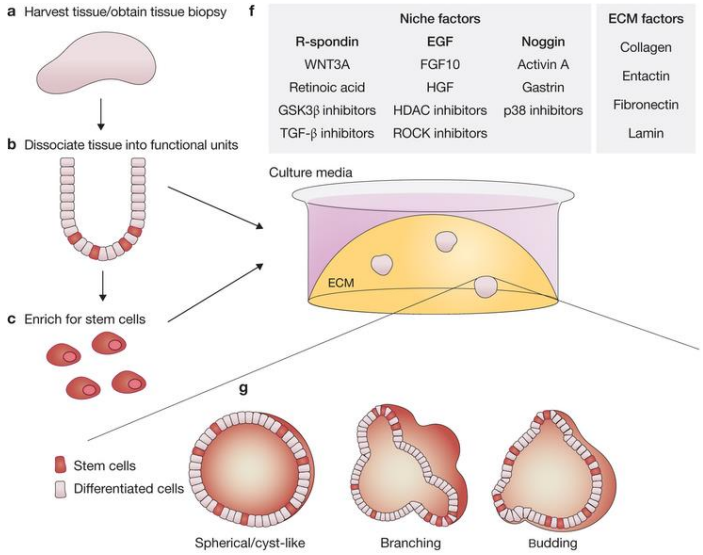


**Figure 1.3:** Organoid model to study human diseases *in vitro*. Organoids can be generated from primary cells. Adult or stem cells can give rise to organoid formation under appropriate conditions. Organoids are typically cultured in an extracellular matrix (ECM) surrounded by culture media supplemented with niche factors specific to the organoid type. Image adapted from [28].

The development of 3D culture models has shown that studying tumors in 3D better represents *in vivo* growth characteristics. For example Bissell et al, showed that when normal mammary epithelial cells were grown in monolayers they divided exponentially through several passages. However, when mammary epithelial cells were grown in 3D Matrigel culture, they responded to micro-environmental cues by reducing proliferation and differentiating into nearly normal-sized mammary acinar structures [55]. Cells derived from breast carcinomas were unable to respond to signals within the matrigel microenvironment, continuing to divide and failing to form a lumen. This suggests that cancer is a disease of not only the tumor cell but also the surrounding microenvironment.

The recent establishment of 3D multicellular tumor organoids from mouse adult stem cells demonstrated to be a valuable tool for the identification of new drugs targets [28-29]. The organoid technology is currently applied to establish a cell culture model for human cancers. In comparison to traditional *in vitro* cultures, organoids are similar to primary tissue in both their composition and architecture, have self-renewing stem cells capacity and are able to differentiate in cell lineages similar to those found in living tissue [27-28]. Organoids represent an important bridge between traditional 2D cultures and *in vivo* mouse/human models, as they are more physiologically relevant than monolayer culture models.

By use of an ECM substitutes and defined niche factors, scientist were able to generate organoid *in vitro* in serum-free conditioned medium and could be maintained in up to at least 2 years without noticeable transformation [28-29]. In addition, organoids can be cryopreserved

as biobanks and easily manipulated using techniques similar to those established for traditional 2D monolayer cultures [30].

Morphologically, organoids form and arrange in a spherical morphology with proliferating cells at the periphery, intermediate quiescent but viable cells and a central necrotic center (lumen). Moreover, organoid cells maintain a high degree of cell-cell contact and cell-matrix interaction similar to tumors found *in vivo* conditions. Currently several organoid model for various organs and tissue have been developed (e.g. intestine, colon and prostate) to study several diseases (table 1) [28].

| Tissue | Source | Organoid morphology | Types of human diseases modeled |
|---|---|---|---|
| **Stomach** | 1. Mouse/human adult tissue<br>2. Mouse/human ESCs<br>3. Human iPSCs | 1. spherical organoids/budding | Cancer |
| **Intestine** | 1. Adult tissue<br>2. Mouse/human ESCs<br>3. Human iPSCs | 1. Normal tissue: branching organoids<br>2. Diseased tissue: cystic and other morphologies | Cancer/ Cystic fibrosis |
| **Colon** | 1. Adult tissue<br>2. Mouse/human iPSCs | 1. Normal tissue: budding organoids<br>2. Diseased tissue: cystic morphologies | IBD/Cancer |
| **Liver** | 1. Mouse adult tissue<br>2. Human iPSCs | 1. Mouse organoids: spherical<br>2. Human organoids: cystic | Cystic fibrosis |
| **Prostate** | 1. Mouse/human adult tissue | 2. Normal tissue: spherical<br>3. Diseased tissue: branching similar to cancerous organoids | Cancer |

**Table 1:** Examples of organs used to establish a 3D organoids model, including descriptions of the typical organoids morphologies observed and the various diseases that have been modelled in the organoids. ESCs, embryonic stem cells; iPSCs, induced pluripotent stem cells [28].

# 1.5 Single cell isolation

The study of cell heterogeneity in cancer research requires the handling and isolation of single cells and is of great importance in applications such as single cell analysis or for emerging diagnostic methods. Analysis of cell heterogeneity in bulk populations results in an averaged signal from the population, hereby missing important information about a small but potentially relevant subpopulation in the background [31-33]. The isolation and analysis of single cells can provide detailed information which eventually can be used for therapeutic

purposes, hereby increasing personalized medicine. Single cells analysis is especially needed in the field of CTC detection and characterization [33]. However, at the moment, the isolation and separation of single cells is still technically challenging. The main challenges are the yield and quality as well as the throughput and the sensitivity of the single cell isolation method. A large number of different technologies for single-cell separation, isolation, and sorting are available. Examples of frequently used technologies for single cell isolation are: flowcytometry (FACS), random seeding or serial dilution, laser microdissection, manual cell picking, and microfluidic (lab-on-a-chip) devices (Fig. 1.4) [31].

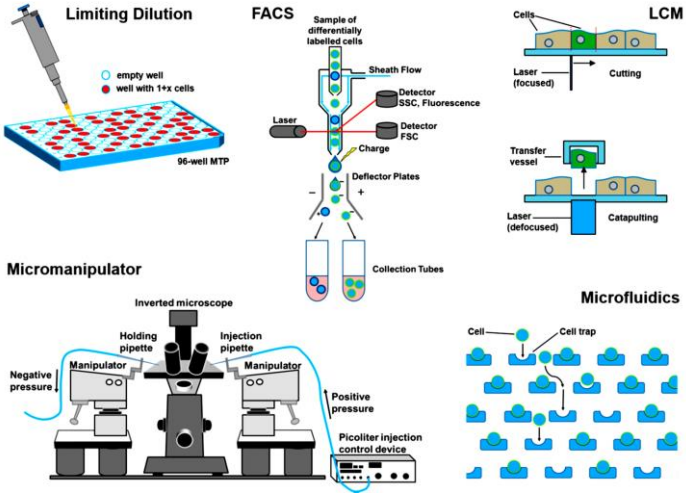


**Figure 1.4:** Some of the most frequently used technologies for the isolation of single cells; FACS, laser microdissection (LCM), micromanipulator, random cell seeding/dilution and microfluidic technologies are depicted. FACS and random seeding represent the most used technologies for single cells isolation. Image adapted from [31]

In general, the use of each of these methods strongly depends on the nature and origin of the sample and the analysis to be performed on the cells once being isolated. FACS systems have the main benefit of high throughput and sorting capability but are cost-intensive and can affect cell vitality. Laser microdissection is ideal for isolation of single cells from solid tissue. Micromanipulator assisted cell picking is a manual process and therefore slow, but provides maximum control over individual cells. Limiting dilution relies on statistical distribution, is simple to implement and can be automated. However, the presence of single cells often needs to be verified. Although these technologies have shown their value within the field of single cell isolation, they are hampered typically by low throughput, labor intensiveness, show high cell losses and affect cell viability. Apart from these established technologies, microfluidic technologies are ideally suited to addressing these problems by providing reduced reagent costs, small volumes, scalability, ease of automation, improved cell handling, and multi-step integration [31-33]. Many different microfluidic devices for single cell separation and handling have been published in the literature. Most of these devices use at least one of the three following microfluidic principles to isolate single cells: droplet-in-oil-based isolation, pneumatic membrane valving and hydrodynamic cell traps as for example published [31].

## 1.5.1 VyCAP microfluidic wells

Recently, Swennenhuis *et al*. reported the use of a microfluidic chip as a platform for the isolation of single cells for downstream analysis. This microfluidic chip combines single cell seeding in microwells with an efficient method to isolate and recover single cells after characterization by fluorescence microscopy (Fig. 1.5A-B). The microfluidic chip is composed of 6400 microfluidic wells in an effective area of 8 × 8 mm. Each individual microfluidic well has a diameter of 70 ± 2 µm, a depth of 360 ± 10 µm and a volume of 1.4 nL. The bottom of the microfluidic well is made from an optical transparent silicon nitride (SiNi) membrane, with a thickness of 1 µm and a single pore with a diameter of 5 µm. The supporting material is made from silicium oxide (SiO2). Comprehensive description about the fabrication of the self seeding microfluidic well chip can be found in [33]. The principle of single cell isolation using the self-seeding microfluidic well chip is shown in Fig. 1.5C. The chip is inserted in the filtration holder, the cell suspension is transferred on top of the microfluidic wells, and subsequently a small negative pressure of 5-10 mbar is applied across the microfluidic wells (Fig. 1.5D). This result in a fluid flow from top to bottom, fluid enters the microfluidic wells from the upper (top) side and leaves the microfluidic wells through the pore at the bottom of the well. Single cells follow the hydrodynamic flow profile and are directed into the wells towards the pore at the bottom of the microfluidic well. Because the diameter of the pore is smaller than dimension of cells of interest, cells are trapped and cannot pass [33]. Once a pore is blocked the fluid flow is restricted. This results in that no other cell will enter the same microfluidic well. The next cell is then diverted to a neighboring well. In this manner single cells are seeded in individual wells across the entire microfluidic well chip until all well have been occupied [33].

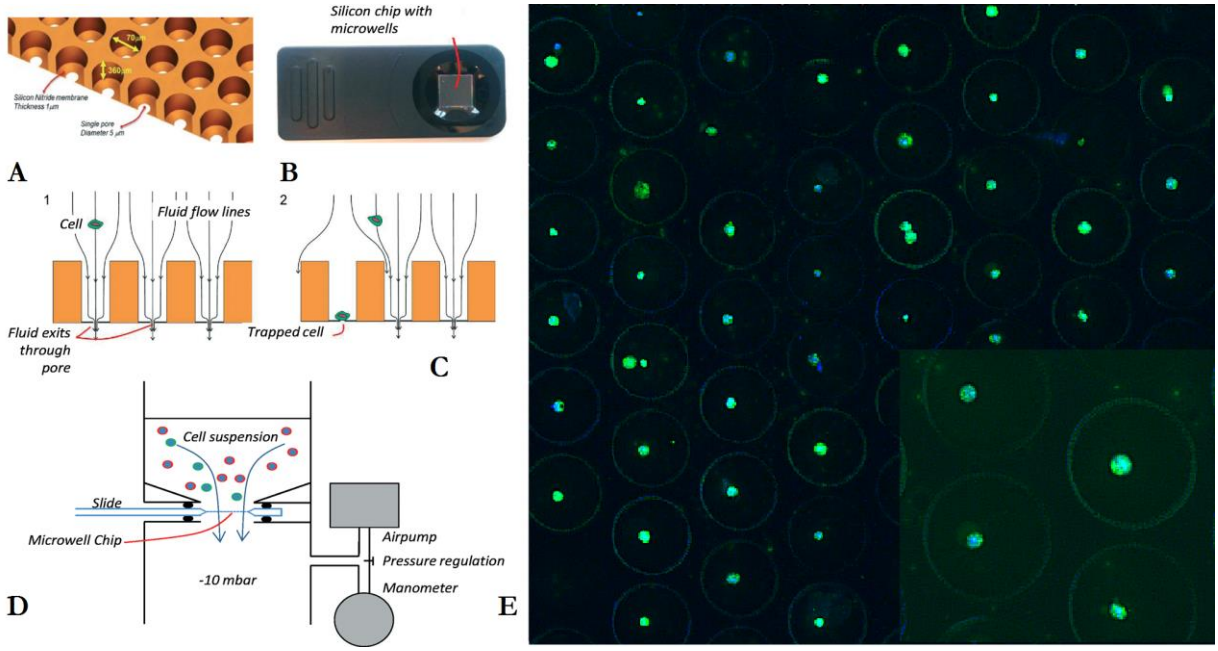


**Figure 1.5:** A) Dimensions of the microfluidic chip (10 × 10 mm). The microfluidic wells have a diameter of 70 µm and a depth of 360 µm. The bottom membrane is made from SiNi (1 µm thick) with a 5 µm pore in the center of the microfluidic well. B) The microfluidic wells chip is mounted in a plastic slide for handling. C) The principle of the seeding method is illustrated; fluid enters the wells from the top and exits through the pore at the bottom. Cells are

directed inside the well and land onto the pore at the bottom of the microfluidic well. D) Schematically illustrates the filtration system. Negative pressure is applied and cells are forced into the microfluidic wells. E) Microfluidic wells seeded with cells from breast cancer cell line MCF-7 is shown, blue for nucleus (Hoechst), green cytoplasm (Cell Tracker Orange) partly adapted from [33].

Once cells have been seeded in the microfluidic wells the chip is scanned using an inverted fluorescence microscope that acquires images of the entire microfluidic well chips in an automated fashion. Figure 1.5E represents a typical image of a microfluidic chip which contains fluorescent labeled single cells residing in microwells. Image shows that most microfluidic wells contain a single cell at the centre (pore). If desired, cells can be retrieved from the microwells for further analysis. Schematic representation of this method is presented in Fig. 1.6A and B. Fluorescence images are used to select the desired cells for punching (recovery). Subsequently, a needle is directed to punch the selected cells from the microfluidic wells. The punched cell plus the bottom fragments fall down into a designated collection vessel (cell culture plate) that is placed on a different X-Y stage beneath the microfluidic chip (Fig. 1.6C-D).

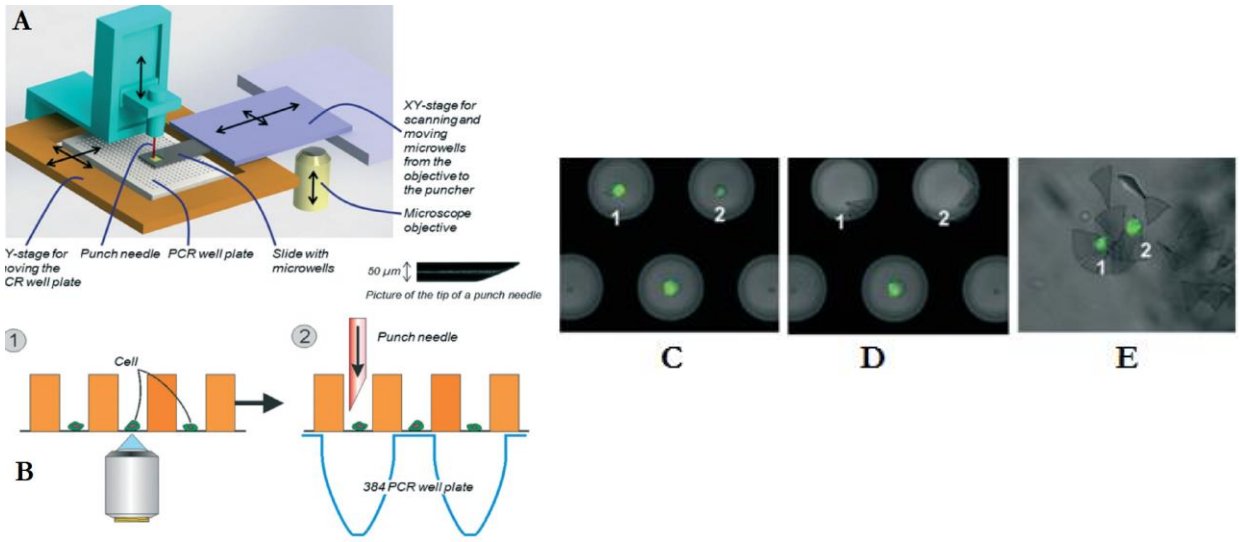


**Figure 1.6:** Illustration of the punching set up. A) The punching principle is shown, the stage for the collection vessel (wells-plate) and the magnet holder for the microfluidic wells both can move in the X-Y direction. Punching needle is able to move in the Z-direction (Up/down). B) Cells are imaged through the transparent membrane. The selected cells are punched from the microfluidic well into a collection vessel that is positioned below the microfluidic well. C-D) Example of cell recovery from microfluidic wells; two cells are punched and recovered. Images adapted from [33].

## 1.6 Aim of the study

Circulating tumor cells (CTCs) are rare heterogeneous cell populations shed by primary tumors and circulate in blood of patients. CTCs can be used as noninvasive biomarkers for disease prognosis and tumor recurrence. Molecular characterization of CTCs allows us to better understand the process of metastasis and will improve treatment strategies. However, CTCs are present at low concentrations in the blood, limiting detailed molecular characterization. Most of these cells, which are thought to be involved in metastasis, die in the circulation. Nonetheless, if CTCs can be isolated from cancer patients as viable cells and expanded (ex-vivo culture), this would provide a tool to noninvasively monitor the changing patterns of drug susceptibility in individual patients as their tumors acquire changes in DNA (e.g. epigenetic and mutations) and RNA [34, 40]. Importantly, it was hypothesized that the generation of cultures from single CTC clones, can provide very detailed information about the genomic landscape (heterogeneity) of the tumor and may be used for therapeutic decisions in personalized medicine.

Currently, a variety of technologies for single-cell separation, isolation, and sorting are already available. However most of these established technologies affect cell viability or cannot isolate cells from rare samples with low numbers of cells or experience low throughput. In contrast, microfluidic technology plays an increasing role in establishing entire workflows for single-cell separation, isolation, and analysis. Therefore microfluidic technologies are promising platforms for single cell isolation.

In this study we aimed to characterize a microfluidic chip with 6400 microwells for the isolation and culture of cells.

In addition, tumors release cell free DNA (ctDNA) into the blood, but the majority of circulating DNA is often not of cancerous origin, and detection of cancer-associated alleles in the blood has long been impossible. Alterations in the patterns of DNA are among the earliest and most common events in tumorigenesis. Many gene promoters contain GC-rich regions of

DNA known as CpG islands. Methylation of CpG islands located within the promoter region of genes may result in abnormal gene inactivation, including those involved with control of cellular growth (*i.e.*, tumor suppressor genes) and has been reported in a wide spectrum of human cancers. Therefore we aimed to determine if DNA methylation can be used as molecular diagnostic marker for cancer detection.

# 2 Materials and Methods

## 2.1 Cell culture

MCF-7 (human breast cancer, ATCC® HTB-22) and LNCaP (human prostate cancer, ATCC® CRL-1740) cell lines were used. Prior to experiments cells were thawed and cultured onto polystyrene flasks. MCF-7 cells were kept in culture with Dulbecco's Modified Eagle medium (DMEM, Gibco) with 10% fetal bovine serum (FBS, Greiner Bio-One), 100,000 IU/l penicillin and 100mg/l streptomycin (Lonza), 4mM L-Glutamine (Lonza). LNCaP cells were cultured in RPMI-1640 supplemented with 10% FBS, 100,000 IU/L penicillin and 100 mg/L streptomycin (Lonza), 4mM L-Glutamine (Lonza).When reached 90% confluence cells were trypsinized (0.05% trypsin-EDTA, Gibco) and replated in fresh flasks and incubated at 37° C and 5% CO2. For experiments, flasks which showed 70% confluency were used. MCF-7 cells used in the experiments were from passage 95 to 120 and LNCaP from passage 55 to 70. Prior to seeding cells in microfluidic wells, cells were spun down at 300 × g for 5 minutes and resuspended in cell culture medium.

## 2.2 Organoid Culture

Human colorectal cancer cells (CRC organoids) from patients undergoing resection for primary tumors expressing Green fluorescence Protein (GFP) were kindly provided by the lab of H. Snippert (University of Utrecht/Hubrecht Institute). Organoid cells were cultured in DMEM/F12 stem cell medium (advanced Dulbecco's Modified Eagle medium/F12; Life Technologies Europe BV, The Netherlands). Suplemented with 10% R-Spondin conditioned medium (Peprotech), 10% Noggin conditioned medium (Peprotech), 1× B27 (Invitrogen), 1.25 mM n-Acetyl Cysteine (Sigma-Aldrich), 10 mM Nicotinamide (Sigma-Aldrich), 50 ng/ml human EGF (Peprotech), 500 nM TGF-β type I receptor inhibitor A83-01 (Tocris), 10 uM P38 MAPK inhibitor SB202190 (Sigma-Aldrich) and 10 uM Rock inhibitor LY27632. For passaging organoids medium was removed and organoids were incubated with (0.05% trypsin-EDTA, Gibco) for 10 min with pipetting up and down to break the matrigel and frequently checking under microscope to investigate the dissociation of cells from the organoids/BME slurry. Once organoids dissociated into single cells, the supernatant was transferred to a new tube. Basal culture medium (DMEM/F12 supplemented with penicillin/streptomycin, 10 mM HEPES, 10 mM Glutamax and 10% FBS) was added and the CRC cells were spun down at 650 rpm for

3 min. The pellet was washed in basal culture medium and resuspended in Basement Membrane Extract type 2 (BME, Cultrex Amsbio Trevigen Inc, Gaithersburg, MD). Cells were plated in 10 µL BME droplets and left to solidify at 37°C. Finally, cell culture medium was added and cells were incubated at 37°C and 5% CO2.

## 2.3 Microfluidic wells preparation

Microfluidic chips were supplied by VyCAP BV, the Netherlands. Prior to cell seeding microfluidic wells were degassed in Phosphate buffered saline (1X PBS) with 0.1% Tween at a pressure of -0.5 bars for 15 minutes. Subsequently, wells were sterilized in 70% ethanol for 30 minutes and washed with 1X PBS to remove ethanol. Finally microwells were incubated in cell culture medium.

## 2.4 Live cell tracking

To track cell growth on microfluidic wells cells were stained with Cell Tracker Orange, 1:5000 v/v (CTO, Life Technologies). Briefly, fresh cell culture medium with CTO was added to flask and incubated at 37º C and 5% CO2 for overnight. Medium was removed and cells were washed with 1X PBS and incubated for 30 minutes in culture medium.

## 2.5 Cell viability in microfluidic wells

For viability assay cells were cultured as previously described. Briefly, MCF-7 cells were grown to 70% confluency in TCP; cells were then collected by trypsin, resuspended in cell culture medium, spun down and counted. Cells were then stained with LIVE/DEAD Cell Imaging Kit (488/570) (Invitrogen) as described by the manufacturer's protocol. Cells were incubated in 4 µM ethidium homodimer (EthD) and 2 µM calcein-AM in 1X PBS for 20 min at 37°C. Live cells stain green due to enzymatic conversion of the non-fluorescent cell-permeant Calcein-AM to fluorescent Calcein. Dead cells stain red after binding of EthD1 to the DNA of membrane-compromised cells. Finally, cells were seeded in microfluidic wells. To determine viability in microfluidic wells over time cells were stained in microfluidic wells by removing culture medium from the bottom of the microfluidic wells. 50 µL Live/Dead staining solution was added on top of the microfluidic wells and incubated at 37º C for 30 min. Cells were imaged on fluorescent microscope. As control a number of 20 cells per well was seeded in TCP with FACS or by manual pipette. The number of viable and non-viable cells was counted.

## 2.6 Cell culture in microfluidic wells

For each microfluidic chip a number of 6400 cells was resuspended in a mixture of medium and BME. For cell lines BME type 1 and for CRC cells type 2 was used with a protein concentration between 15,05-16,06 mg/ml. BME was thawed overnight at 4º C on ice. To prepare cell/BME mixture, medium was chilled on ice followed by addition of desired concentration of BME and cells (6400 cells).The cell/BME suspension was thoroughly mixed and kept on ice before seeding into microfluidic wells. Microfluidic chips were cooled on ice to avoid matrigel gelling during cell seeding. The microfluidic chip was inserted in the filtration holder which was connected to the pump unit. The complete volume of cell/BME

mixture was added on top of the microfluidic wells and a pressure of 5-10 mbar is applied to seed cells in microfluidic wells. Subsequently, microfluidic chips were incubated for 30 minutes at 37º C to allow matrigel to gel. Finally, cell culture medium was added on top of the microfluidic wells and incubated at 37º C and 5% CO2. Figure 2.1 illustrates the workflow used for cell culture in microwells. As a control for cell culture in microfluidic wells, cells were seeded with FACS and pipette. Cells were seeded in wells-plate coated with 10% BME.

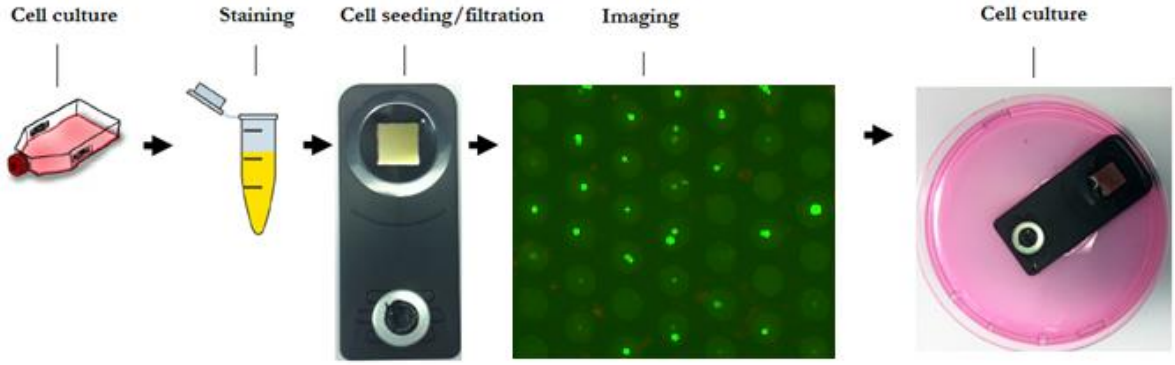


**Figure: 2.1**: Schematic representation of the culture method used to grow cells in microfluidic chip. Cells were harvested, stained and seeded (filtered) in microfluidic wells. Subsequently, cells were incubated in medium for cell culture.

# 2.7 Quantification of cell growth

For quantification of cell growth, the microfluidic wells were scanned and images were taken at different time points. Images for all time points were then stacked using Image J software. From these images the number of cells at t=0 and t=1, 2, 3, etc was determined. Microfluidic wells containing single cells directly were counted automatically using Image J software. In practice, the fluorescent images were first converted to grayscale images (Fig. 2.2A), then thresholded in Image J (Fig. 2.2B). Subsequently, the plugin particle analyzer in Image J software was used to determine the total number of single cells directly after seeding. The mask image was used for comparison with initial fluorescent image (Fig. 2.2C). Wells which showed proliferated cells were counted manually in Image J. The growth efficiency was calculated by dividing the total amount of proliferated cells by the total amount of cells present directly after cell seeding (single, doublets or more cells). Finally, from the obtained numbers a graph was plotted which depicts the amount of cells which have proliferated over time.

**Fluorescent image** **Thresholded image** **Mask image**

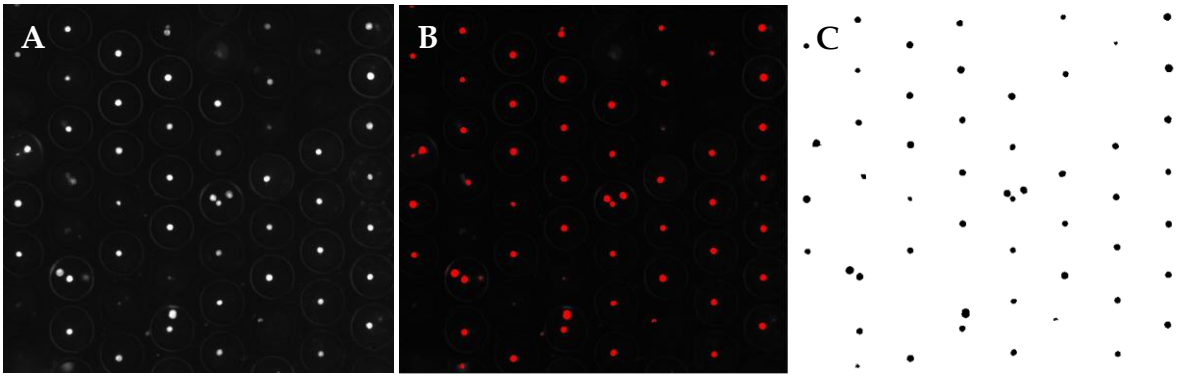


**Figure 2.2:** For quantification of cell proliferation in microfluidic wells, total number of single cells was counted automatically using image. Fluorescence images were converted to a grayscale images (A) and thresholds manually in Image J software (B). The plugin particle analyzer in Image J was used to count the number of cells in each microfluidic well. The masked image depicts the particles counted and was used for comparison with the original image (C).

# 2.8 Punching cells

Cells were retrieved from the microfluidic chip by punching SiNi-membranes from the microwells (Fig. 2.3). Single cells or colonies were stained for viability and scanned. From the obtained fluorescent images viable cells were selected. Punching was performed in immersion mode. Medium contact between the well of a 96 wells-plate and the back of the microfluidic was made. Once liquid contact was established cells were punched out and recovered in TCP.

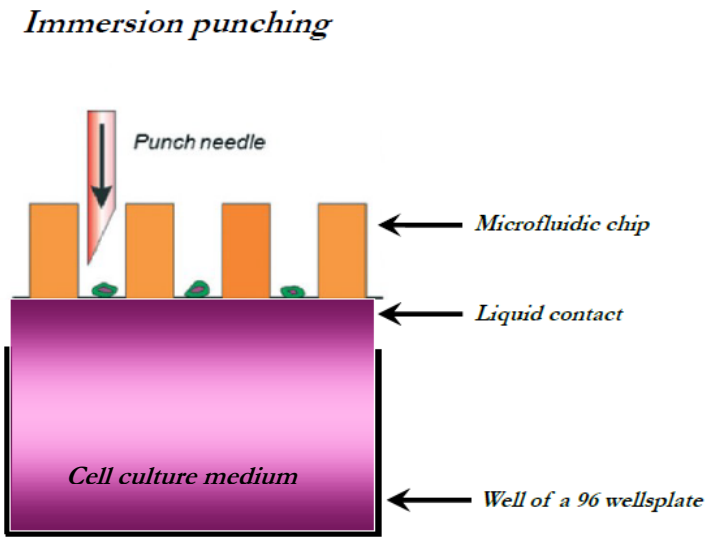


**Figure 2.3:** Schematic representation of immersion punching. Medium contact between back of microfluidic chip and well is made. Cells were punched out with a needle that breaks the SiNi glass membrane.

# 2.9 Cell recovery after punching

Cell recovery after punching was determined by counting total number of successful punched cells and the amount of cells recovered in TCP. These numbers were used to quantify the recovery efficiency. Overall a number of 100-150 cells were punched.

## 2.10 Growth efficiency after punching

For growth efficiency after punching cell were stained for viability after 4 hours and total number of viable cells was counted. Cells growth was monitored for 14 and total number of cells which proliferated was determined. Cell growth efficiency was calculated as the total number of cells which proliferated divided by the total number of viable cells at 4 hours.

## 2.11 Immunostaining

For immunofluorescence staining of cells grown into microfluidic wells, cells were washed twice with 1X PBS for 5 minutes. A sponge was used to remove wash buffer (1X PBS) from bottom of wells. Cultures were fixed with 1% formaldehyde in 1X PBS (v/v) for 30 minutes at room temperature and washed twice with 1X PBS. Next, cells were incubated with Hoechst 33342 (1:500, v/v) for 30 min at room temperature. Finally cells were washed once with 1X PBS followed by imaging.

## 2.12 Spiking and enrichment

MCF-7 cells were pre-labeled with cell tracker violet (1:5000) (Invitrogen) and a number of 1500 cell was spiked in 1 mL fresh whole blood. The RosetteSep™ Human CD45 Depletion kit was used to enrich epithelial tumor cells from whole blood using a combibation of density gradient separation with an antibody-mediated enrichment step. Enrichment was done through negative selection. Unwanted cells were cross-linked to multiple red blood cells by bispecific tetrameric antibody complexes including CD45, CD66b and glycophorin A. As the density of these unwanted cells increases (rosette formation), they accumulate in the lower compartment after density gradient centrifugation. In practice, after spiking 1500 MCF-7 cells in blood, the mixture was incubated with 50 µL Rosettesep tetrameric antibody cocktail and incubated for 20 minutes at RT. Hereafter, 1 mL of 2% BSA in 1X PBS was added and mixed. The total volume was gently layered on top of 1.5 mL Ficoll gradient and centrifuged at 1200 × g for 20 minutes. The purified epithelial tumor cells were present as a highly enriched population at the interface between the plasma and the buoyant density medium (Ficoll). This enriched cell fraction was gently collected and washed in 1X PBS. Subsequently, this fraction was stained with APC conjugated anti-EpCAM (1:50 v/v), PerCP conjugated anti-CD45+ (1:25 v/v) and with 50 µL viability dye (Calc AM and EthD1, Invitrogen). Finally, cells were seeded in microfluidic wells and imaged. Cells positive for Cell tracker violet, EpCAM and Calcein AM were selected and punched out from microfluidic wells into BME coated or non-coated 96 wells-plate.

## 2.13 Image Acquisition

To determine and evaluation cell behavior (e.g. proliferation, cell-morphology and migration) in microwells images were acquired using a fluorescence microscope (Nikon Eclipse TE2000S, Nikon); images were taken with a Zeiss AxioCam HRM camera and custom made imaging software to image microfluidic wells (VyCAP.BV). Cells cultured in 96 wells-plates were imaged using inverted microscope Olympus IX73.

## 2.14 Image Analysis

Aqcquired images were analyzed using an image processing and analysis software (Image J, version 1.46).

## 2.15 DNA isolation from plasma

Plasma DNA was purified using the MinElute spin kit (Qiagen) according to manufacturer protocol. All steps were performed at room temperature. A volume of 300 µL plasma was added to 30 µL proteinase K (Qiagen) in 2 mL tube and mixed. Buffer AL (300 µL) containing 5,6 µg carrier RNA was added and mixed thoroughly, followed by incubation at 56º C for 30 minutes in water bath. Then, samples were centrifuged briefly and 375 µL of absolute ethanol was added and mixed by pulse vortex for 15 seconds. The samples were incubated for 5 minutes at room temperature, followed by a short centrifugation step. Subsequently, samples were transferred to QIAamp MinElute columns and spun down at 8000 × g for 1 minute. The flow-through was discarded and columns were washed with 500 µL buffers AW1 and AW2 respectively. Finally, the columns were washed once in 500 µL absolute ethanol and the DNA was eluted in 20 µL AVE buffer followed by a second elution step in 20 µL AVE buffer. The isolated DNA samples were pooled and stored at -20º C or directly used for bisulfite treatment or MBD enrichment.

## 2.16 Isolation of genomic DNA

LNCaP cells were harvested by trypsin and cells were pelleted at 300 × g. Cells were washed once in sterile cell 1X PBS. Finally, cells were diluted in 200 µL 1X PBS. gDNA DNA from LNCaP cell and WBC was extracted with QIAmp DNA mini kit (Qiagen, cat 55704 )and used according to manufacturer's protocol. First 20 µL of proteinase K and 200 µL of Buffer AL was added to samples and mixed for 15 seconds by pulse vortex followed by incubation at $56^0$ C for 10 minutes. Subsequently, 200 µL absolute ethanol was added to samples and mixed. This mixture was loaded onto QIAamp mini spin column and centrifuged at 6.000 × g for 1 minute. The column was washed with 500 µL buffer AW1 and once with 500 µL buffer AW2 and centrifuged at 6000 × g for 1 minute and at 20000 × g for 3 minutes respectively. Finally, genomic DNA was eluted by incubation for 5 minutes in 25 µL AE buffer. Isolated genomic DNA was finally stored at -20 $^0$ C or directly used for sodium bisulfite conversion.

## 2.17 Sodium Bisulfite treatment

Isolated plasma- or genomic DNA (from cell lines or white blood cells) was subjected to bisulfate conversion using EZ DNA Methylation Kit (cat D5002-2, Zymo Research, Irvine, CA). All steps were performed at room temperature. 5 µL M-dilution buffer was added to each sample and total volume was adjusted to 50 µL with Milli-Q. Subsequently, samples were incubated at 37º C for 15 minutes in water bath. 100 µL CT conversion reagents (prepared in advance by adding 750 µL water and 210 µL M-dilution buffer to CT conversion reagent) was added and samples were incubated at 50º C for 12-16 hours in dark. Converted DNA was cleaned-up using Zymo-spin IC columns and buffers provided with EZ DNA Methylation kit.

First, 100 µL of M-Binding Buffer was loaded onto spin columns to wet the column then another 300 µL of M-Binding Buffer was added directly to each sample and mixed thoroughly. Samples were then loaded onto spin columns and spun down at 10.000 × g for 30 sec. The flow-through was loaded again twice more into the spin column to achieve higher DNA yield. The columns were then washed with 100 µL M-Wash buffer and samples were incubated with 200 µL M-desulphonation buffer for 20 minutes according to manufactures protocol. Finally, samples were washed in 100 µL M-Wash buffer and DNA was eluted in 25 µL M-Elution Buffer (≥20.000 × g). The amount of DNA was determined by fluorometric quantitation (Qubit, Thermo Fisher Scientific Inc.). Isolated bisulfite treated DNA samples were stored at -20º C before use in PCR.

# 2.18 Methylated DNA enrichment

Plasma DNA was isolated from DNA samples using the EpiMark® Methylated DNA Enrichment Kit (cat E2600, New England BioLabs), with slight modifications. For each enrichment reaction, 10 µL of human MBD2 protein fused to the Fc tail of human IgG1 (MBD2−Fc) was coupled to 1 µL of paramagnetic protein A beads (MBD2−Fc/Protein A Magnetic Bead). MBD2−Fc/Protein A Magnetic Beads were then concentrated using a magnetic rack and washed twice using 1 mL 1X Bind/Wash Buffer before being re-suspended in 11 µL 1X Bind/Wash Buffer. For each sample 10 µL of beads was mixed with plasma DNA (~50 µL), 20 µL of 150 mM NaCL and 20 µL MilliQ (to make a total volume of 100 µL) and incubated for 20 minutes at RT with agitation. The DNA fraction bound to MBD2−Fc/Protein A Magnetic Beads was concentrated using a magnetic rack. The supernatant was saved as the fraction could not bind to the MBD2−Fc/Protein A Magnetic Beads (unmethylated fraction). MBD2−Fc/Protein A Magnetic Beads were washed three times with 1 mL of 1X Bind/Wash Buffer. The bound DNA fraction (methylated fraction) was incubated at 65 °C for 15 minutes in Milli-Q (60 µL) with frequent mixing. Finally, the samples were briefly spun down at 14.000 rpm and the beads were concentrated on magnet rack. The supernatant which contained the enriched methylated DNA was collected and stored at -20 °C.

# 2.19 Methylation Specific PCR

Methylation Specific Polymer Chain Reaction (MSPCR) was performed on converted plasma DNA samples to specifically detect methylation at specific gene sites. To achieve high specificity we performed nested MSPCR. As a target gene the methylation in the GSTP1, known to be highly methylated in prostate cancer patients and unmethylated in healthy donor was exploited. Bisulfite-converted plasma DNA was subjected to two rounds of PCR to amplify GSTP1 CpG island alleles, using primers that recognize GSTP1 sequences after conversion of C to T. Primers targeting the promoter region of the GSTP1 gene were adapted from Shilpa et al [54]. The first PCR reaction was performed using 1 µL (1 ng/µL) bisulfite-converted template DNA, 0.5 µL external GSTP1 primers (5 pmol/L), 0.2 µL deoxyribonucleotide triphosphates (DNTPs, 2 pmol/L), and 0.05 µL *Taq* polymerase (0.25 Units, biolabs), 1 µL 10X Reaction buffer and 7.25 µL of nuclease free water (Thermo Fisher Scientific Inc.) in a total reaction volume of 10 µL. Sequences of external primers were GSTP1-

F: GGG-ATT-TTA-GGG-CGT-TTT-TTT-G; GSTP1-R: ACC-TCC-GAA-CCT-TAT-AAA-AAT-AAT. PCR was done by the following procedure: initial denaturation at 95°C for 5 minutes followed by 35 cycles at 95°C for 30 seconds, 50°C for 30 seconds, 72°C for 30 seconds and a final extension at 72°C for 5 minutes. The second PCR reaction mixture was performed in a total volume of 10 µL. Two primer sets were used. The first set targeting the methylated (GSTP1-M pair) and second set of primers targeting the unmethylated (GSTP1-U pair) gene. The reaction mixture contained 1 µL of 500× diluted DNA-template (product from first PCR round), 0.1 µL GSTP1 primers, 0.2 µL DNTPs (2pm/L), 0.05 µL of *Taq* polymerase (0.25 Units), 1 µL Reaction buffer and 7.65 µL of nuclease free water. PCR cycling conditions for methylated primers consisted of an initial denaturation step for 5 minutes at 95 °C, followed by 35 cycles of 30 seconds denaturation at 95 °C, 30 seconds annealing at 52 °C and 30 seconds elongation at 72 °C followed by final elongation at 72 °C for 5 minutes. For unmethylated primers the same cycling protocol was used; however only the annealing step was performed at 51 °C for 30 seconds. Primer sequences used were GSTP1-MF: TTC-GGG-GTG-TAG-CGG-TCG-TC; GSTP1-MR: GCC-CCA-ATA-CTA-AAT-CAC-GAC-G and GSTP1-UF: GAT-GTT-TGG-GGT-GTA-GTG-GTT-GTT; GSTP1-UR: CCA-CCC-CAA-TAC-TAA-ATC-ACA-ACA for methylated and unmethylated respectively.

# 2.20 Gel electrophoresis

Agarose gel electrophoresis was used to analyze samples. 2% (w/v) agarose (Sigma.) was prepared in 0,5X TBE buffer. ) SYBR safe DNA gel stain 1:10000 (v/v) (Invitrogen) was added and gel was poured. Samples (10 µL) were loaded on gel with 2 µL loading dye. A 100 kb ladder was added and gel was run for 10 minutes at 90 Volt and for 25 minutes at 120 Volt. Images were taken with Gel Doc Ez Imager (Bio-rad) supplemented with imaging software Image Lab 5.2.1(Bio-rad).

# Part 1

## Characterization of self-sorting microwells

# 3 Results

## 3.1 Cell seeding efficiency

Cell seeding efficiency in the microfluidic wells was investigated for dynamic seeding technique (filtration). Cells were fluorescently labeled and a number of 6400 MCF-7 cells were seeded in microfluidic wells using a pressure of -10 mBar. Cells were seeded in the presence of different BME concentration. The number of recovered cells was counted to determine the seeding efficiency. Figure 3.1A and B demonstrates fluorescently labeled cells seeded in the presence or absence BME in microfluidic wells. In the absence of BME we clearly identify the presence of a single cell per well located at the pore and thus showing optimal seeding efficiency.

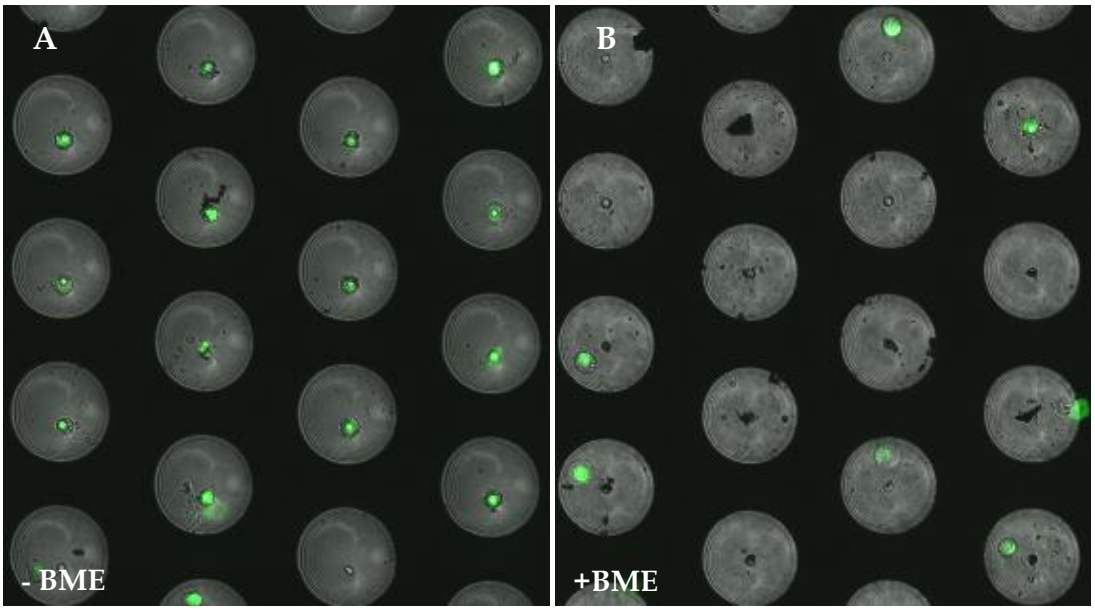


**Figure 3.1**: Cell seeding with or without BME to determine the seeding efficiency using dynamic seeding technique. Fluorescence labeled cells seeded in microfluidic wells. In image A cells were not suspended in matrigel (-BME), which resulted in the presence of a single cells per well. For cells seeded with 20% matrigel (+BME) we see a lower number of seeded cells per well. This indicated that matrigel affects overall cell seeding efficiency.

For cells resuspended in 20% BME not all the wells show the presence of a single cell per well. This indicates that BME affects cell seeding efficiency. We further observed that the cell distribution across the microfluidic wells was uniform, indicating that cells could be found all over the microfluidic well and not in one particular area. The relationship between BME and cell seeding efficiency is shown in Fig. 3.2. In the absence of BME (medium), 89% of the cells are found back in the microfluidic wells, while for cells in 2% BME a decrease of 14 % (75% cell seeding efficiency) was seen when compared to medium group. Cell seeding efficiency decreased with increasing BME concentration. Cell supplemented with 5% BME shows a seeding efficiency of only 64%.The highest amount of BME showed lowest recovery efficiency (35%).

For BME samples (especially for higher BME concentration) we observed that during seeding the applied cell-suspension volume did not completely pass through the microfluidic wells. This could explain the decrease in efficiency in BME samples. Seeding method used here is dependent on fluid flow through 5µm pores located at the bottom of the SiNi-membrane. A clogged pore limits fluid flow in that particular well, which results in that no cell can enter. Perhaps during cell seeding BME gels due to increase in temperature which in turn results in the clogging of pores and consequently limits entrance of cells in microwells. This could explain the decrease in efficiency seen in BME samples.

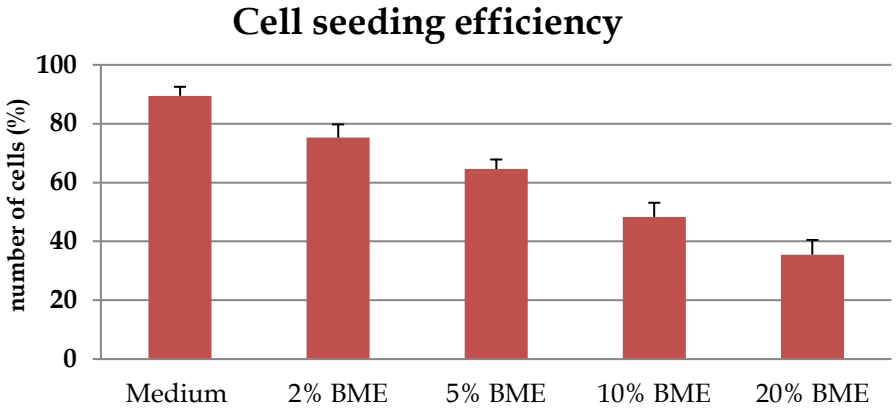


**Figure 3.2:** Cell seeding efficiency in microfluidic wells. Cell were resuspended in different BME concentration and seeded in microfluidic wells. Cell seeding efficiency in microfluidic wells decreases with increasing BME concentration. Data represents mean ± sd (n=4).

# 3.2 Cell viability

We next, assessed whether microfluidic wells have the potential to be used as a platform for the isolation of viable cells for *in vitro* cell culture. Cell viability directly after cell seeding and during incubation for several days was investigated. MCF-7 cells were seeded in microfluidic wells and cultured for 4 days. Figure 3.3 shows fluorescent labeled cells in microfluidic wells at different time points. Directly after seeding (30 minutes) most of the cells were viable, most of the cells were positive for Calc AM (alive cells) and negative for the nucleic dye Eth-D1

(dead cells). However, prolonged culture of cells in microfluidic wells resulted in a further decrease of cell viability over time. After 24 and 48 hour culture in microfluidic wells cell viability further decreased. Nevertheless we still could detect viable cells (see Fig. 3.3). Majority of dead cells was found in microwells which only contained single cells. Microfluidic wells with 2 or more cells, MCF-7 cells clustered together to form cell clumps. Furthermore, at 24 and 48 hours proliferating cells were detected indicating that MCF-7 cells could proliferate in microfluidic wells.

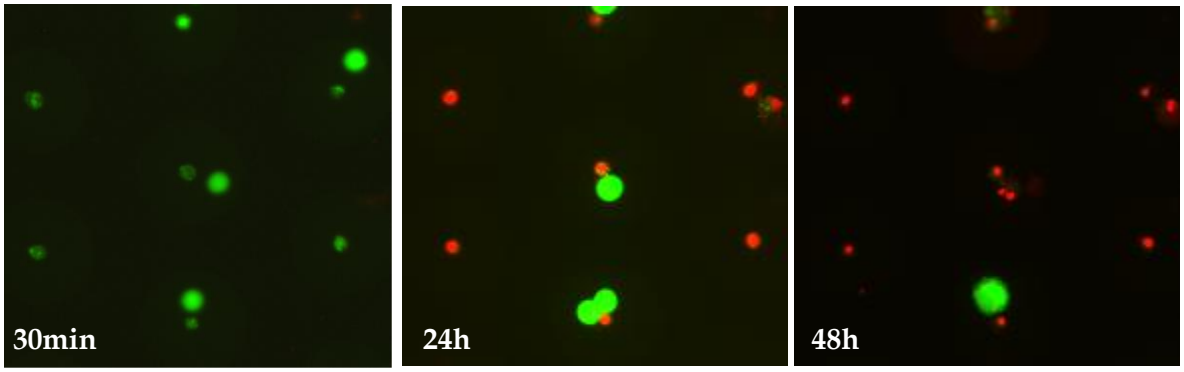


**Figure 3.3:** Images of MCF-7 cells seeded in microfluidic wells and stained at different intervals to determine the viability in microfluidic wells. Fluorescent images show a decrease in cell viability. Red indicates dead cells (EthD1) and green alive cells (Calc AM).

Next we quantified the number of viable and non-viable cells in microfluidic wells. The number of live and dead cells was counted at each time point. Filtration seeding (microfluidic wells) was compared with 2 different methods, flowcytometry and pipette. The bar graph of Fig. 3.4 demonstrates the number of viable cells in microfluidic wells cultured for several days and stained for viability at each time interval. Directly after seeding (0h and 4h), cell viability was similar to control groups (FACS and pipette). The number of viable cells in microwells decreased from >90% viability (at 0h) towards <57 % at day 2. For cells seeded with flowcytometry and pipette this number decreased from 96% to 39% and from 98% to 76% cell viability respectively (Fig. 3.4).

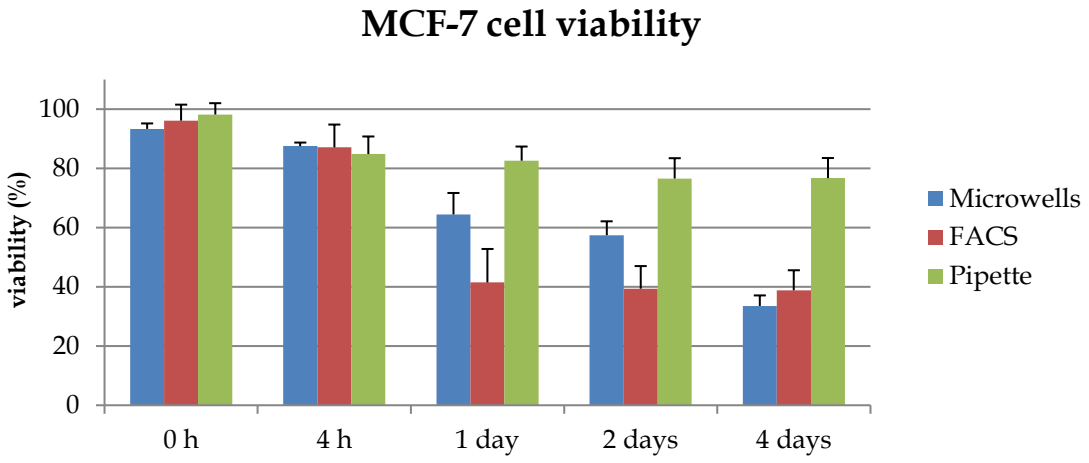

**Figure 3.4:** Bar graph shows viability of MCF-7 cells cultured in microfluidic. Cells cultured in microfluidic wells were compared with 2 different seeding methods (FACS and pipette). For cell viability in microfluidic wells cells were stained and imaged. For control group (FACS and pipette) viable and dead cells were counted directly under fluorescent microscope. From these numbers the percentage viability was calculated and plotted. Data represents mean ± s.d n=2.

For FACS a large decrease in cell viability is seen between 4 hours and day 1. At day 4, cell viability continued to decrease for cells cultured microfluidic wells. However for the control group (FACS and pipette) cell viability remained constant. Overall, cells cultured in microfluidic wells show a linear decrease in viability while for the FACS group cell viability drops instantly at day 1 and does not show a significantly change over time. For the pipette group viability drops slightly but remains constant over time.

# 3.3 Cell growth in microfluidic wells

From the viability experiment we learned that cell viability in microfluidic wells was affected. Nevertheless, in some microfluidic wells cell proliferation was observed. To induce cell proliferation in microwells we chose to culture cells in the presence of BME. Tumor cells lines MCF-7 (breast cancer) and LNCaP (prostate cancer) and primary CRC (colorectal cancer) cells were used as model cells for culture in microfluidic wells. Cell lines were grown with or without BME. In order to establish 3D intestinal tumor organoid in microfluidic wells, CRC cells were grown in the presence of different BME concentration. For each cell type, cell behavior and growth in microfluidic wells was investigated.

## 3.3.1 LNCaP cell morphology and growth efficiency

LNCaP cells were fluorescently labeled with cell tracker orange (CTO) and seeded into microfluidic wells. Bright field images and CTO staining showed that LNCaP cells in BME adhered and spread on SiNi-membranes demonstrating a spindle-like morphology. This cell behavior (spreading) also seen in cells cultured on TCP was not observed in the control group (control). This indicates that the presence of BME induces LNCaP spreading on SiNi-membrane. Furthermore, in some wells lamelli- and filopodia formation could be detected indicating that cells were migrating on the SiNi-membrane surface. Some LNCaP cell showed a spreading morphology spanning over the entire diameter of the well (Fig. 3.5 A and B). Overall cells in the presence of ECM proteins (10% BME) showed a higher amount of cell-spreading and lamellipodia formation when compared to control (medium only).

Next, we attempted to culture cells inside the microfluidic wells by incubating cells in microfluidic wells with culture medium. To determine the growth of cells in microfluidic wells images were taken at different time points. The number of microfluidic wells displaying cell proliferation was counted. Figure 3.6(A-D) shows LNCaP proliferation in microfluidic wells. LNCaP cells cultured in TCP were used as control. Figure 3.6A and B represent cells cultured in the presence of BME and C and D illustrate cells cultured without BME. In Fig. 3.6A we

observe cells at the periphery of the well at day 1. At day 3 the cells proliferated and at day 8 a cluster of cells can be seen. In Fig. 3.6B two cells can be seen, only one cell was able to proliferate. Loss of fluorescent staining of one cell indicated that this cell gave rise to daughter cells (indicated by the loss of CTO fluorescence), while the non-proliferated cells still showed CTO staining at day 8 (green arrow). Furthermore this cell showed a morphology resembling dead cells, with cell shrinkage and a black non-transparent appearance. At day 8 in Fig. 3.6A and B a large cell cluster can be seen. In addition, we observed that cell grew and formed spheroids, indicating that cells assembled into a 3D morphology (day 8, blue arrow). However, we cannot clearly distinguish the number of cells presents at day 8, nuclear staining would provide more information about the number of cells present. For cells grown without BME (Fig. 3.6C and D) a single and a pair of cells is shown at day 1. The cells did not show any growth at day 3. However, culture for more days showed an increase in cell surface. CTO staining was dim and more distributed in the cytoplasm. This characteristic was also seen in microfluidic well with 2 cells (Fig 3.6D). Here, one cell showed appearance of a dead cell with intense CTO fluorescence staining at day 8. The second cell doubled at day 3 and at day 8 a cell cluster is observed (Fig. 3.6D). We further noticed that in some wells cells proliferated in 2 or 3 cells but did not continue to grow to bigger spheroids.

For cells seeded on TCP (control) we clearly distinguish cell growth from a single cell towards a cluster of cells at day 3 and this cluster increased in size (day 8), (Fig. 3.6E and F). For the +BME group, cells displayed a 3D spheroid like morphology with high cell-cell contact. However, LNCaP cells cultured without BME illustrate a spindle-like morphology with less cell-cell contact and high degree of cell spreading.

After 14 days cell were stained with hoechst (nucleic dye) and number of proliferated cells was counted Figure 3.7 demonstrates the growth efficiency from single LNCaP cells cultured in microfluidic wells or in TCP. BME cultures showed a growth efficiency of 9% and 39% for microfluidic well and TCP respectively. In the control group only 6% proliferated in microfluidic wells and 33% for cells cultured in TCP. We expected that BME supplementation would induce cell proliferation in microfluidic wells. Results do show a difference, but growth efficiency is still much lower than cell grown in TCP. Perhaps, the concentration used is too low to observe a significant difference. Furthermore, most of the cells which proliferated did not continue to grow to larger spheroids. Most of the cells in microfluidic wells exhibit morphology of dead cells. Overall, the growth efficiency of LNCaP cell cultured in microfluidic wells is low when compared to cells grown in traditional TCP.

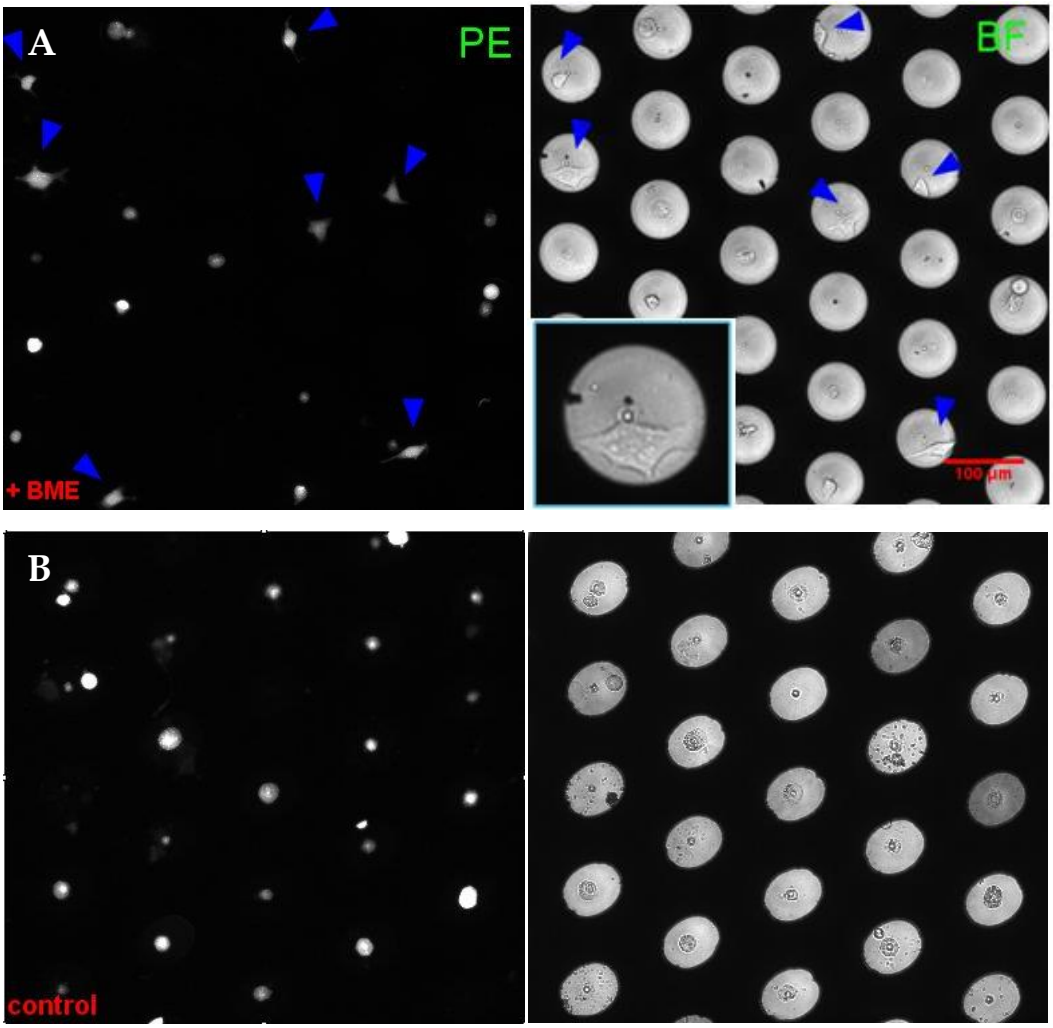


**Figure 3.5:** LNCaP cells were stained with cell tracker orange and seeded in microfluidic wells supplemented with or without 10 % BME. Images represent CTO fluorescence (PE) and bright field (BF). A) LNCaP cells in BME (+BME). B) Cells without BME (control). Cells cultured with BME (A) show a spread spindle like morphology indicative of LNCaP. This behavior is not seen in cells cultured without BME (B). Enlarged image shows a spreading LNCaP cell in the microwell. Bleu arrows indicate spreading cells.

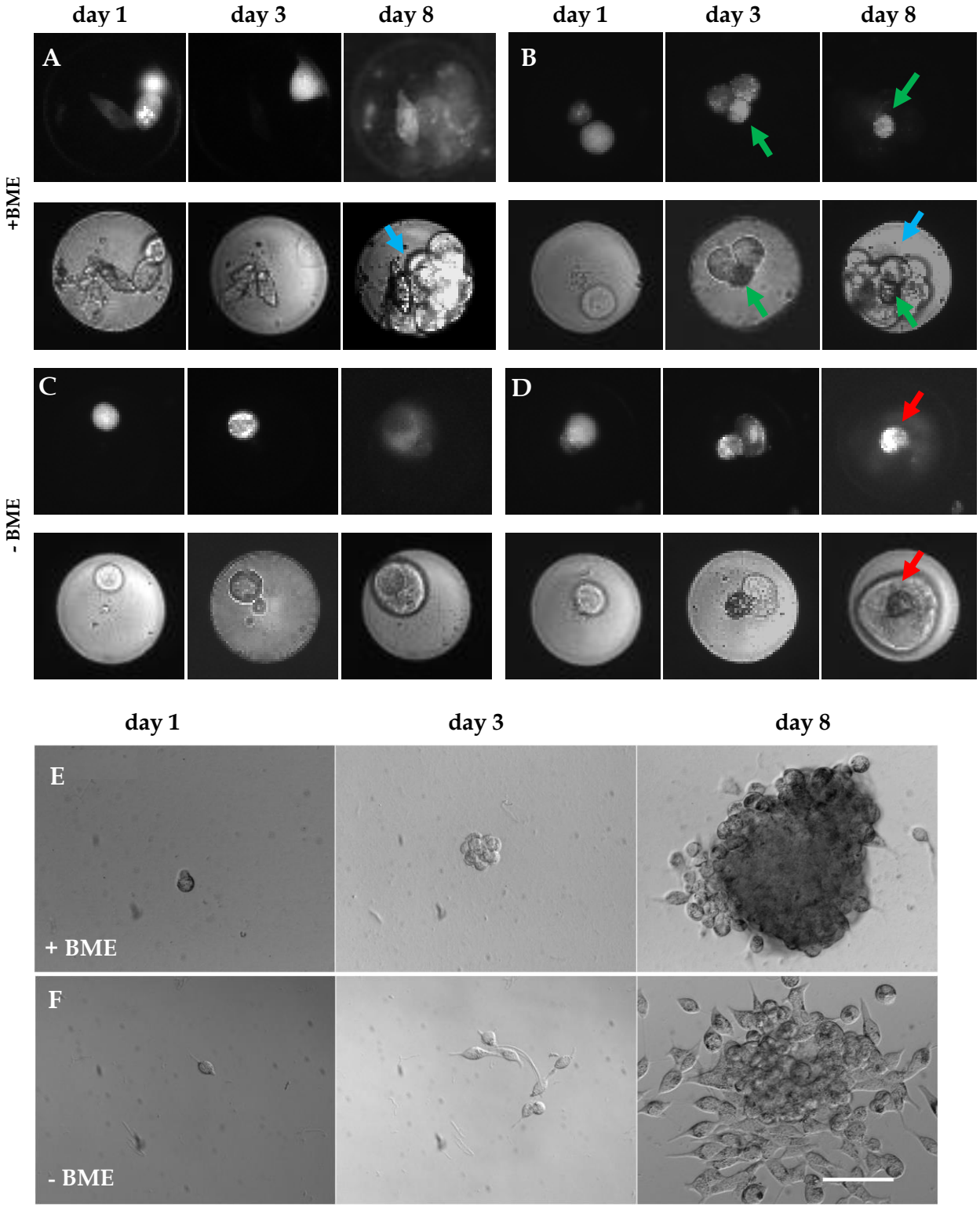


**Figure 3.6:** Fluorescent images (CTO) and bright field images showing LNCaP cell cultured in microfluidic wells or TCP. Cells were cultured in presence (+BME) or without (-BME). A-B) single cell and pair of cells grown in microfluidic wells in the presence of BME. C-D) Cells cultured without BME. E-F) Cells cultured in TCP were used as control. Scale bar: 50 µm.

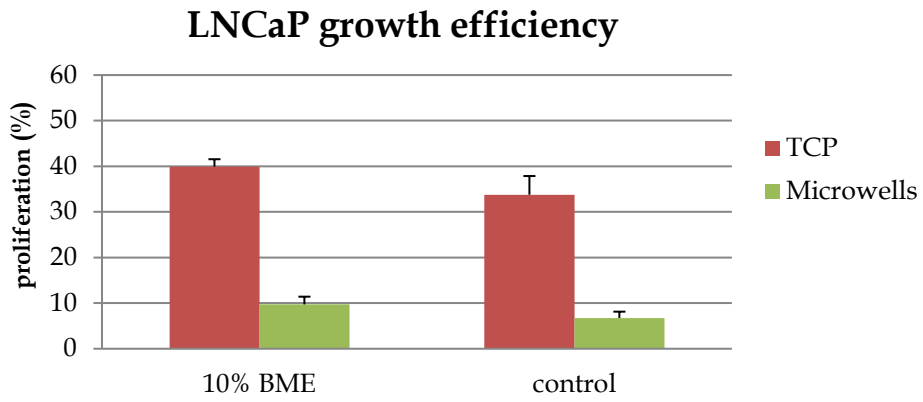


**Figure 3.7:** Bar chart reflects LNCaP growth efficiency in microfluidic wells from single cells. Cells cultured on TCP were used as control for microfluidic well. To induce proliferation, cells were supplemented with or without BME. For the control group a number of 10-15 cells per well was seeded. Data represents mean ± s.d, n=2.

## 3.3.2 MCF-7 cell morphology and growth efficiency

Next we seeded MCF-7 cells in microfluidic wells. MCF-7 cells which under *in vitro* conditions grow in colonies and display cobblestone appearance did not show a change in cell morphology (with or without BME). However, after a few days MCF-7 cells proliferation could be observed. MCF-7 cells in BME formed cell-clusters while cells in medium (-BME) formed a monolayer (Fig. 3.8A). Cells without BME adhered to the glass membrane (SiNi), while cell in BME arranged and acquires spheroid morphology. The majority of cells in both conditions, with our without BME, were located at the periphery of the wells (Fig. 3.8B). MCF-7 adhered to the wall of the microwells (SiO2), due to the higher surface area. Incubation for more days showed that MCF-7 cells assembled in a more 3D morphology (Fig. 3.8C). At this stage cell grew on top of other cells and formed spheroids/aggregates. After 12 days the aggregates/spheroids grew larger and at this time point individual cells could not be determined (Fig. 3.8D).

The potential of MCF-7 to grow from a single cell in microfluidic wells was assessed. MCF-7 cell were fluorescently labeled with CTO and seeded in microfluidic wells with or without BME. Culture of cells in TCP was used a control. Figure 3.9A shows an example of MCF-7 cells proliferating in microfluidic wells with or without BME. At day 1 single cell can be seen. At day 3 MCF-7 cells proliferated into a group of cells (4 cells). Continued culture for 9 day showed an increase in cell number. The formed spheroids/aggregates filled the entire well. Figure 3.9B illustrates typical growth of a single cell cultured in TCP (control). MCF-7 cells in BME formed spheroids which is a typical for BME supplementation, while cells without BME formed monolayers.

Subsequently, we determined MCF-7 growth efficiency in microfluidic wells. Microwells which showed proliferated cells were counted and growth efficiency was calculated for respectively single cells, a pair (2 cells) or a triplet (≥3 cells) (Fig. 3.10). Growth efficiency in

microwells was compared to cells grown in TCP (control). MCF-7 cells in BME show almost 2-fold increase growth efficiency when compared to cell grown without BME (13% vs 7%). However, these numbers are still much lower when compared to MCF-7 cultured in TCP. The growth of MCF-7 cells from 2 or more cells per well demonstrate an increase in growth efficiency when compared to growth from single cells. We found that for BME cultures 34% and 47% of the cells was able to grow in microfluidic wells starting from 2 and ≥3 cells per microfluidic well respectively. For cell without BME 18% and 31% of the cells proliferated starting from 2 and ≥3 cells. For wells with 2 cells growth efficiency almost. This indicates that next to cell-substrate interaction the contribution of cell-cell interaction is an important factor as well. Cell seeded with a pipette and cultured in TCP show higher growth efficiency when compared to microfluidic cultures.

To summarize, MCF-7 cells do proliferated in microwells (with or without BME). Results further indicated that cells could be kept in culture for weeks. BME addition showed to induce MCF-7 cell proliferation. In addition, increasing cell number per well resulted in an increases in growth efficiency.

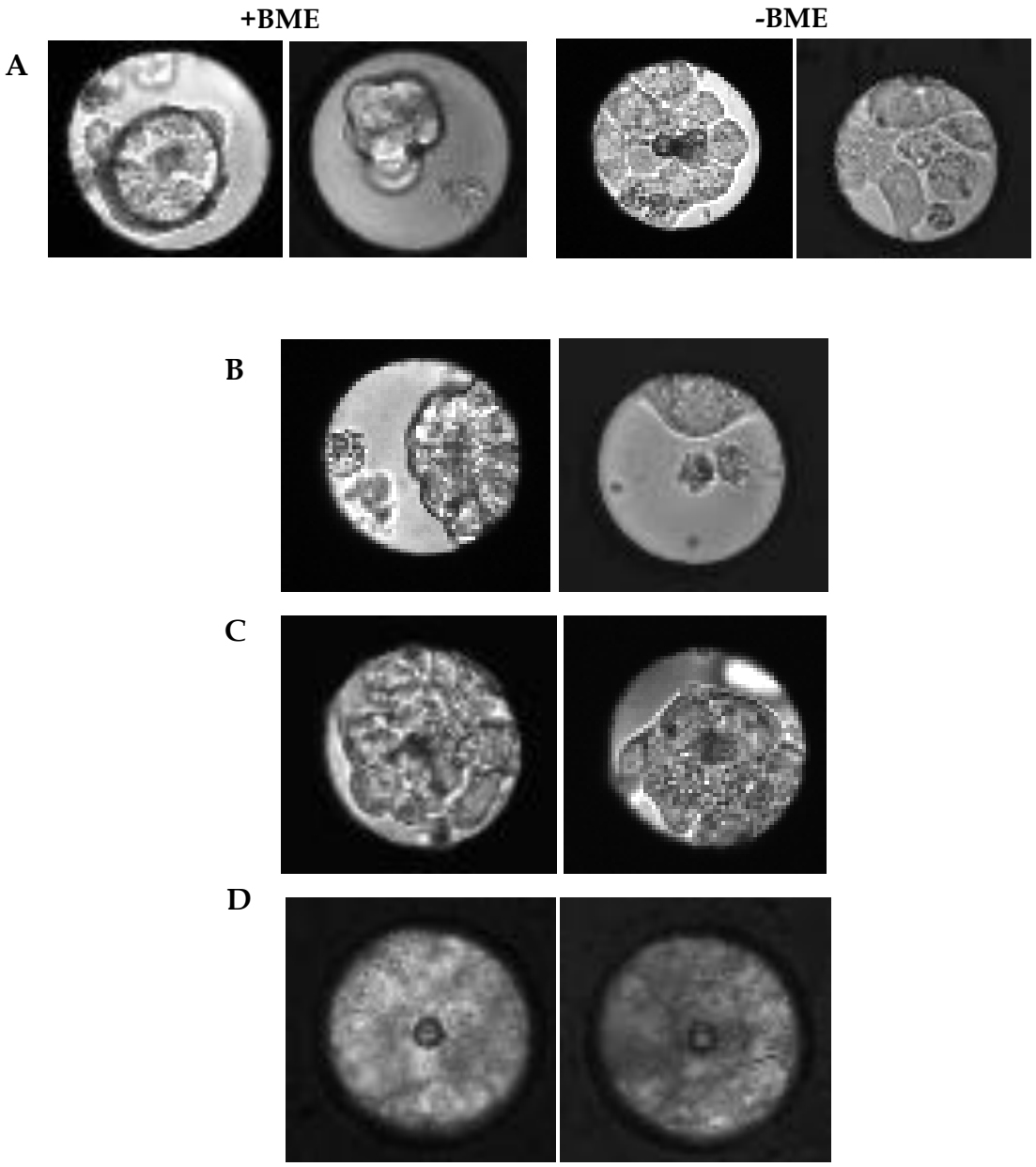


**Figure 3.8:** Bright field images illustrate MCF-7 cell morphology in microfluidic wells. A) MCF-7 cell formed spheroids (+BME) or 2d monolayer (-BME). B) Cells adhered to walls of microwells. C) Cells which were not grown in BME formed aggregates and grew on top of others cells. D) After 12 days culture cell MCF-7 show a non-organized morphology and individual cells could not be identified.

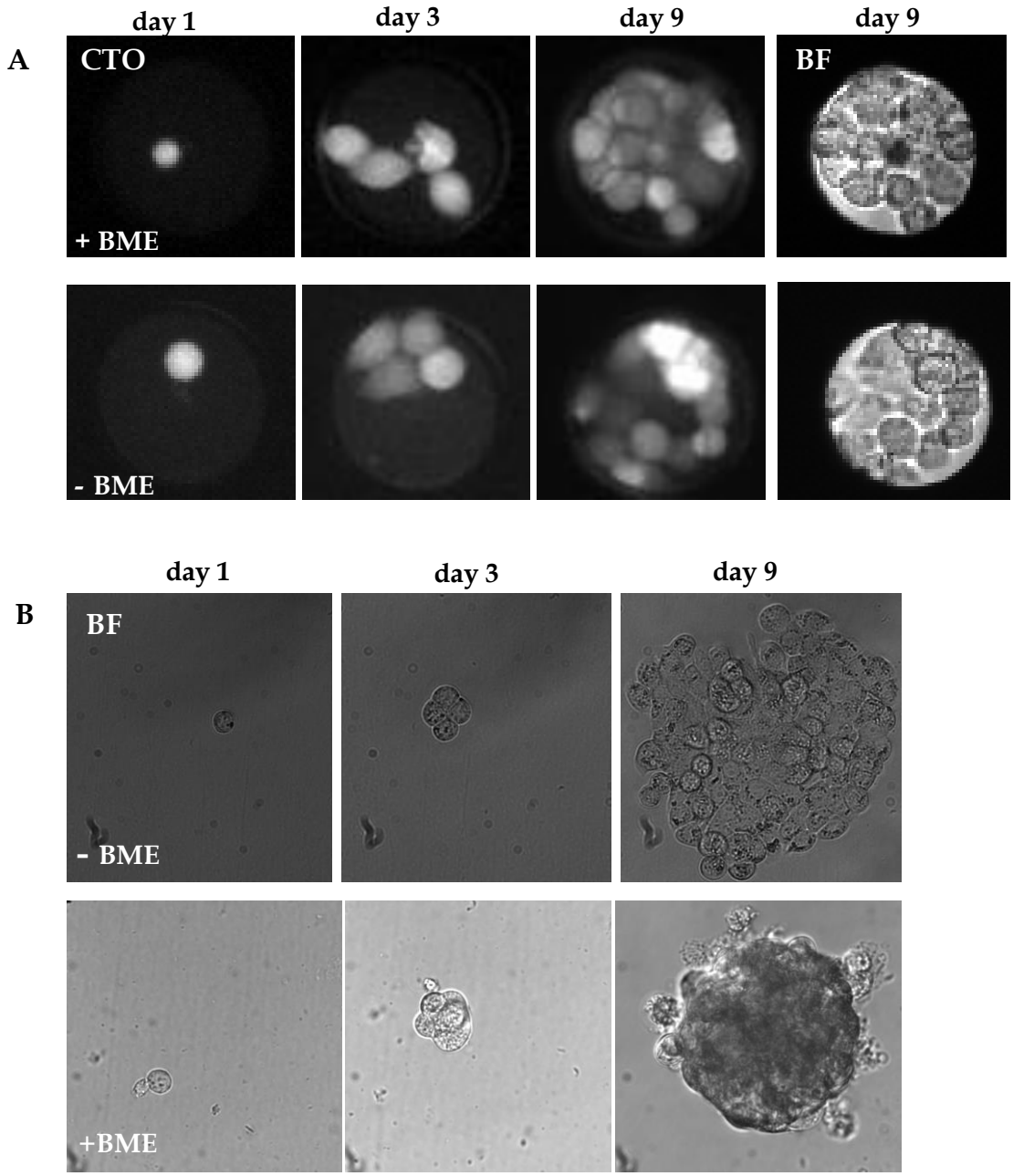


**Figure 3.9**: Cell proliferation from single MCF-7 cells. Cells were labeled with cell tracker orange (CTO) and seeded in microfluidic wells with or without 10% BME. Cells cultured in TCP were used as control. A) Growth of single MCF-7 cells in microwells with (+BME) and without (-BME) is shown. B) The growth of single MCF-7 in TCP is illustrated (BF, bright field images. Cell without BME formed a monolayer (-BME) and cells in BME grew in an aggregated 3D morphology (spheroids, +BME).

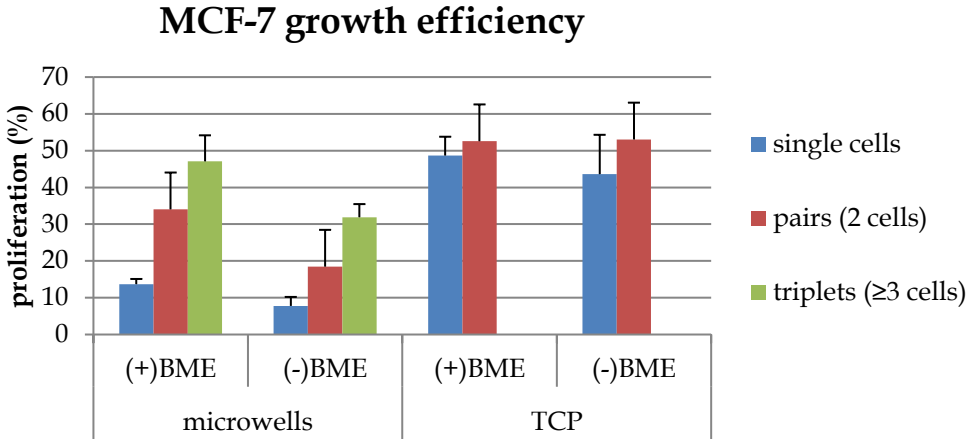


**Figure 3.10:** Growth efficiency in microfluidic wells or TCP (control) from 1, 2 or ≥3 was quantified. Cells were cultured with or without 10% BME. Cell cultured in microfluidic wells with BME show an increase in cell proliferation compared to microfluidic wells without BME. Data represents mean ± s.d, n=2.

# 3.4 Organoid culture

Next, results obtained from cell line culture (experiments) were used to grow organoids from CRC cells. Traditionally, for the generation of organoid, cells are suspended in 100% BME which provides a 3D micro-environment and enables cells to grow and form organoid structures. We choose to culture CRC cells in 0%, 2%, 10% and 20%. Cells were mixed with different BME concentrations and seeded in microfluidic wells. Culture medium supplemented with EGF, noggin, R-spondin1 and Rho kinase inhibitor Y-27632 was added and cells were cultured in microfluidic wells. Images were taken at different time points to track organoid growth and development. Images at day 1 in Fig. 3.11 show CRC cells cultured in microfluidic wells. For all investigated conditions CRC cells formed intestinal tumor organoids within 3 days. With 3 more days of culture, the organoids developed a specific morphology. While organoids were growing in size cells arranged into a spherical conformation and this morphology was stable up to 10 days of cultivation. Figure 3.11 demonstrates organoid formation in microwells from single CRC cells. Directly after seeding, single cells displayed dim GFP signal. During organoid growth, GFP signal increased indicating an increase in cell number and subsequent organoids development. Matching bright field images show the increase in organoids size in time (Fig 3.11). GFP expression showed that cells arranged in a nested pattern, with highly active cells at the periphery. Quantification of organoid size at day 9, showed that majority of organoids had an average diameter between 50 and 60 µm and occupied the complete microwell surface area. Hence, culture for 3 more days resulted in the outgrowth from the microfluidic well onto the supporting area of the microfluidic wells.

Organoid development of non-tumorigenic cells is characterized by a proliferative stage where single cells grow into multicellular clusters. Subsequently, the outer layer of cells becomes polarized to the basement membrane and cell growth is arrested. However, because CRC cells are tumorigenic, growth was not arrested which resulted in cell outgrowth from microwells. Organoids cultured in 20% BME grew fast and displayed the highest amount of

outgrowing cells. These organoids kept expanding in size and merged with organoids from neighboring wells and formed large organoid aggregates on the chip (Fig. 3.12). Focusing on the morphology, the established organoids exhibit morphology similar to cells cultured in TCP (100%) BME (Fig. 3.13A and B).

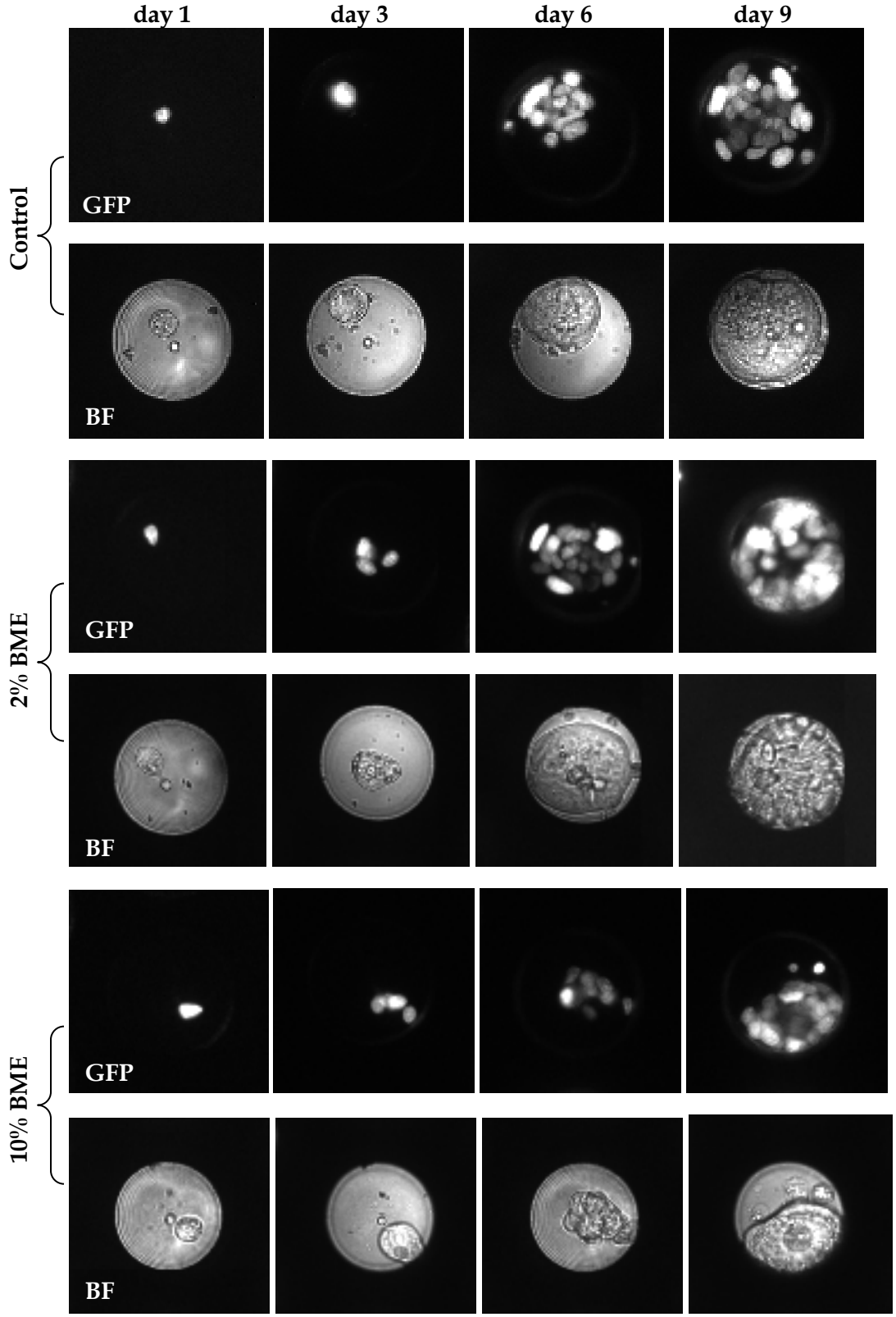

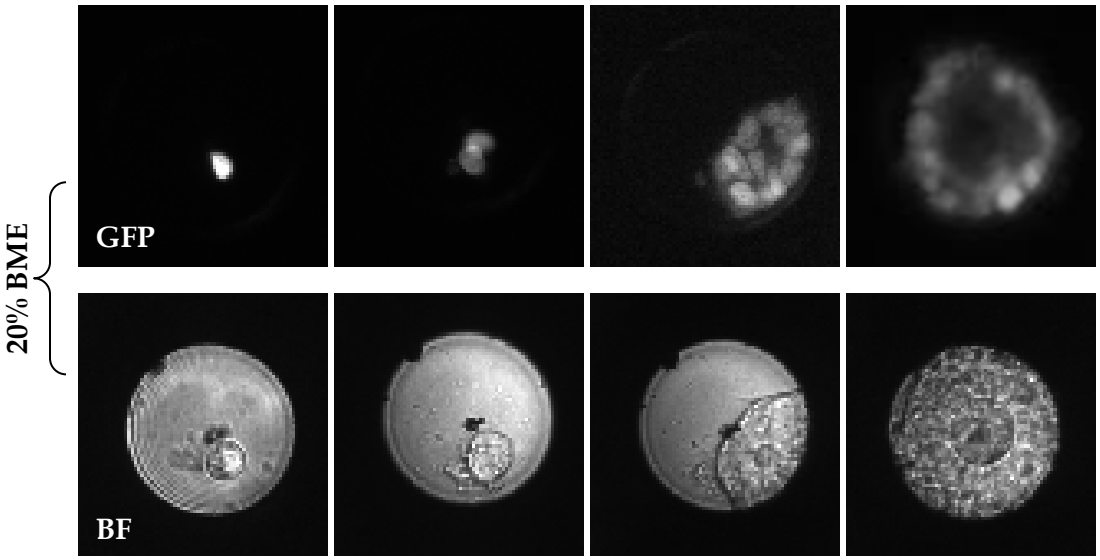


**Figure 3.11**: Typical images representing organoids growth in microfluidic wells established from a single cells. CRC cells were grown in different BME concentration and cultured in microfluidic wells. Fluorescence images of GFP expression in the nucleus and bright field demonstrates the development of organized structures with a spherical geometry growing in 3D. Round-shaped organoids with concentric cell arrangement were generated in all conditions.

Focusing on organoid morphology, a lumen formed *de novo* and expanded within the cell aggregates starting on day 6 (Fig. 3.13A, red arrows) and its morphology closely resembled that of CRC organoid cultured in TCP (compare Fig. 3.13A and B). Close inspection of the spheroids revealed 3 forms on day 6: spheroids lacking a lumen (Fig. 3.13C), spheroids featuring a developing lumen, and spheroids containing a fully formed lumen (up to 41 µm in diameter); these presumably reflect distinct stages of the development of cell aggregates into organoids. Perhaps the lumen formed as a result of apoptosis and clearance of inner cells. Organoid absent of a lumen were mainly found in cultures without BME. In addition, cells grown without BME displayed a spread grape-like morphology, which was not displayed by CRC cells supplemented with BME. Nevertheless, the majority of generated organoids in the control group displayed similar morphology to organoids generated with BME and followed the same developmental process. Subsequent culture of organoids for more days revealed the disappearance of the lumen and the outgrowth of cells from the microfluidic wells (Fig. 3.13A, at day 14). These results indicate that organoids can be established in microwells with or without the use of BME.

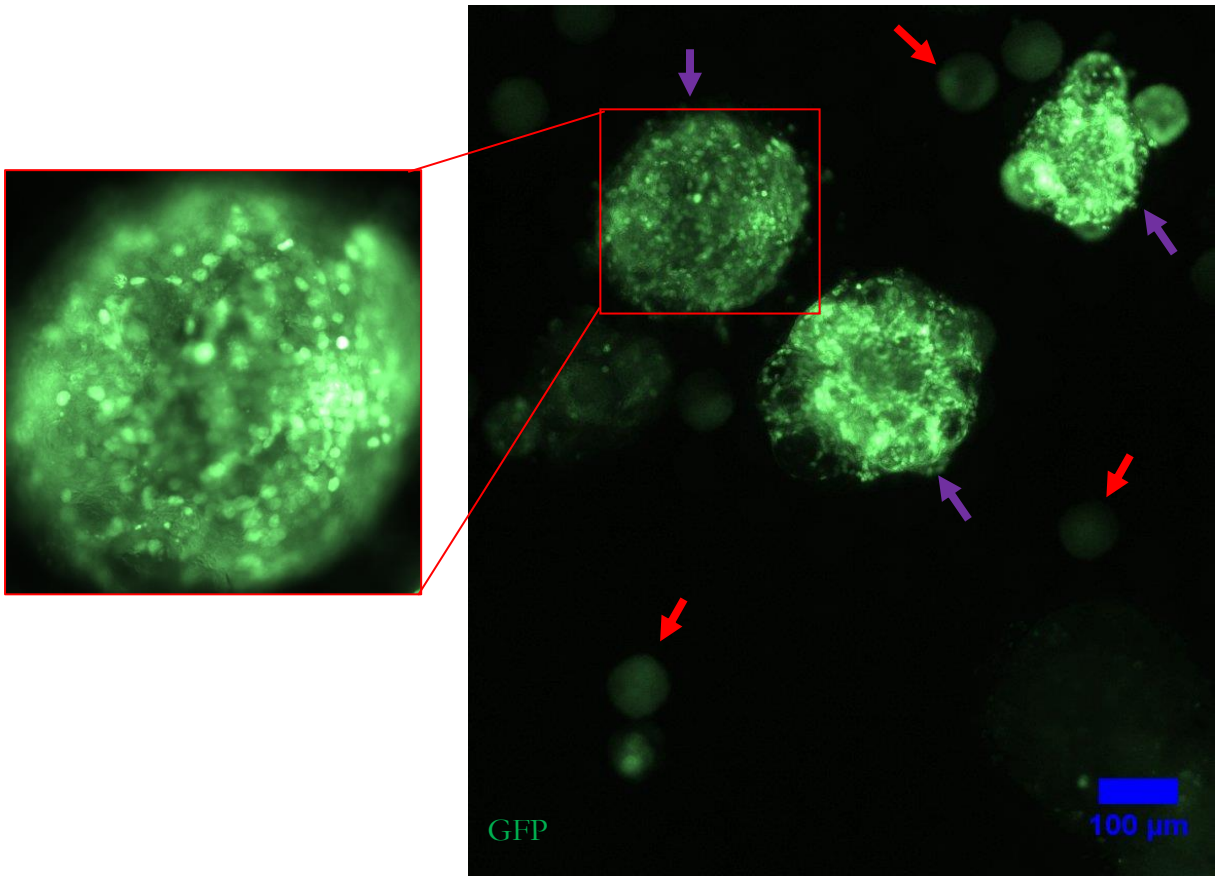


**Figure 3.12:** The outgrowth of CRC organoids from microwells is shown. Image was taken from the top of the microfluidic wells. Red arrows depict individual microwells with CRC organoids and purple arrows indicate the outgrowth and merging of organoids from different microwells and growing on top of multiple wells.

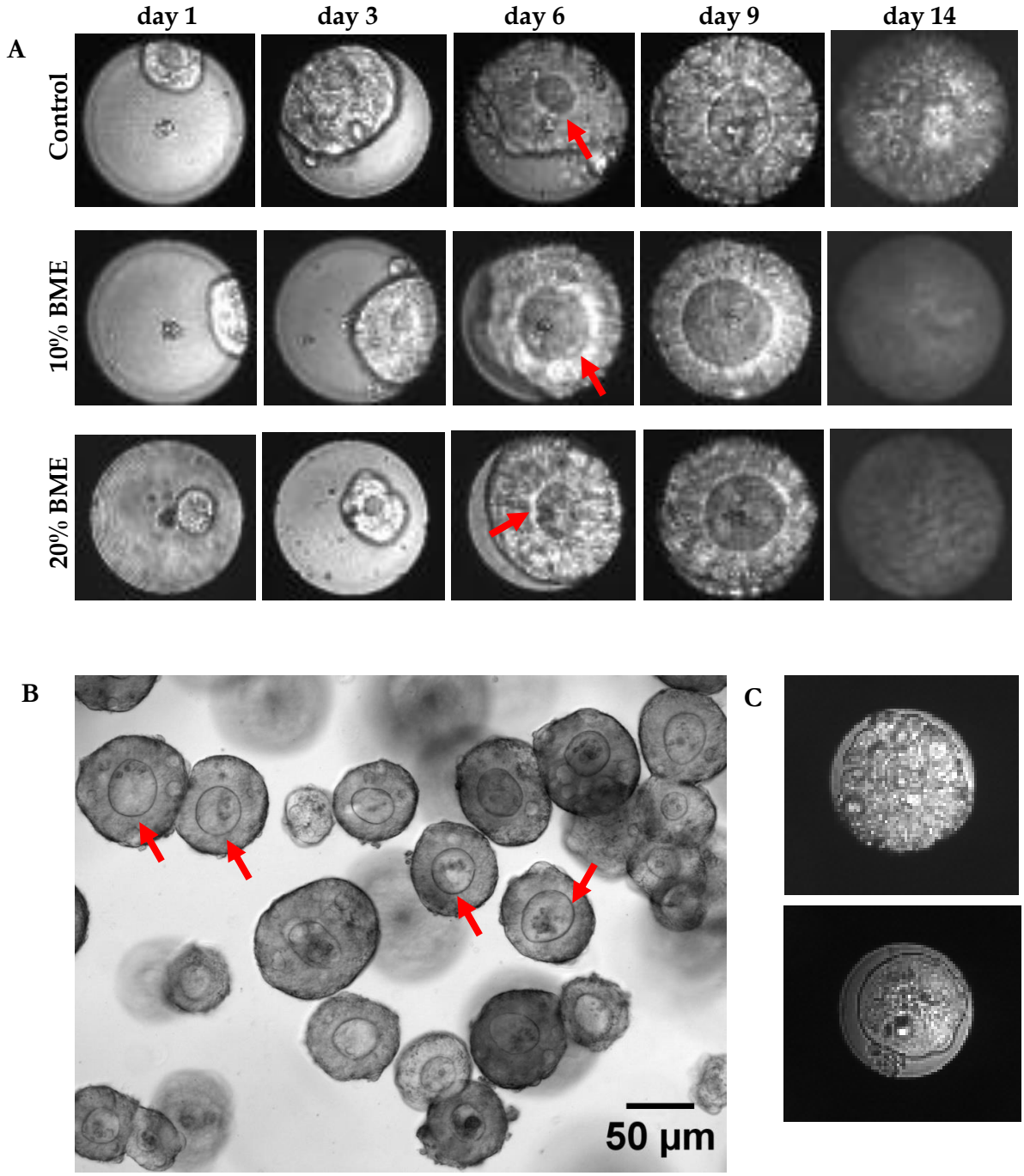


**Figure 3.13:** A): Bright field images illustrate organoid development and morphology in microfluidic wells. B) Organoids grown in BME in TCP. C) Typical bright field images showing morphology of organoids without the presence of lumen and was mainly found in cultures absent of BME.

We further determined CRC cell growth efficiency in microfluidic wells from single cells, a pair of cells (2 cells) or triplets (≥ 3 cells). CRC cells which proliferated and developed into spherical organoids were determined. From the GFP expression in the cell nucleus and bright field images at different time points organoids were counted and growth efficiency after 14 days was calculated. Graph in Fig 3.14 shows organoid growth efficiency with respect to BME concentration in microwells.

Apart from the effect on organoid morphology BME also has an inducing effect on organoid growth efficiency. For the control group only 10% of the single cells were able to grow and generate organoids. An increase in growth efficiency was observed for organoids cultured in

the presence of BME. The highest efficiency was found for cells grown in 20% BME. At this BME concentration, 28% of the single cells proliferated and generated organoids. For 2% and 10% BME the growth efficiencies were 13% and 20% respectively. Single CRC cells grown without BME displayed the lowest growth efficiency (Fig. 3.14, control). For microwells with pairs (2 cells per well) or triplets (≥ 3 cells per well) growth efficiency increased significantly when compared to growth from single cells. This was seen in all conditions with or without BME addition. However, cultures in 20% BME showed by far the highest percentage of organoid formation from pairs and triplets (65% and 80% respectively).

Overall, results reveal that intestinal organoids can be grown inside microfluidic wells from single cells with or without the addition of BME. Moreover, the generated organoids could be maintained in culture for weeks and show similar characteristic morphology to organoids generated in TCP.

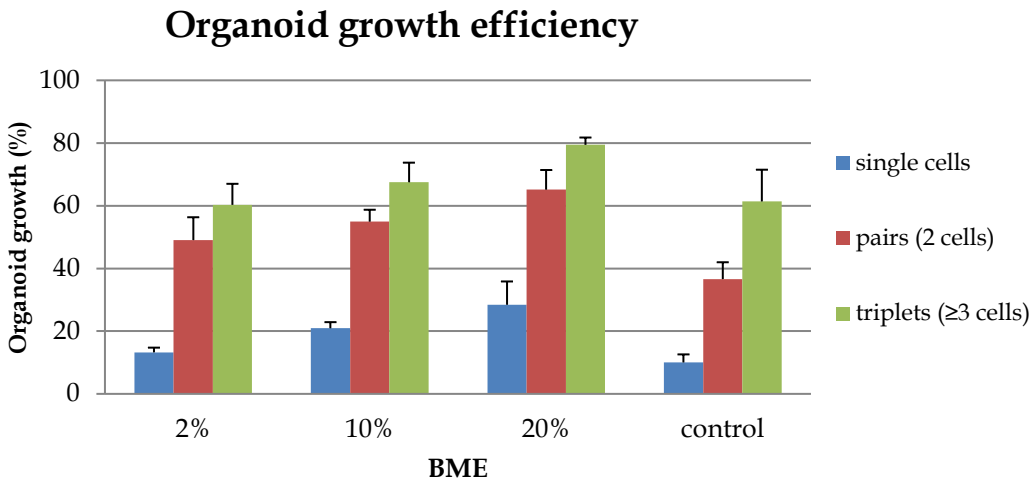


**Figure 3.14**: Organoid growth efficiency in microfluidic wells. CRC cells were cultured in microfluidic wells with or without BME. Total number of generated organoids was determined after 14 days. Number of grown cells is plotted against BME concentration. Each value represents the mean ± s.d, n=2.

## 3.4.1 Organoid recovery

Having established organoids in microfluidic wells from primary CRC cells, we investigated whether we could retrieve the established organoids from the microfluidic wells. On day 14, organoids were harvested from microfluidic wells for further growth in 96 wells-plates. Wells-plate was coated with BME type 2 and organoids were punched out from microfluidic wells directly into wells of a 96 wells-plate. Punched organoids settled down by gravitation. Small and large organoids which filled the complete microfluidic well (Fig. 3.15A) were punched. Organoid recovery efficiencies were ~47% for large organoids and ~80% for small organoids. Large organoids were not retrieved intact, but mainly as scattered and spilled cells. This indicates that organoids grew too large for efficient punching. In addition, organoids adhered to walls of microfluidic wells, hereby challenging the proper punching and recovery of organoids. Smaller organoids which did not attached to the walls of the microfluidic wells were found back more often as a whole and intact with less spilled cells (Fig. 3.15B). Punched organoids were recovered attached or detached from the SiNi-membrane and cells still expressed GFP fluorescence (Fig. 3.15B).

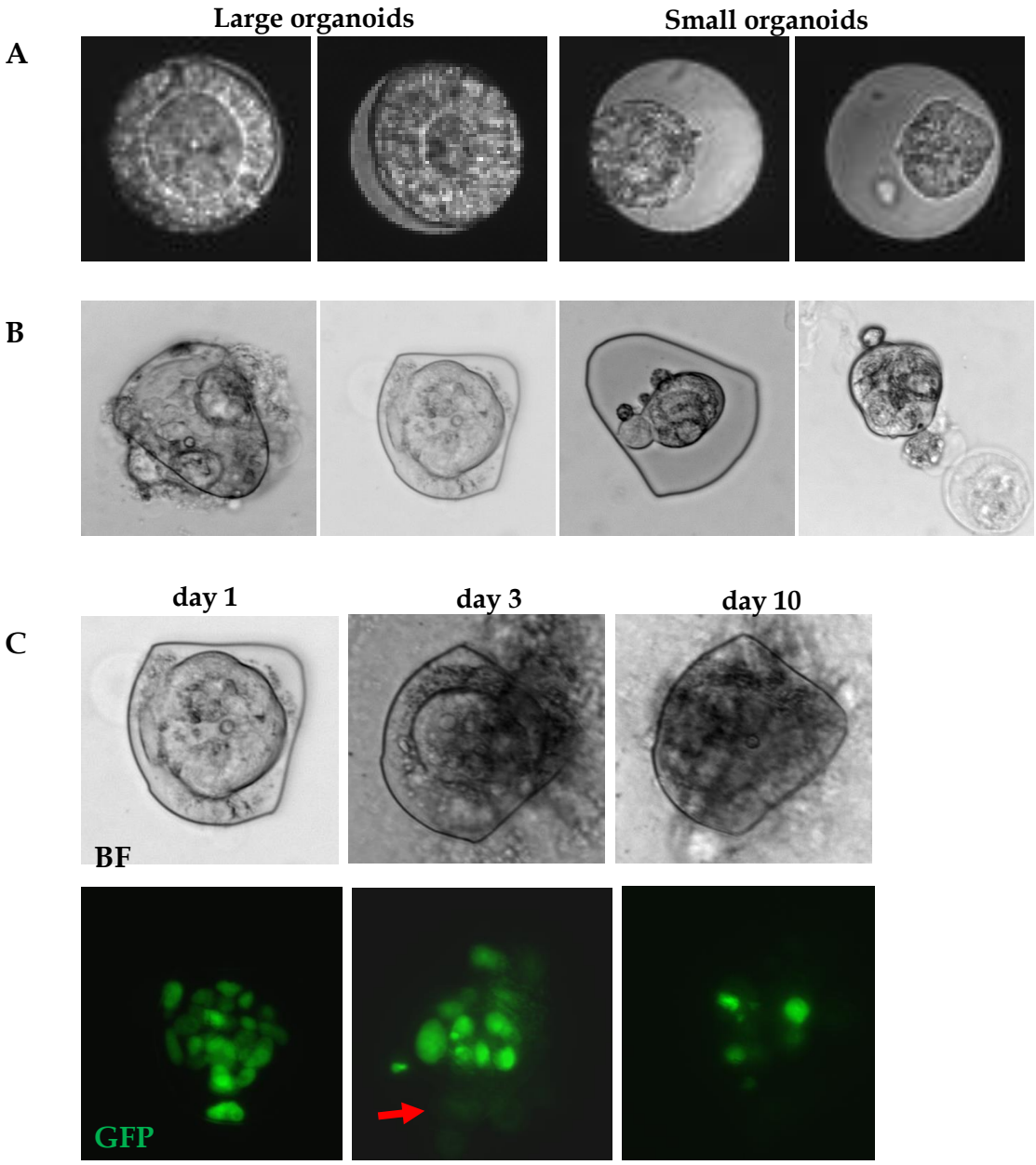


**Figure 3.15:** Organoids punched from microfluidic wells: Organoids were established in microfluidic wells from CRC cells. A) After 14 days culture large and small organoids were punched out from microfluidic wells. B) Represents punched organoids in 96 wells-plate loose or adherent to SiNi-membrane. C) Example of a punched and growing organoid, top panel shows bright field images (BF) and lower panel GFP expression at 1, 3, and 10 days culture of the same organoid. Red arrows indicated the invasion CRC cells into BME layer. SiNi-membrane size ~70 µm.

Recovered organoids were incubated and growth was monitored. Out of 30 punched CRC organoids only 4 showed modest cell growth (Fig. 3.15C). Most of the punched organoids lost GFP expression at day 3 and did not invade in the BME layer. Organoids which did invade in the BME layer (Fig. 3.15C, red arrows at day 3) showed a non-spherical morphology and GFP expression was dim. None of the punched organoids grew towards larger proportions. This could indicate that culture for 14 days before punching resulted in cellular stress and cell death. Although organoid expressed GFP, we did not determine whether the organoids were really viable before recovery from the microfluidic wells and after punching.

# 3.5 Live cell punching

## 3.5.1 Single cell culture

From previous experiments, it was shown that cells could be cultured in microfluidic wells. Cell lines and primary cells were able to proliferate in microfluidic wells from a single cell. Subsequently, the generated cultures could be easily recovered from the microfluidic wells. However, we could not culture the cells after retrieval. Therefore, we investigated whether we could establish cultures from a single cell after recovery from microfluidic wells. We used 2 methods; the first method exploits the microfluidic wells as a cell sorters followed by direct punching of single cells for culture in wells-plate (Fig. 4.1A);. For the second strategy microfluidic wells were as a tool for single cell isolation and cell culture inside the microwells for 2 days followed by recovery of the generated colonies from microfluidic wells for subsequent culture in a culture plate (Fig. 4.1B).

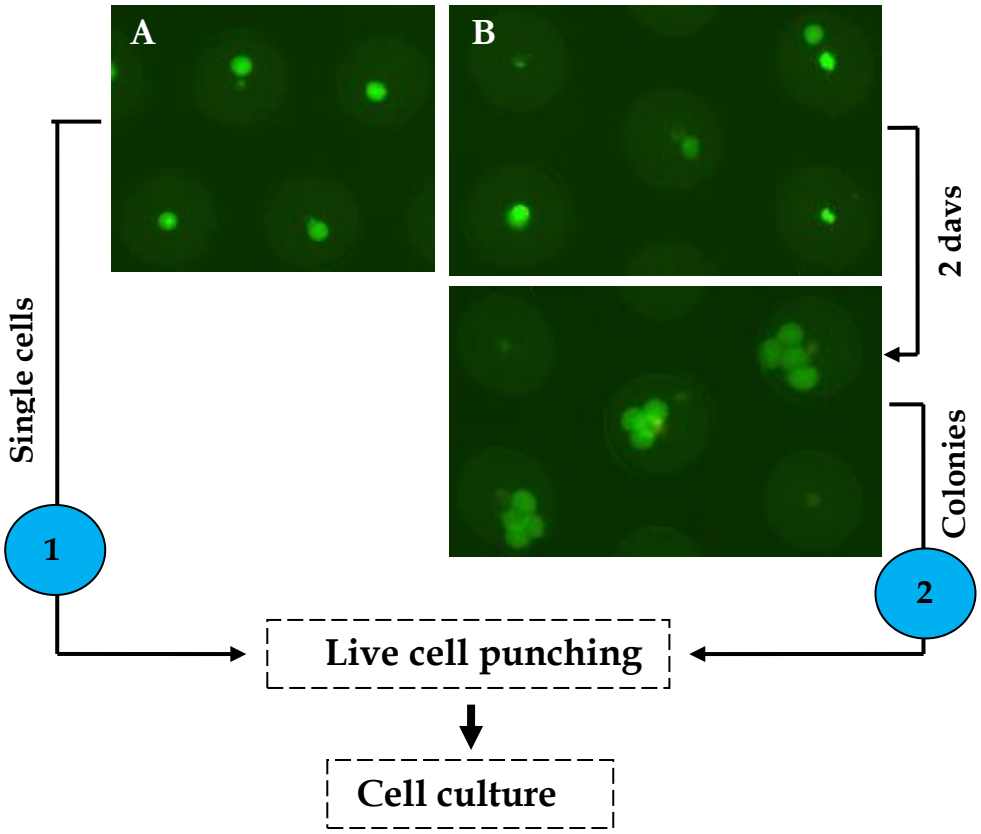


**Figure 4.1:** Scheme illustrated the methods used for live cells punching. A) Cells were seeded in microfluidic wells and viable single cells were punched directly from microfluidic wells (1). B) Single cells were cultured inside microfluidic wells. After 2 days cells were stained for viability, colonies generated from single cells were punched out and cultured in 96 wells-plate (2).

MCF-7 cells were stained for viability with Calc AM and EthD1 and seeded in microfluidic wells. Figure 4.2A shows a typical image of MCF-7 in microwells after staining for viability. Counting total number of Calcein positive cells showed that majority of the cells was viable (~95%). Subsequently, punched single viable cells from microfluidic wells into a TCP and cells were cultured. Next, the same microfluidic chip was incubated to allow cells to grow inside

the microfluidic wells. Cultivation for 2 days demonstrated the growth of colonies composed of 3 to 6 cells. Viability assay after 2 days culture indicated that cells were still viable inside the microfluidic wells. Furthermore MCF-7 cell adhesion at the periphery of the wells was observed (Fig. 4.2B). After 2 days culture inside the microfluidic wells, colonies established from a single cell were punched out and recovered in TCP.

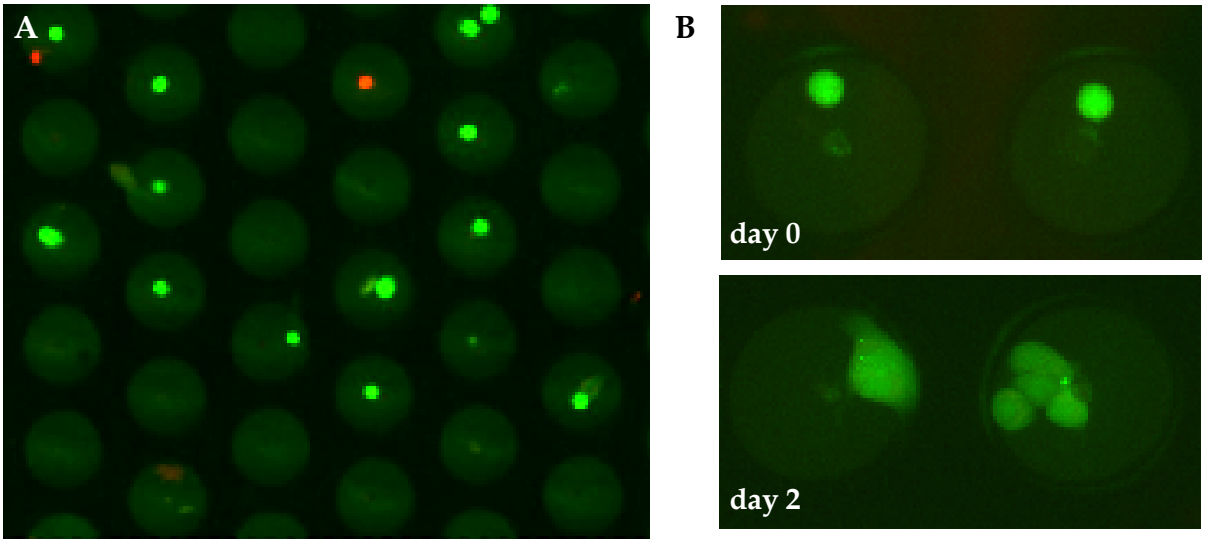


**Figure 4.2:** A) MCF-7 cells stained and seeded in microfluidic wells. Calcein AM staining indicates that most cells were viable. B) Single cells grown inside microfluidic wells for 2 days. Green fluorescence indicates alive cells. (Calc AM); red for dead cells (EthD1).

## 3.5.2 Punching efficiency and viability

Subsequently we determined the cell recovery efficiency. Single cells and cell colonies were punched from the microfluidic wells and the number of punched and recovered cells was counted. In total more than 80 SiNi-membranes with single cells and 78 SiNi-membranes with colonies were punched out. SiNi bottoms that were not detectable after punching were counted as a successful punch. Figure 4.3 displays cell recovery after. Single cells demonstrated a recovery efficiency of 92%, while cell colonies show a recovery efficiency of 76%. An explanation for this difference in recovery efficiency between single cells and colonies is due to fact that most colonies were located at the periphery of the wells or adhered to the wall of the wells, which challenges punching. Furthermore, the recovery efficiency of punched MCF7 colonies is almost similar to the punched small organoids. Majority of punched single cells were recovered off the SiNi-membrane, while colonies were still attached to the SiNi-membrane.

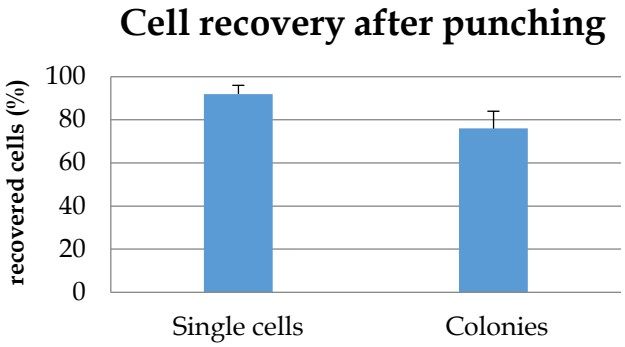


**Figure: 4.3:** Cell recovery after punching; Number of cell recovered in the wells-plate was determined and recovery efficiency was calculated. Data represents mean± s.d. (n=3).

Next, we assessed if punching cell from microwells affect cell viability. Punched cells were incubated for 4 hours to allow cells to adhere to the culture plate. Subsequently, cells were stained for viability (Fig. 4.4A). Number of alive and dead cells was counted and cell viability was determined (Fig. 4.4B). For comparison to cell punching, cell were also sorted by FACS or pipette. Highest amount of alive cells were found for FACS (96%) followed by punching (79%) and pipette (78%). Punched cells were then incubated to determine if cells could proliferate after punching. Cells were cultured and cell proliferation from single cell or colony was monitored.

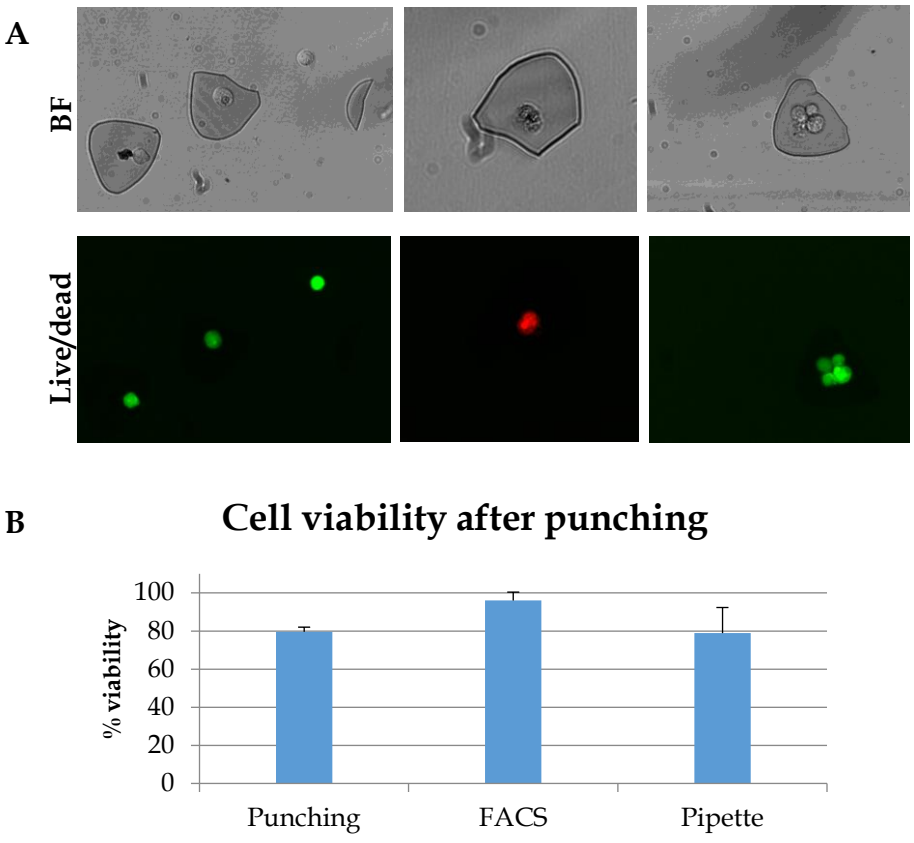


**Figure: 4.4:** A) Typical images of single cells or cell colonies punched from microfluidic and recovered into a wells-plate. After 4 hours cells were stained and number of viable cell was determined. Top panel depicts bright field images and lower panel fluorescent images with (green, alive cells) or EthD1 (red, dead cells. B) Quantification of cell viability for punched, FACS and pipette cells. Data represents mean± s.d, n=2.

## 3.5.3 Growth efficiency after punching

Single cells or colonies, established inside microwells proliferated after punching. Fluorescent image in Fig. 4.5A at day 0 (the top left corner) depicts a typical image of a single cell before punching in a microwell. The bright field image at day 0 represents the same cell directly after punching. Bright field images at day 2 and day 8 depict the growth after punching. Fluorescent image at day 8 indicates that most cells were viable. In addition Fig. 4.6A shows the growth of a single cell in a microfluidic well. Next, cells are punched out, recovered and cultured (Fig. 4.6B). Day 0 represents cells after punching from the microfluidic well. At day 2 cells proliferate and form larger colonies (mammospheres). Incubation for more days (day 2 to day 8) resulted in further increase in cell numbers. Staining for viability at day 8 provided evidence that most cells in the generated colonies were viable.

To assess the growth efficiency after punching, the total number of single cells and colonies which formed mammospheres was determined for the 3 cell sorting methods (Fig. 4.7A). Punching resulted in 80% cell growth from single cells. A decrease in growth efficiency is found for FACS (42%) and pipette (69%). Punched colonies showed lower growth efficiency compared to single cells, 67% and 80%, for colonies and single cells respectively. For the pipette group no difference is observed between single cells and colonies (Figure 4.7A).

In general punched colonies were still attached to SiNi-membrane. Recovered colonies which were not able to escape (push the membrane upwards or migrate out) from the SiNi-membrane did not form mammospheres. Perhaps the ability to detach from SiNi-membrane, followed by adhesion to TCP and subsequent migration from underneath the membrane is an important factor determining the potential to initiate cell proliferation (Fig. 4.7B). In contrast, single cells were mainly found loose from the membrane after punching, which could explain the difference in growth efficiency between single cells and cell colonies.

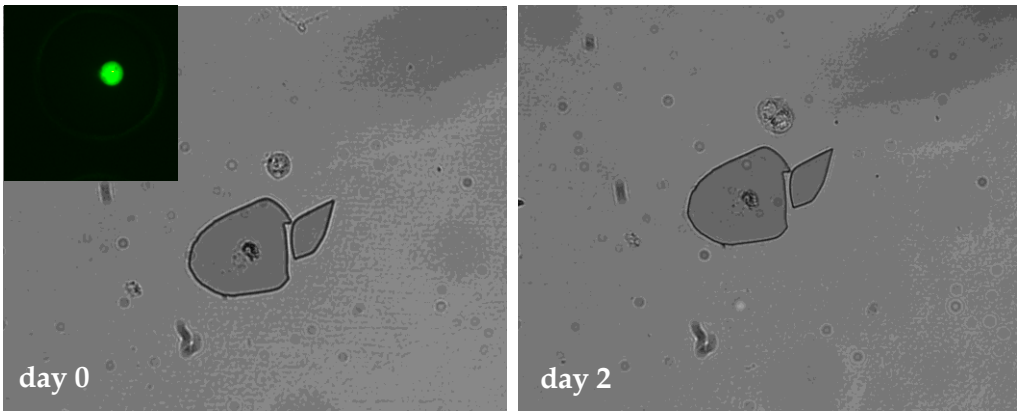

A

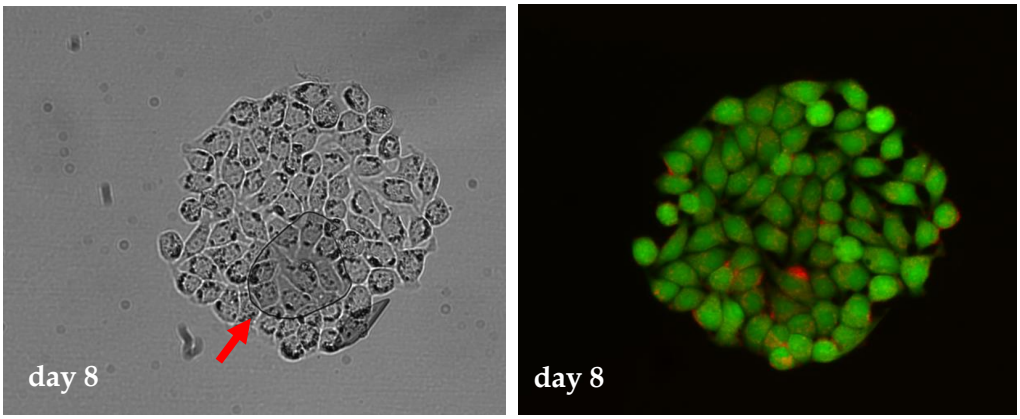


**Figure 4.5** Series images show the growth of a single MCF-7 cells after punching out from the microfluidic wells. Fluorescent image at the left top image show the single cells residing in a microwell stained with Calc AM (before punching). Image at day 0 represents the cell directly after punching. Fluorescent image at day 8 shows that cells are viable. Calc AM green (alive) and EthD1 red (dead) fluorescence. Red arrow depicts SiNi-membrane on top off the monolayer, size membrane ~70µm.

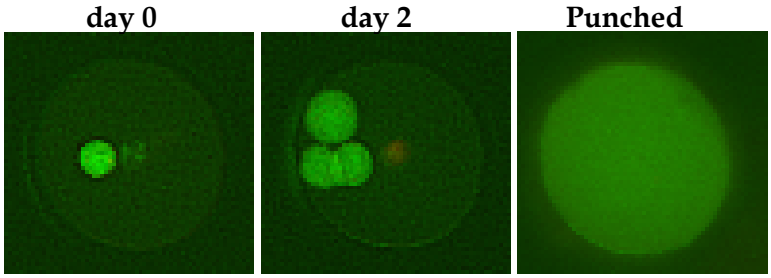


B

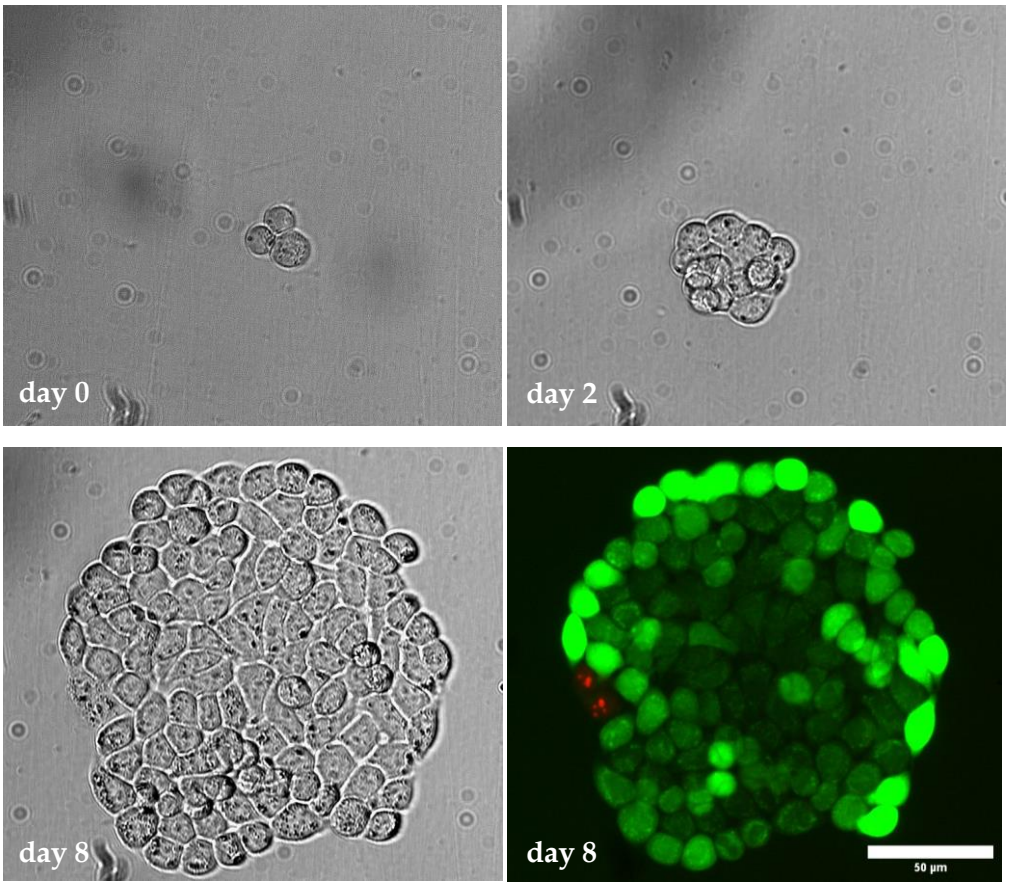


**Figure 4.6**: Typical example of punching and culture of a colony MCF-7. Single cell grown in a microfluidic well cultured for 2 day. Subsequently the established colony is punched out from the microwell and cultured in TCP. A) Represents the growth of the cell in the microfluidic well and punching. B): illustrates the growth of the punched colony in time.ies. Staining with Calc AM/EthD1 at 8 day, indicates that majority of cells were viable. Scale bar 50 µm.

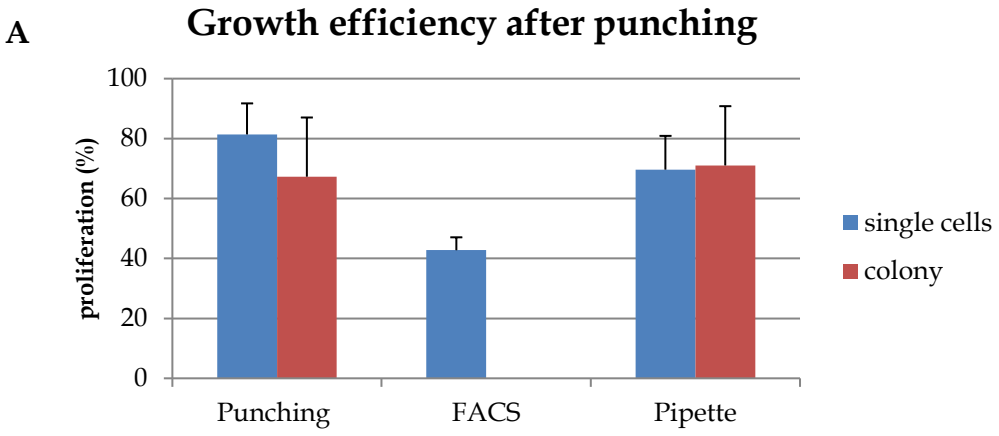


**Figure 4.7**: A) Growth of single cell and colonies after sorting. Number of cells forming colonies (3-5 cells) after 14 days culture is quantified. For FACS only growth from single cells is shown. B) Escape from SiNi-membrane: MCF-7 cells punched from microfluidic well and recovered in TCP. Red arrow shows proliferating cells which probably detached from SiNi-membrane. Data represents mean ± s.d. (n=2). Scale bar 50 µm.

# 3.6 Spiking and punching

## 3.6.1 Cell viability and growth in microfluidic wells

To further determine whether we could use the model (workflow) described in Fig. 4.1 for the isolation and recovery of CTCs, we performed an *in vitro* study and MCF-7 was used as model CTCs. A number of 1500 MCF-7 cells was pre-labeled and spiked in 1 mL of whole EDTA-blood. MCF-7 cells were enriched by depleting hematopoietic cells. A tetrameric antibody complex was used to target CD45+ cells. Subsequently, buoyant density medium was used to pellet unwanted cells. Enriched MCF-7 cell fraction was stained for viability, epithelial marker (anti-EpCAM) and CD45 (WBCs) (Fig. 4.8). Subsequently, the isolated cell fraction was seeded in microfluidic wells. Next, similar to previous experiment cells were either punched directly

or first cultured for 2 days inside microfluidic wells followed by punching of established colonies.

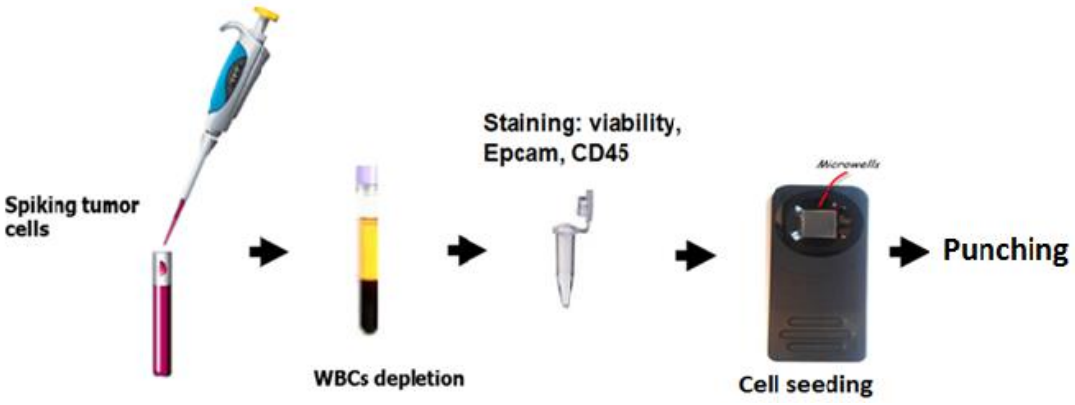


**Figure 4.8**: Scheme showing workflow used for spiking and isolation of MCF-7 cells for live cell punching. MCF-7 cells were spiked in blood. Rosettesep antibody cocktail was used to deplete cells from non-epithelial origin. Isolated epithelial cells were stained and seeded in microfluidic wells. Viable single cells or colonies were punched out.

We found that 53% of the spiked tumor cells were recovered and majority was viable (Fig. 4.9A). Furthermore, MCF-7 cells could be identified based on the fact that they were positive for anti-EpCAM, indicating that these cells were of epithelial origin and true MCF-7 (Fig. 4.9B). Live-dead assay showed a cell viability of ~95%, based on Calc. AM and EthD1 fluorescence. Isolated MCF-7 cells were incubated and cultured inside microfluidic wells. Figure 4.10A demonstrates the growth of single MCF-7 cells in microwells (numbered 1, 2 and 3). Cell proliferation in microwells further confirmed that cells were viable and able to initiate growth. In addition, cells at day 2 showed anti-EpCAM fluorescence (Fig. 4.10A). At day 6, anti-EpCAM fluorescence was more spread out and distributed among the new clones (Fig. 4.10A).

Figure 4.10B shows identical microwells (number 1, 2 and 3) after 8 days culture in microwells stained for viability and EpCAM. These images illustrate that cell were still viable. The majority of cells formed a monolayer at day 2 and at day 6 cells started to form aggregates. Cells grouped themselves into a spherical arrangement induced by the shape of the microwells and cells showed high cell–cell interaction. Furthermore, in some microfluidic wells MCF-7 cells showed spread morphology and adhered to the microwell wall and SiNi-membrane.

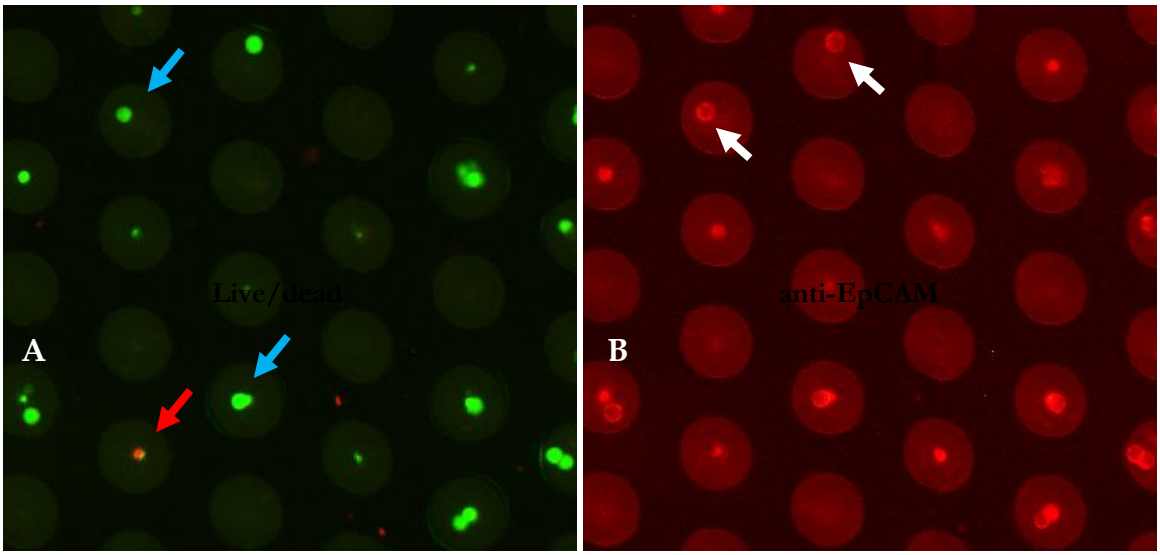


**Figure 4.9:** Representative images showing MCF-7 cells in microfluidic wells after spiking and sorting. A) MCF-7 cell viability in microwells stained with Calc AM (alive cells) and EthD1 (dead cells). B) MCF-7 cells could be easily identified in the microfluidic wells based on anti-EpCAM fluorescence located at the cell-membrane. Blue arrow depicts Calc AM (alive), red arrow EthD1 (dead) and white arrow anti-EpCAM.

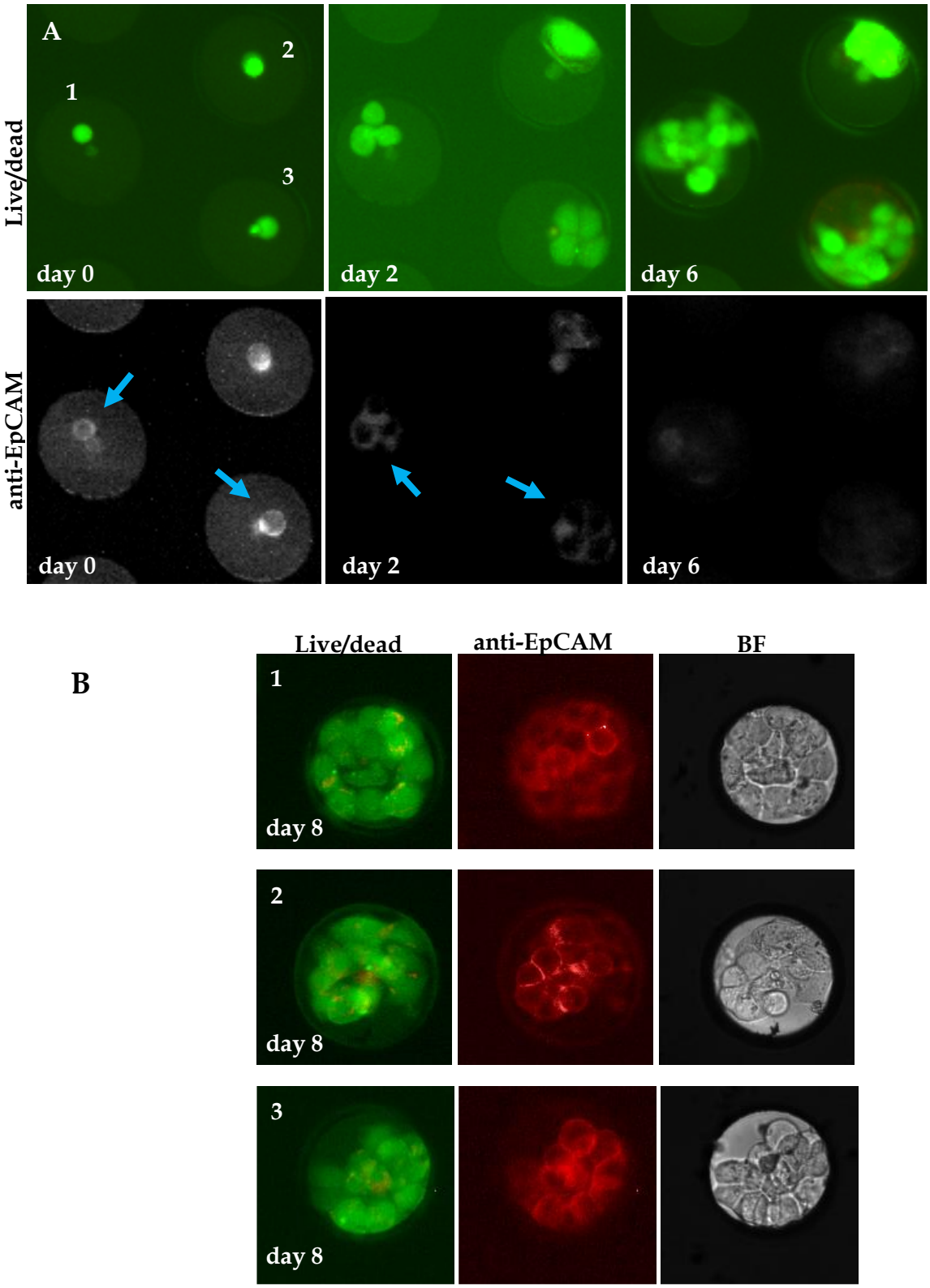


**Figure 4.10**: Representative images showing single MCF-7 seeded in microfluidic wells 1, 2 and 3). A) Images illustrating the growth of MCF-7 cells inside the microfluidic wells. Images in the top panel show single viable cells (day 0) and the growth of these cells at day 2 and day 6. Lower panel illustrate anti EpCAM. B) Identical microwells (1, 2 and 3) stained for viability and EpCAM after 8 days culture. Blue arrow indicates anti-EpCAM. BF denotes bright field images.

## 3.6.2 Viability after punching

Single cells and colonies (3-5 cells) were selected and retrieved from the microwells. MCF-7 cells were selected based on the expression of epithelial marker EpCAM and viability (positive for Calc AM and negative for Eth-D1). Selected cells were punched out in BME coated or non-coated 96 wells-plate. After 4 hours cells were stained again for viability and total number of viable cells was determined (Fig. 4.11). For single cells 77% was shown to be viable after 4 hours. Punched colonies showed a viability of 70%. Focusing on the punching of colonies we observed that most established colonies were recovered as a complete intact colony. Subsequently, cells were incubated and the potential to grow and generate mammospheres after punching was monitored.

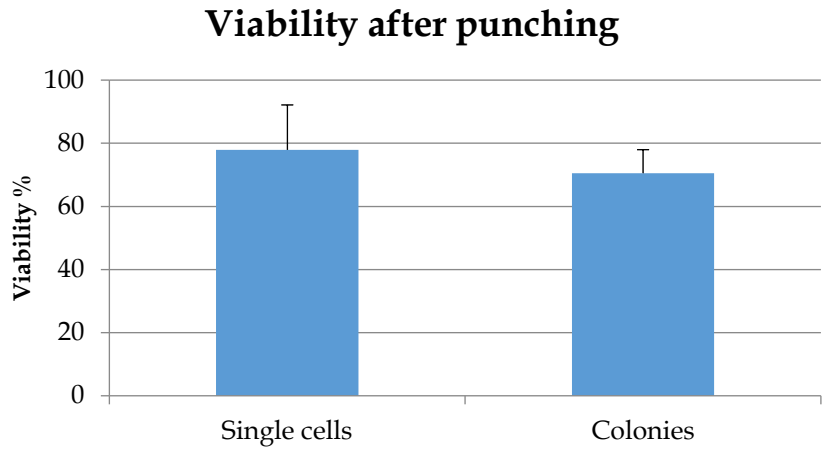


**Figure 4.11**: Cell viability after punching: MCF-7 punched as a single cell or as a. Single cells were punched out directly after seeding (0 hours); colonies were punched after 2 days culture inside microfluidic wells. Cells were stained after 4 hours and number of viable cells was determined. Data represents mean± sd, n=2.

## 3.6.3 Growth after punching

In Fig. 4.12 (from A to D) a selection of single cells or colonies is displayed. Selected cell were punched out from microwells and recovered in BME coated or non-coated TCP. Fig. 4.13 (A-D) shows identical single cells or colonies after punching from microfluidic wells. The punched cells grow rapidly and in well-defined structures. Cells punched in BME (at 3 days) display a very different appearance from cells punched in plastic (2d). MCF-7 cells punched in non-coated plates cells adhered to TCP (Fig 4.13A and B, at day 1). With longer culture times cells proliferated and formed a monolayer (Fig. 4.13A and B, day 3 to 14). MCF-7 cells punched in BME were able to grow into spheroid with a high degree of cell-cell contact (4.13C and D). The presence of the SiNi-membrane did not seem to affect cell proliferation. After 14 days, cells continued to proliferate and formed large spheroids. Interestingly, in BME cultures the majority of punched cells arranged and invaded into the BME layer (4.14A). The SiNi-membrane was often seen horizontally oriented. In non-coated plates (Fig. 4.14B) the SiNi-membrane was often observed to be located on top of the growing cell colony.

Continued culture after 14 days showed that MCF-7 cells punched in BME began to exhibit a darkened central area when analyzed by light microscopy. Over time, this region increased, and on day 19 of culture, the dark region became stable in size (Fig. 4.15C). Simultaneously with the increasing area of the central region, the region at the periphery of the spheroid showed cell budding and cells migration. Perhaps in larger spheroids cell death at the centre of the spheroid could be due to increased hypoxia and nutrient deficiency (Fig 4.15C).

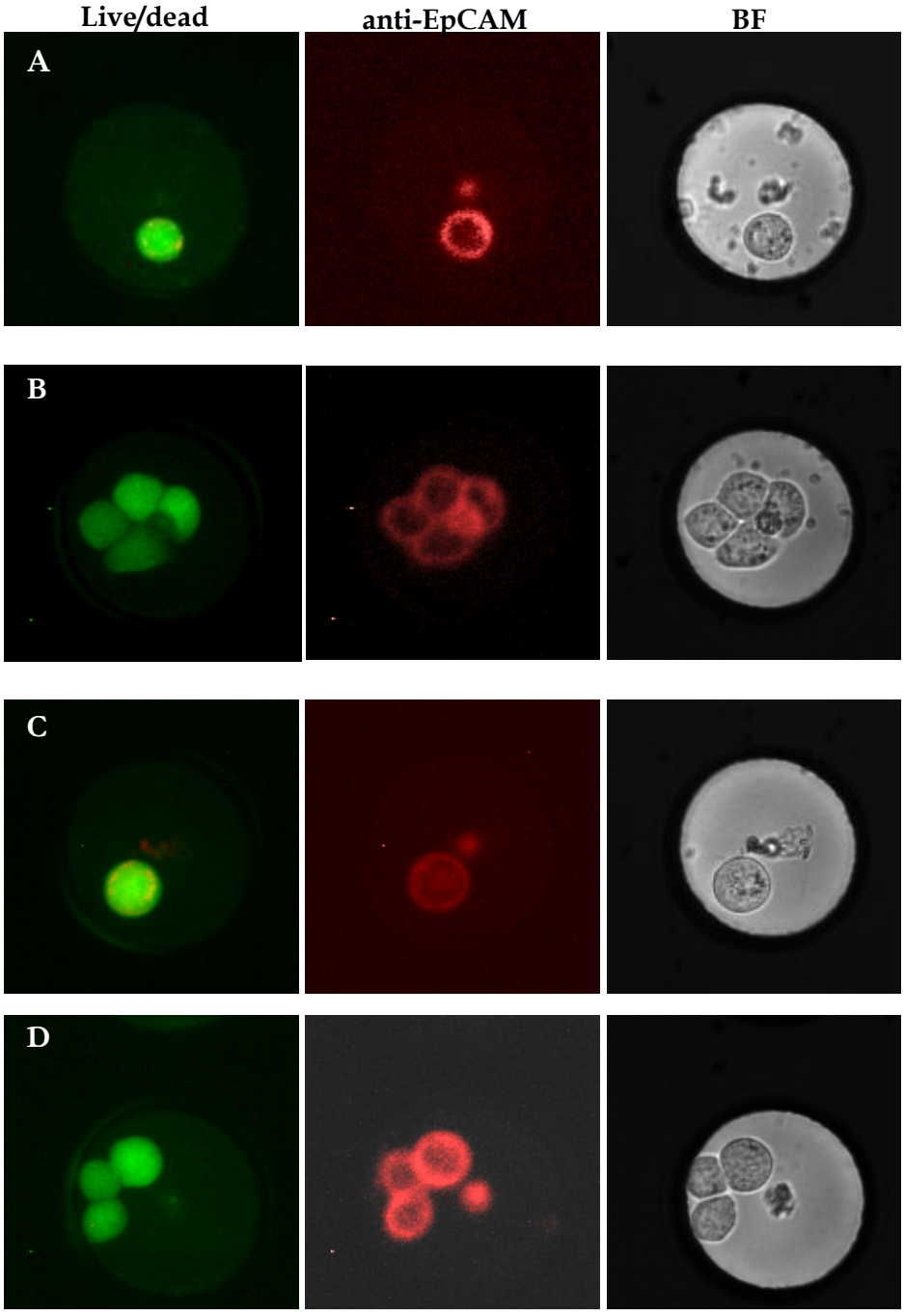


**Figure 4.12:** Single cells or colonies inside the microfluidic wells before punching. Cells were selected based on viability and EpCAM expression. Colonies were stained inside the microfluidic wells after 2 days culture with epithelial marker (anti-EpCAM), Calc AM (live) and EthD1 (dead).

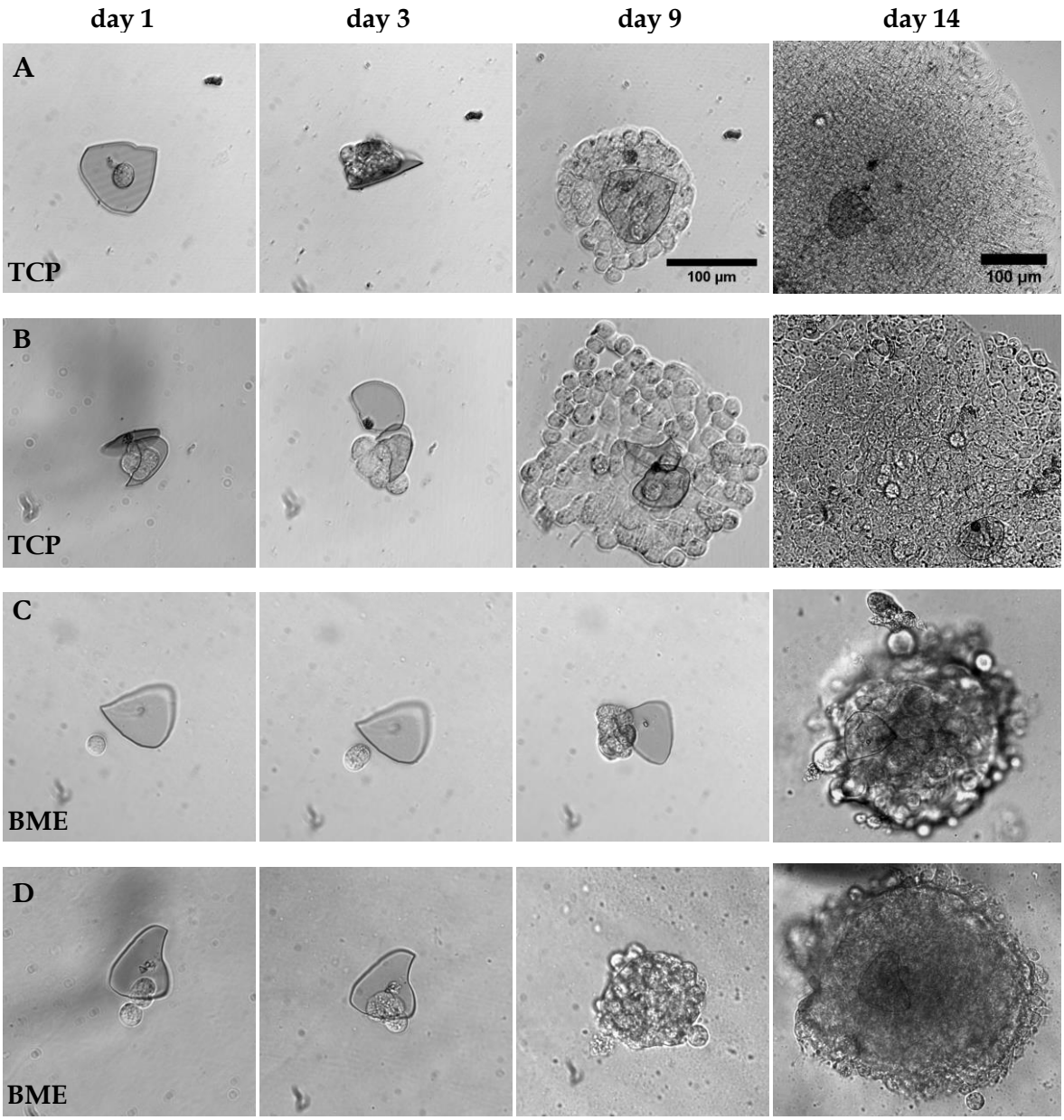


**Figure 4.13:** Cell growth after punching: MCF-7 cells were isolated from blood and sorted in a microfluidic chip. Cells were punched and recovered in TCP or BME for cell culture. Images A and B represent single cell and colony grown in TCP. C and D illustrate punched cells grown in BME. Proliferation was monitored for 14 days. Punched cells proliferated and formed a monolayer on TCP and spheroids in BME.

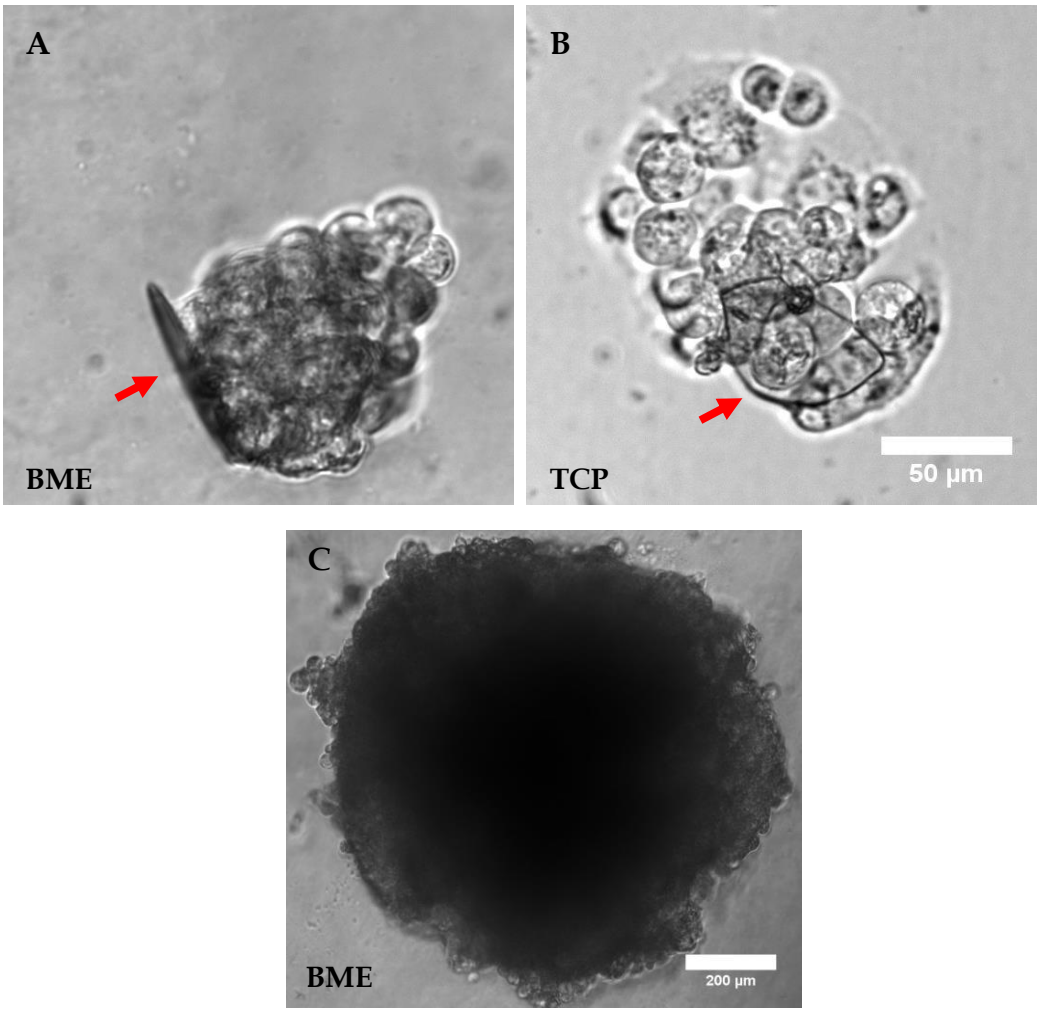


**Figure 4.14:** Typical bright field images of cells punched in BME coated or non-coated plates. A) Cells arrange and invade into the BME layer. B) In non-coated plates, SiNi-membranes were often located on top of the monolayer. C) Prolonged culture (19 days) of spheroids resulted in the formation of darkened central area. Red arrow indicates the SiNi-membrane.

Figure 4.15 shows the growth efficiency after punching. A distinction was made between cells cultured in BME coated plates and non-coated plates. Cells punched in BME showed higher growth efficiency when compared to non-coated. Only 44% of single cells generated mammospheres in non-coated plates (TCP) while in BME punched cells, 55% successfully proliferated and formed spheroids. Punched colonies showed an efficiency of 39% for TCP cultures and 62% for BME cultures. These results indicate that BME has an inducing effect on cell proliferation.

In contrast, it was expected that punching a colony of cells would results in higher growth efficiency due to the presence of more cells which could initiate proliferation. Instead, for cell punched in TCP we found lower growth efficiencies for colonies. In BME we find a higher efficiency for colonies which is in agreement with our expectation.

In summary, the microfluidic chip was used for the sorting of cells. The microfluidic chip enabled the sorting of viable single cells and we confirmed that cells could be cultured inside

the wells. In addition, single cells or colonies could be recovered from the microfluidic chip by punching. Subsequently, cultures were established from these punched cells. Theoretically, if the generated cell cultures where from real CTCs, the cells could be put back on the microfluidic wells for the sorting of single cells. Single cells could be subjected to a second round of culture inside the microfluidic wells or punched out in TCP to establish a cell line derived from CTC. The results obtained here indicate that the microfluidic chip could proof to be a valuable tool for sorting single viable CTC.

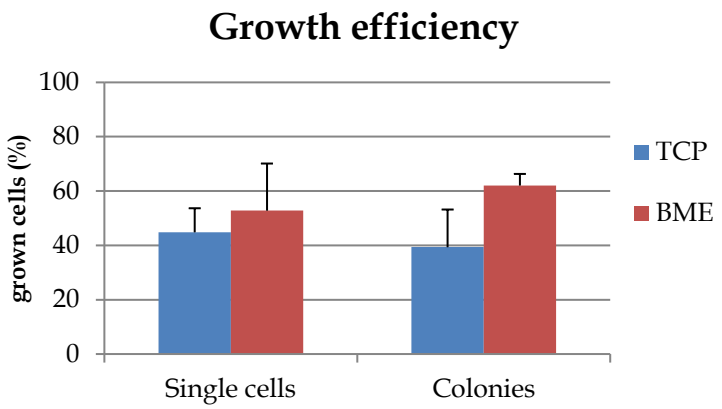


**Figure 4.15**: Growth efficiency after punching, the number of single cells or colonies which proliferated in TCP or BME was quantified. Cells were tracked for 14 days and growth efficiency was determined. TCP for non-coated plates and BME for matrigel coated plates.

# 4 Discussion

## 4.1 Microfluidic wells for cell sorting and culture

Swennenhuis *et al.* showed that different cell types could be seeded as single cells in microfluidic wells. In that study, the microfluidic wells were used for the isolation and sorting of single cells for downstream applications [33]. However, the culture of cells in the microwells was not investigated. In the present study we aimed to identify if the microfluidic chip could be used as a tool for the culture of cells, which in the future could be used for the sorting or culture of viable CTCs. In addition, the sorting and recovery of viable single cells or cell colonies from the microfluidic chips was investigated.

## 4.2 Cell seeding and viability

First we determined the cell seeding efficiency in microfluidic wells. MCF-7 cells were seeded in microfluidic wells with different BME concentrations (ECM proteins) and seeding efficiency was determined. It has been found that BME negatively affects cell seeding efficiency in microwells. Cells seeded in medium only showed an efficiency of ~90%. BME addition to the cell-suspension resulted in major decrease in cell seeding efficiency. Seeding cell in absence of 10% and 20% BME showed an efficiency of 48% and 35% respectively. This observed effect was expected, because BME is a viscous at (>4° C). At higher temperatures (> 4° C) BME gels and becomes viscous, which results in clogging the pores of the microfluidic wells. Clogged pores limit fluid flow, which affects cell seeding in microfluidic chip. We aimed to keep the cell-suspension and the microfluidic chip as cool as possible to avoid BME gelling and pore clogging however, this did not resulted in an increase in seeding efficiency. Perhaps seeding cells in a cold room (4° C) could result in an increase in efficiency.

Subsequently, the effect of the seeding method on cell viability was assessed. We observed that for the breast cancer line MCF-7, 90% of the cells was viable immediately after seeding. Incubation of cells inside the wells for 4 hr and 24 hr, showed a decrease in viability. Further incubation resulted in a further decline of viability inside the wells. FACS and pipette sorting showed similar viability directly after seeding (0h) and at 4h. But after 24h the number of viable cells decreased drastically for FACS (41%) when compared to cells in microfluidic wells (64%). Further incubation resulted in a decrease in viability for cells in microwells while FACS and pipette sorted cells showed almost no change in viability.

We believe that during the filtration process cells are exposed to hydrodynamic shear forces and endure physical stress [43]. In our study a negative seeding pressure between 5-10 mBar was used. Although cells experience a level of stress during seeding, they are exposed only for short period of time to shear stress (5-10 minutes) indicating that cells do not experience continues flow induced stress. Nevertheless we cannot explain why cells died in the microfluidic wells. In our study we clearly see a difference in cell viability between pipette and the other two methods for cell sorting. Cells seeded with pipette experienced less stress during

seeding and showed a higher number of viable cells. In addition, we assume that cell-cell and cell-substrate interaction is likely to play a significant role in regulating cell viability [44]. To determine whether this is also applies for our study, 500 microfluidic wells with single or pair of cells was randomly selected and viability for both conditions was determined. It was found that ~54% single cells were viable, while pair of cells showed a viability of ~73% after 1 day incubation. This difference in cell viability could be attributed to the process of cell-cell contact. Focusing on cancer cells, others studies reported that cell–cell contact rescues cancer cells and, partially, normal epithelial cells from cell death [45].

# 4.3 Cell culture

## 4.3.1 Cell lines

Next, cancer cells were cultured in microfluidic wells. Prostate cancer (LNCaP) cell and breast cancer (MCF-7) cells proliferated from single clones and formed spheroids inside fluidic wells. We observed that SiNi substrate did not facility cell spreading (LNCaP cells); only after the addition of ECM proteins cell spreading was observed. LNCaP cell cultured in BME adhered to the SiNi-membrane and showed a spread spindle like morphology similar to cells cultured in TCP. However at later time points, LNCaP exhibit a round morphology similar to cells cultured without BME. These results indicate that SiNi substrate did not facilitate LNCaP cell spreading.
MCF-7 used in this study and cultured in microwells did not show a change in morphology when compared to cell grown in TCP. MCF-7 in migrated in the microfluidic wells and were mainly located at the periphery of the wells. In addition, due to the quasi-3D properties of the fluidic wells, cells experience a 3D environment, this enabled cells to grow in a 3D morphology (with or without BME). There is only little scientific data regarding the cell adhesion on SiNi substrates. One study showed that mouse fibroblasts did not attach or spread to bare SiNi substrate. In addition, coating with fibronectine enhanced cell adhesion onto SiNi substrates [48]. In general, cell adhesion to silicon nitride membranes is typically weak, and cell proliferation is limited [56].

We aimed to culture cancer cell lines and provide cells with BME to induce cell growth. Single LNCaP cells grown in 10% BME showed a growth efficiency of 9,7% while cells in medium showed an efficiency of 6,7%. LNCaP cells grown in TCP with or without BME displayed growth efficiency between 39% and 33% respectively. It was observed that the majority of the LNCaP cells showed a morphology resembling dead cells. Overall LNCaP show poor growth in microfluidic wells, even for wells with more than 1 cell, growth efficiency was low.
MCF-7 cell showed higher growth efficiency when compared to LNCaP cells. Overall 13% and 7,7% of the single proliferated in microfluidic wells for respectively with and without BME. MCF-7 colony formation efficiency in microfluidic wells was shown to increase with increasing number of cell per microwell. Wells with respectively 2 or ≥3 cells resulted in a growth efficiency of 34% and 47% for BME supplemented cells and 18%, 31% for medium only. Again we believe that the combination; absence of neighboring cells (cell-cell contact), cell-

substrate interaction (SiNi) and the experienced stress during seeding are the main cellular properties affecting cell viability and cell proliferation. Especially, the process of cell-cell contact has been demonstrated to be an important factor to induce cell proliferation. For example Chen and colleagues used quasi-3D microwell substrates to determine the effect of cell-cell signaling on cell proliferation. They demonstrate that the presence of cell–cell contacts increased proliferation via paracrine signalling [47].
The effect of the substrate (SiNi) on cell behavior (e.g. spreading, adhesion and proliferation) is not well documented. In this research we showed that SiNi substrates did not have any cytotoxic effect on cell, which is also confirmed by others. Medina Benavente et al. recently reported the successful growth of PC12 cell on (poly-L-lysine) PLL coated SiNi-membrane (2d) [46]. They compared the growth on SiNi and TCP and found that the proliferation rate of PC12 cultured on the PLL coated SiNi surface was higher than in the plastic dish during the initial phase of the experiment. But, the proliferation rate decreased on the SiNi substrates when cells were cultured for longer periods [46].
In our study we have shown that cell growth in microwells is cell dependent. In addition because the microwells used here for cell culture are composed not only from SiNi but also from SiO2. Therefore it is difficult to determine which material is preferred by cells in term of cell growth. Nevertheless, although the characteristics of these microfluidic wells have not yet been fully determined, there is already evidence that they can be potentially useful as substrates for cell culture.

### 4.3.2 Organoids

An interesting aspect of microfluidic wells is that they enable to control the size of cell aggregates. Due to their small volumes and highly controllable environments, microwells could be attractive for creating miniaturized organoids to study cell heterogeneity. Here, we attempted to apply the microfluidic array for the generation of tumor organoids. Human CRC cells were cultured in microfluidic wells at different BME concentrations. In all conditions (with or without BME) organoids were generated. Organoids established in microwells shared similar morphologies to organoids grown in TCP (100% BME). In general for the generation of organoid in vitro, cells are resuspended in an ECM, herby providing cells with 3D microenvironment [28, 30]. We have shown that CRC organoids could established from single, two or three cells without the use of ECM. Perhaps the 3D-microwell environment combined with the non-adhesive properties of the SiNi substrate induces CRC cells to grow and assemble into organoid morphology.

Organoid growth efficiency was determined to be proportional to BME concentration. Largest percentage of organoids growth from single CRC cells was found in 20% BME cultures (28% efficiency) and lowest in the control group (0% BME) (10% efficiency). Further, we observed that growth efficiency was related to number of cells per microfluidic well. Increase in cell number per microfluidic well resulted in an increase in growth efficiency. The established organoids could be maintained in culture for more than 14 days. In addition organoids were successfully retrieved from the microfluidic wells and cultured in BME coated TCP. The retrieved organoids could not be maintained in culture after retrieval. Only a low amount of

organoids were able to invade in the BME layer and proliferate. Most organoids died after retrieval, probably due to the long incubation time in the microfluidic chip. Nevertheless, these results provided insights regarding the growth of organoids in the microfluidic chip.

## 4.4 Live cell punching

The microfluidic chip was further characterized and its potential to be used a platform for the sorting or culture of single cell was investigated. We aimed to establish cultures from single cells to study cell heterogeneity. Therefore, the microfluidic well array was exploited for its dual function; as a cell sorter (1) and for the culture of cells (2). MCF-7 cell were sorted with the microfluidic chip and single cells were recovered from the wells by punching. In addition colonies established from single cells in microfluidic wells were recovered. Live-dead assay showed that majority of recovered cells was alive and almost similar to control groups. Only cell sorted with FACS showed a higher viability after 4 hours. In addition the retrieval efficiency was found to be 92% and 76% for single cells and colonies respectively. The lower recovery found for colonies is probably because cells did not only adhere to the bottom membrane but also to the walls of the microfluidic wells. Single cells were punched directly after sorting and were mainly located at the centre of the SiNi-membrane. The affect of adhesion was further confirmed by the fact that cell colonies were still attached to the SiNi-membrane after punching while single cells were found detached from the membrane. This mean growing cell to larger number in the microwells could affect the cell recovery.

Results showed that 80% of the single cells and 67% of the colonies grew after punching. Pipette seeded cells showed a growth efficiency of 69% (single cells) and 71 % (colonies). Growth efficiency for punched single cells seems to be two-fold higher when compared to FACS sorted cells. Sorting cells with FACS seems to affect cell MCF-7 cell viability. Probably, during cell sorting process (FACS), cells are pushed through narrow tubing under high pressure, rapidly depressurized after passing through a nozzle, and then jetted through the air at high speed. While in the punching methods cells are continuously in contact with cell culture medium and do not experience high degree of stress. In addition for punched colonies the presence of the SiNi-membrane on top of cells did affect cell growth. In general cells which were not able to escape from the membrane did not proliferate. Comparing the punching of single cell colonies, results indicate that punching single cells after isolation is more efficient in generating cell growth after recovery.

Finally in a proof of principle study we aimed to test the previously described workflow, which in the future could be used to sort and culture CTC from real patients. In this study MCF-7 cells were spiked in whole blood. Tumor cells were enriched and stained in order to differentiate between tumor cell and WBC. Finally tumor cells were sorted in the microfluidic chip. Subsequently single cells or cell colonies were punched out in BME coated or non-coated culture plates. Spiked cells showed al lower viability after 4 hours when compared to non-spiked cells (77% vs 92%) while colonies showed almost similar viability (70% vs 77%). Punched single cells or cell colonies invaded into BME and formed spheroids, while cells punched in TCP formed 2d monolayers. Cell growth efficiency in BME was higher when

compared to TCP. In this experiment single-cell punching demonstrated a much lower growth efficiency when compared to colonies or non-spiked single cells.

Spiking resulted in 1.8 fold decrease in growth efficiency for single cells when compared to non-spiked single cells (previous experiment). This indicates that during the handling procedures; spiking, cell enrichment, staining, cell seeding and finally punching, cells experienced stress which could have affected cell viability. However, viability assay performed after 4h did not indicate a decrease in viability. Furthermore the results from the two experiments do not clearly indicate which method is most efficient for generating cell growth from a single clone. Nevertheless, our aim in this study was to show that single cell or group of could be recovered from the microfluidic chip and cultivated hereafter. Therefore, the workflow described here, can be used for the isolation of cells (single or colonies of cells) for further analysis.

Although the results presented here look promising, more experiments need to be performed to gain more data and determine the reproducibility. Especially, because in our study we used a large amount of cells which is not realistic as CTC are rare and only available in low numbers [51]. We are aware that the culture of CTCs from patients with low amount of CTC is challenging. However, if we could this would provide an opportunity to noninvasively study CTC heterogeneity and determine new drug targets. For CTC culture from real patients it is important to determine the appropriate method capable of effectively depleting leukocytes from a blood specimen while preserving viable tumor cells for *in vitro* expansion [53]. Furthermore, for CTCs expansion an appropriate culture model needs to be identified. Perhaps the use of the organoid culture model developed to establish in vitro growth of patient-derived samples at higher efficiency could proof to be useful in establishing cell lines from CTCs.

# 5 Conclusion

This thesis describes a preliminary study performed to characterize a microfluidic chip with an array of well for the sorting and culture of cells. In summary, from several experiments we determined that the microfluidic chip enables the seeding and sorting of viable cells. We showed that cells from different origin could be grown in microfluidic wells. In addition, 3D tumor organoids derived from CRC cells were generated in the microfluidic chip with or with the use of BME. Quantification of growth efficiencies, indicate that cell growth is dependent on cell type and cell number per well. Furthermore we showed that the microfluidic chip could be used as a cell sorter. Single-cell or colonies established in the microwells could be easily sorted and retrieved from the microfluidic chip for further culture or analysis. Taken together all the experiments performed here give a good indication of the characteristics and potential use of the microfluidic chip.

# Part 2

## DNA methylation

# 6 Characterization of ctDNA

## 6.1 GSTP1 methylation

To detect the hypermethylation of the GSTP1 CpG in prostate cancer, plasma DNA from 3 patients and 2 healthy donors (HD) was extracted. Plasma DNA samples were subjected to bisulfite treatment, including a positive control (LNCaP gDNA) and negative control (WBC gDNA). After conversion, MSPCR with 2 primers sets was performed. MSPCR analysis of plasma specimens is shown in Fig. 7.1. The LNCaP prostate cancer cell line was used as a positive control for methylation and is almost exclusively methylated at the GSTP1 promotor site as demonstrated by an absent band in the "U" (unmethylated) lane and a strong intensity band in the "M" (methylated) lane. Genomic DNA isolated from human WBC was used as a negative control for methylation at the GSTP1 site. HD plasma DNA was used as another negative control for methylation. GSTP1 promoter methylation was observed in the following samples shown in Fig. 7.1. We observe a faint band in the "M" lane for the blank control which could indicate contamination (red arrow). In all 3 patient samples GSTP1 hypermethylation is observed (Fig. 7.1). For the patient samples P1 and P2 an intense band in "M" can be seen which indicates to be highly methylated. In addition, we also observe bands in "U" lane for patient samples. This was expected because plasma DNA contains a mixture of ctDNA derived from tumors but also a high amount of "healthy" WBC DNA. These data show that GSTP1 can be detected in plasma samples.

Next, to separate methylated plasma DNA from the unmethylated fraction, MBD2 proteins were used. Plasma DNA from a prostate cancer patient (P) and HD was extracted. Subsequently, methylated and unmethylated fraction in each sample was separated in an MBD+ ("M") and an MBD- ("U") fraction. Figure 7.2 demonstrates the methylation profiles obtained after MSPCR analysis. We observe an intense band for the patient MBD+ fraction, in the "M" lane. This indicates that the GSTP1 promoter site is methylated. We do not observe a band in the "U" lane for patient sample. This suggests that the MBD+ fraction contains only methylated DNA. The MBD- fraction shows a band in "U" lane which represents unmethylated GSTP1. For HD a single band can be seen in MBD- fraction demonstrating that this fraction is unmethylated. In the MBD+ fraction for HD no band is observed which shows that this fraction does not contain any methylated GSTP1 DNA. We only mis a single band in the positive control group LNCaP, known to be highly methylated at GSTP1 promotor site (Fig. 7.2). Nevertheless, we showed that we could sensitively detected GSTP1 hypermethylation from only 300 µL plasma derived from cancer patients. However the method used here to detect mutation from ctDNA need to be applied to larger patients group.

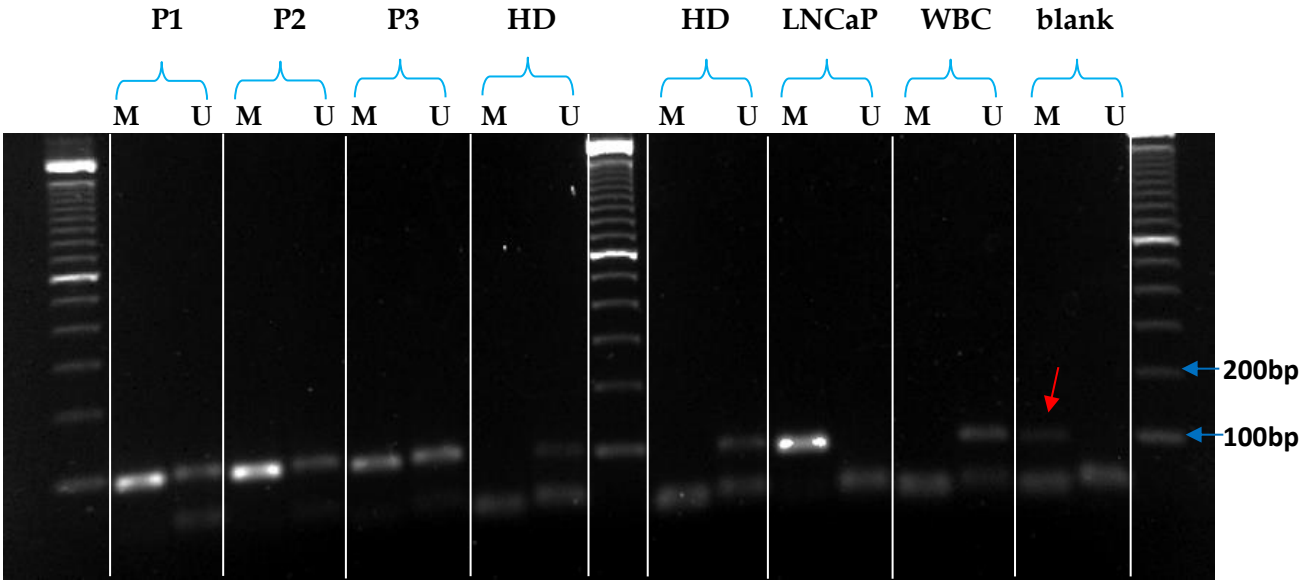


**Figure 7.1:** Agarose gel (2%) analysis showing the molecular analysis of GSTP1 by MSPCR in plasma samples of patients with prostate cancer. Generation of a PCR product indicates the presence of unmethylated (U) or methylated (M) GSTP1 alleles. LNCaP gDNA (positive control for methylation); WBC DNA (negative control for methylation); HD plasma, negative control for methylation; Blank for water control. Red arrow indicates non expected band in the blank control.

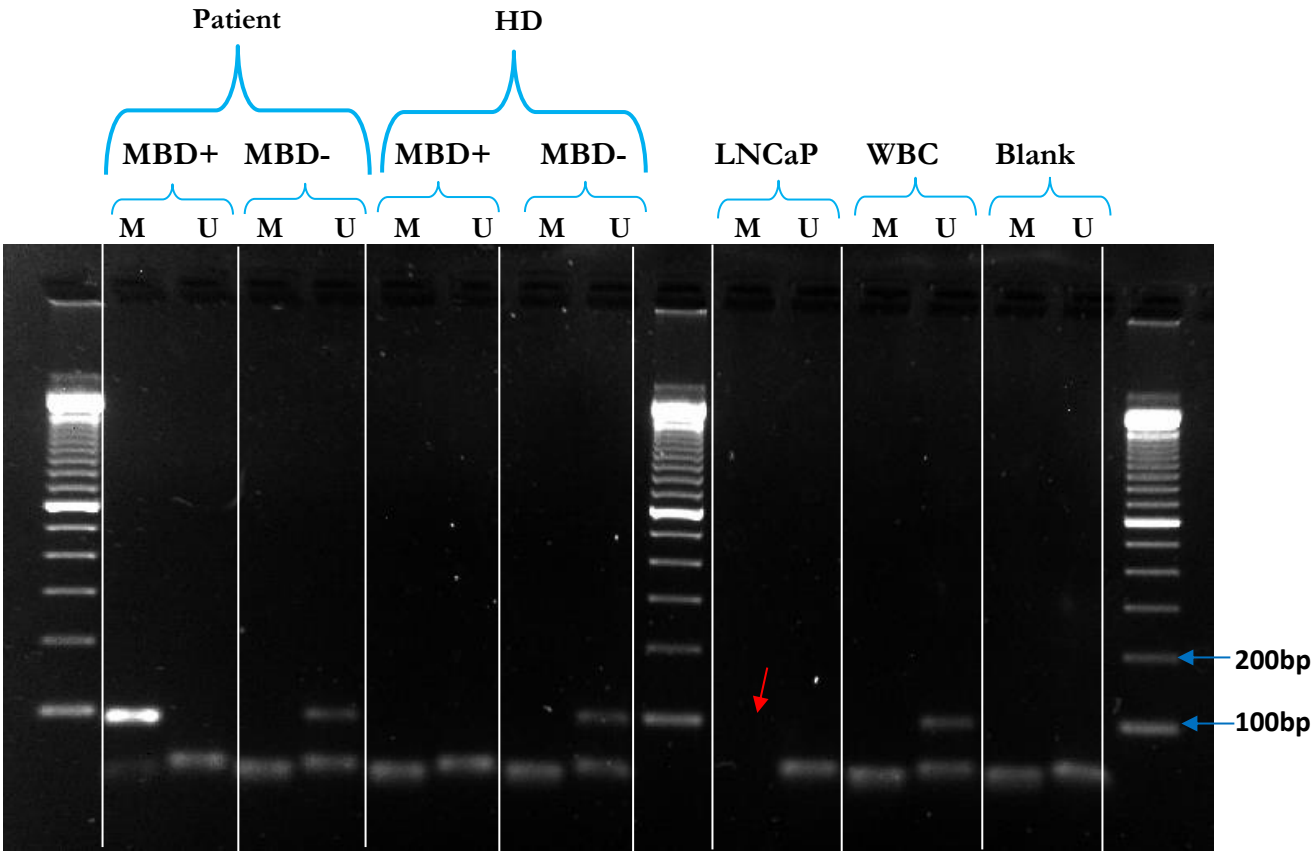


**Figure 7.2:** MSPCR after MBD2 enrichment. Prostate cancer and HD DNA was enriched, bisulfite treated and amplified. Image of the gel shows the molecular analysis of GSTP1 methylation. Generation of a PCR product indicates the presence of unmethylated (U) or methylated (M) GSTP1 alleles. LNCaP, gDNA (positive control for methylation); WBC DNA (negative control for methylation); HD plasma, negative control for methylation; Blank, water control. Arrow denoted the absence of an expected band for positive control (LNCaP).

# 7 Discussion

DNA methylation analysis of cell free ctDNA from blood samples has a substantial potential to serve as a minimally invasive tool for early diagnosis and clinical monitoring of diseases with considerable heterogeneity, especially in cancer and cancer-related diseases. Blood samples, often referred to as 'liquid biopsies' have several advantages over tissue biopsy including being noninvasive, easily accessible and can be repeatedly drawn from the same patient. Therefore changes in ctDNA methylation found in bodily samples can be a suitable biomarker. The goal of our study was to determine if we could detect the methylation status of the GSTP1 promotor site in plasma samples derived from prostate cancer patients. The GSTP1 promotor region is considered to be highly methylated in prostate cancer but unmethylated in healthy individuals. Using bisulfite conversion followed by MSPCR it was shown that hypermethylation of the GSTP1 promotor site can be detected in plasma from 3 prostate cancer patients. In addition the use of bisulfite as a tool to discriminate between methylated and unmethylated DNA, is hampered by the loss of DNA. This chemical treatment introduces various DNA strand breaks and results in highly fragmented single-stranded DNA. It has been shown that degradation affects between 84–96% of the DNA which renders PCR amplification impossible [49]. To overcome this, a different method was used to separate methylated from unmethylated DNA. Methyl-CpG-binding domain (MBD) proteins were used to bind specifically to methylated DNA fragments. MBD enrichment avoids the manipulation of DNA by methylation-sensitive restriction endonucleases or bisulfite treatment. However, we subjected the enriched DNA fractions to bisulfite to determine the methylation status of the GSTP1. MSPCR analysis showed that the two fractions contained only methylated or unmethylated DNA and GSTP1 methylation was detected in the methylated plasma DNA fraction.

Apart from plasma, GSTP1 methylation was also found in urine samples. Cairns *et al.* reported the detection of GSTP1 methylation in 6 out of 22 (27%) patients. Furthermore, they did not observe a case where urine ctDNA harbored methylation when the corresponding tumor was negative [50]. This indicates that molecular diagnosis of prostate cancer from body fluids is feasible. Although bisulfite is the gold standard in methylation analysis, MBD can proof to be a valuable tool in detecting methylation in rare samples with a low amount of starting material (e.g single cells). Gebhard *et al.* describes a rapid and sensitive procedure for detecting methylated DNA target sequences from limited sample material. They showed that MBD-PCR can reliably detect the methylation degree of a specific genomic DNA fragment from <30 cells [52]. MBD-PCR can be particularly useful in screening methylation levels of candidate genes not only in body fluids but also in single CTCs.

# 8 Conclusion

DNA methylation at the GSTP1 promoter site can be detected within the pool of cell-free ctDNA of human plasma from prostate cancer patients and not in healthy donors. After further validation, plasma DNA methylation of GSTP1 could potentially be used to non-invasively diagnose prostate cancer in patients.

# 9 Literature


[1] Crowley, E., et al. (2013). "Liquid biopsy: monitoring cancer-genetics in the blood." Nat Rev Clin Oncol **10**(8): 472-484.

[2] Diaz-Cano, S. J. (2012). "Tumor Heterogeneity: Mechanisms and Bases for a Reliable Application of Molecular Marker Design." International Journal of Molecular Sciences **13**(2): 1951-2011.

[3] Karachaliou, N., et al. (2015). "Real-time liquid biopsies become a reality in cancer treatment." Annals of Translational Medicine **3**(3): 36.

[4] Lodish H, et al. (200) Molecular Cell Biology. 4th edition. New York: W. H. Freeman;Section 24.1, Tumor Cells and the Onset of Cancer.

[5] Hanahan, D. and R. A. Weinberg (2000). "The Hallmarks of Cancer." Cell **100**(1): 57-70.

[6] Pantel, K. and C. Alix-Panabières (2016). "Liquid biopsy: Potential and challenges." Molecular Oncology **10**(3): 371-373.

[7] Nguyen, D. X., et al. (2009). "Metastasis: from dissemination to organ-specific colonization." Nat Rev Cancer **9**(4): 274-284.

[8] Allard, W. J., et al. (2004). "Tumor cells circulate in the peripheral blood of all major carcinomas but not in healthy subjects or patients with nonmalignant diseases." Clinical Cancer Research **10**(20): 6897-6904.

[9] Kidess, E. and S. S. Jeffrey (2013). "Circulating tumor cells versus tumor-derived cell-free DNA: rivals or partners in cancer care in the era of single-cell analysis?" Genome Medicine **5**(8): 1-4.

[10] Wu, S., et al. (2015). "Classification of Circulating Tumor Cells by Epithelial-Mesenchymal Transition Markers." PLoS ONE **10**(4): e0123976.

[11] Harouaka, R. A., et al. (2013). "Circulating tumor cell enrichment based on physical properties." Journal of laboratory automation **18**(6): 10.1177/2211068213494391.

[12] Haber, D. A. and V. E. Velculescu (2014). "Blood-Based Analyses of Cancer: Circulating Tumor Cells and Circulating Tumor DNA." Cancer discovery **4**(6): 650-661.

[13] De Mattos-Arruda, L., et al. (2013). "Circulating tumor cells and cell-free DNA as tools for managing breast cancer." Nat Rev Clin Oncol **10**(7): 377-389.

[14] Li, L.-C., et al. (2004). "DNA methylation in prostate cancer." Biochimica et Biophysica Acta (BBA) - Reviews on Cancer **1704**(2): 87-102.

[15] Hoque, M. O. (2009). "DNA methylation changes in prostate cancer: current developments and future clinical implementation." Expert review of molecular diagnostics **9**(3): 243-257.

[16] Heyn, H. and M. Esteller (2012). "DNA methylation profiling in the clinic: applications and challenges." Nat Rev Genet **13**(10): 679-692.

[17] Baylin, S. B. "DNA methylation and gene silencing in cancer." Nat Clin Prac Oncol.

[18] Frommer, M., et al. (1992). "A genomic sequencing protocol that yields a positive display of 5-methylcytosine residues in individual DNA strands." Proceedings of the National Academy of Sciences of the United States of America **89**(5): 1827-1831.

[19] Li, Y. and T. O. Tollefsbol (2011). "DNA methylation detection: Bisulfite genomic sequencing analysis." Methods in molecular biology (Clifton, N.J.) **791**: 11-21.

[20] Leontiou, C. A., et al. (2015). "Bisulfite Conversion of DNA: Performance Comparison of Different Kits and Methylation Quantitation of Epigenetic Biomarkers that Have the Potential to Be Used in Non-Invasive Prenatal Testing." PLoS ONE **10**(8): e0135058.

[21] Kolostova, K., et al. (2014). "Circulating tumor cells in patients with urothelial tumors: Enrichment and in vitro culture." Canadian Urological Association Journal **8**(9-10): E715-E720.

[22] Cayrefourcq, L., et al. (2015). "Establishment and Characterization of a Cell Line from Human Circulating Colon Cancer Cells." Cancer Research **75**(5): 892-901

[23] Gao, D., et al. (2014). "Organoid cultures derived from patients with advanced prostate cancer." Cell **159**(1): 176-187.

[24] Zhang, Z., et al. (2014). "Expansion of CTCs from early stage lung cancer patients using a microfluidic co-culture model." Oncotarget **5**(23): 12383-12397.

[25] Drost, J., et al. (2016). "Organoid culture systems for prostate epithelial and cancer tissue." Nat. Protocols **11**(2): 347-358.

[26] Gong, X., et al. (2015). "Generation of Multicellular Tumor Spheroids with Microfluidic well-Based Agarose Scaffolds for Drug Testing." PLoS ONE **10**(6): e0130348.

[27] Dyson, R. J., et al. (2016). "An investigation of the influence of extracellular matrix anisotropy and cell–matrix interactions on tissue architecture." Journal of Mathematical Biology **72**(7): 1775-1809.

[28] Fatehullah, A., et al. (2016). "Organoids as an in vitro model of human development and disease." Nat Cell Biol **18**(3): 246-254.

[29] Sato, T., et al. (2009). "Single Lgr5 stem cells build crypt–villus structures in vitro without a mesenchymal niche." Nature **459**(7244): 262-265.

[30] van de Wetering, M., et al. "Prospective Derivation of a Living Organoid Biobank of Colorectal Cancer Patients." Cell **161**(4): 933-945.

[31] Gross, A., et al. (2015). "Technologies for Single-Cell Isolation." International Journal of Molecular Sciences **16**(8): 16897-16919.

[32] Yaron, J. R., et al. (2014). "A convenient, optimized pipeline for isolation, fluorescence microscopy and molecular analysis of live single cells." Biological Procedures Online **16**: 9-9.

[33] Swennenhuis, J. F., et al. (2015). "Self-seeding microfluidic well chip for the isolation and characterization of single cells." Lab on a Chip **15**(14): 3039-3046.

[34] Yu, M., et al. (2014). "Ex vivo culture of circulating breast tumor cells for individualized testing of drug susceptibility." Science (New York, N.Y.) **345**(6193): 216-220.

[35] Alix-Panabieres, C. and K. Pantel (2014). "Challenges in circulating tumour cell research." Nat Rev Cancer **14**(9): 623-631.

[36] http://www.who.int/mediacentre/factsheets/fs297/en/.

[37] Hanahan, D. and Robert A. Weinberg "Hallmarks of Cancer: The Next Generation." Cell **144**(5): 646-674.

[38] Alix-Panabieres, C. and K. Pantel (2014). "Technologies for detection of circulating tumor cells: facts and vision." Lab on a Chip **14**(1): 57-62.

[39] Joosse, S. A., et al. (2015). "Biology, detection, and clinical implications of circulating tumor cells." EMBO Molecular Medicine **7**(1): 1-11.

[40] Haber, Daniel A., et al. (2011) "The Evolving War on Cancer." Cell **145**(1): 19-24.

[41] Cooper GM. The Cell: A Molecular Approach. 2nd edition. Sunderland (MA): Sinauer Associates; 2000. The Development and Causes of Cancer. Available from: http://www.ncbi.nlm.nih.gov/books/NBK9963/

[42] Khavari, D. A., et al. (2010). "DNA methylation and epigenetic control of cellular differentiation." Cell Cycle **9**(19): 3880-3883

[43] Hua, J., et al. (1993). "A Review of the Effects of Shear and Interfacial Phenomena on Cell Viability." Critical Reviews in Biotechnology **13**(4): 305-328.

[44] Wei, Q., et al. (2011). "Cell-Cell Contact Preserves Cell Viability via Plakoglobin." PLoS ONE **6**(10): e27064.

[45] Kondo, J., et al. (2011). "Retaining cell–cell contact enables preparation and culture of spheroids composed of pure primary cancer cells from colorectal cancer." Proceedings of the National Academy of Sciences **108**(15): 6235-6240.

[46] Medina Benavente, J. J., et al. (2014). "Evaluation of Silicon Nitride as a Substrate for Culture of PC12 Cells: An Interfacial Model for Functional Studies in Neurons." PLoS ONE **9**(2): e90189.

[47] Charnley, M., et al. (2009). "Integration column: microwell arrays for mammalian cell culture." Integrative Biology **1**(11-12): 625-634.

[48] Sakata, T., Ueda, A. and Miyahara, Y. (2007), Cell adhesion characteristics of chemically modified silicon nitride surfaces."IEEJ Trans Elec Electron Eng, 2: 295–300. doi: 10.1002/tee.20153.

[49] Ehrich, M., et al. (2007). "A new method for accurate assessment of DNA quality after bisulfite treatment." Nucleic Acids Research **35**(5): e29-e29.

[50] Cairns, P., et al. (2001). "Molecular Detection of Prostate Cancer in Urine by GSTP1 Hypermethylation." Clinical Cancer Research **7**(9): 2727-2730.

[51] Kallergi, G., et al. (2013). "Apoptotic Circulating Tumor Cells in Early and Metastatic Breast Cancer Patients." Molecular Cancer Therapeutics **12**(9): 1886-1895.

[52] Gebhard, C., et al. (2006). "Rapid and sensitive detection of CpG-methylation using methyl-binding (MB)-PCR." Nucleic Acids Research **34**(11): e82-e82.

[53] Ozkumur, E., et al. (2013). "Inertial Focusing for Tumor Antigen–Dependent and –Independent Sorting of Rare Circulating Tumor Cells." Science translational medicine **5**(179): 179ra147-179ra147.

[54] Shilpa V, et al. (2014). "GSTP1 expression and promoter methylation in epithelial ovarian carcinoma." Clin Cancer Investig J;3:487-92.

[55] Weaver, V. M., et al. (1997). "Reversion of the Malignant Phenotype of Human Breast Cells in Three-Dimensional Culture and In Vivo by Integrin Blocking Antibodies." The Journal of Cell Biology **137**(1): 231-245.

[56] Masuda, Y., et al. (2015). "Cell culture on hydrophilicity-controlled silicon nitride surfaces." World Journal of Microbiology and Biotechnology **31**(12): 1977-1982